Università dell'Insubria di Como
Dipartimento di Scienza e Alta Tecnologia
Dottorato in Scienze Ambientali
PhD Course XXVI Cycle

THE MUSSO FAULT AND ITS ROLE IN THE EVOLUTION OF THE NORTHERN LAKE COMO BASEMENT

CARLO MONTORFANO
2015

Università dell'Insubria di Como
Dipartimento di Scienza e Alta Tecnologia
Dottorato in Scienze Ambientali
PhD Course XXVI Cycle

THE MUSSO FAULT AND ITS ROLE IN THE EVOLUTION OF THE NORTHERN LAKE COMO BASEMENT

Tutor:
Prof. Luigina Vezzoli

Co-tutor:
Prof. Silvana Martin

Index

Summary

The main target of this thesis is the study of the Musso Fault in the northern Lake Como region. The Musso Fault is a very important regional tectonic structure, that played a role in the central Southern Alpine basement evolution, similar to that of the Lugano-Val Grande Line and the Orobic Thrust. Along it we found and mapped:

a) Fe-mineralization,
b) Marble lenses,
c) Diffuse mylonitic rocks, pseudotachylytes of metric length, hundred meters long fault walls and cataclastic bands.

Chapter 1 of this thesis is dedicated to the Fe-mineralization; it is proposed a common origin for all the Fe-carbonate mineralizations in the Southern Alps, included that of the Musso Fault, and a clear relationship with the Permo-Triassic rifting-related faults.

The siderite mineralizations, even if distributed over 300 km from W to E, from a stratigraphic point of view belong to the Early Triassic time (≈245-250Ma). They can be found as veins in the basement and covers (BV and SV) but also as stratiform-stratabound metasomatic orebodies in the carbonatic lithologies (SS). The common paragenesis includes siderite±ankerite±sulphides.

The mineralization is associated to Permo—Triassic and Early Triassic extensional faults, generally reactivated during the Alpine Orogeny in a compressive regime. These faults are associated to the Permo—Mesozoic rifting that brought the continental crust to thinning and to the related thermal peak. Alpine reactivation overprinted partly the old Permo—Triassic and Lower Triassic structures.

Siderite has homogenous composition with Mg and Mn content correlated to different types of host-rock. Mg concentration decreases in the metasomatic orebodies probably due to the replacement processes in the carbonatic rocks (Werfen and Servino Fms). Mg tend to be more compatible with the dolomite-ankerite phases than the siderite.

REE elements in the siderite samples show a crystal-chemical driven fractionation. In respect to siderite, both older Permian and younger Ladinian volcanics, have different REE patterns, much richer in REE and very similar to the average continental crust composition. Since currently there are no evidences of a possible deeper source of the fluids (mantle or lower crust related?) it is only likely to confirm that the conditions of the crystallization supported a crystal-chemical fractionation related to the REE^{3+} ionic radii compatibility with the siderite lattice. REE trends show slight variation related to the type of host-rock. The variation is a depletion in REE and a slight enrichment in Eu in the metasomatic orebodies. This can be possibly explained with a

change in the fluid composition that favored the assimilation of the REE by other phases. The Eu positive peaks seem to be correlated to the enrichment in Ca of the siderite and consequent increase of the siderite crystal-chemical compatibility.

Chapter 2 describes the Musso Fault marbles and the included metabasites. Marble lenses, including the main Musso Marble lens (MML) between the villages of Musso and Dongo, are boudinaged along the Musso Fault Zone. The alignment of marble lenses, appear as a structure that divide two different structural units into the Southern Alpine basement.

The marble lenses are composed of four lithotypes: i) dolomitic marble, characterized by compositional layering, ii) coarse grained marble, characterized by large crystal grain size and possibly related to the Triassic thermal peak, iii) fine grained mylonitic marble, diffuse at the border of the marble lenses, possibly related to a Triassic mylonitic deformation, iv) fine grained banded mylonitic marble, characterized by very small grain size and narrow folds, cropping out along main faults. Tabular metabasite bodies crosscut the MML irrespective of its different lithologies.

The structural analysis of the MML and the surrounding basement lead to observe that:

1) The MML is completely bounded by main fragile fault planes and ductile structures.
2) The main foliation of the MML is only partly aligned to the regional E-W trending S2 foliation.
3) The MML has different N-S trending mylonitic foliation and fracture cleavage compared to S/SW dipping mylonitic foliation of the southern basement.
4) The apparent absence of garnet in the MML metabasites suggest a different metamorphic imprint in respect to the surrounding basements.
5) There are not sufficient petrographic data to determine the belonging of the MML to the different structural units recognized in the Southern Alpine basement.
6) The MML reached the Permo-Triassic thermal peak similar to that of surrounding basement.

Within the MML, the marble-metabasite contact has locally characteristics that we interpreted as not correlated to the metamorphic evolution but resembling relicts of primary magmatic intrusion: i) lobes, ii) compositional layering parallel to the contact of the lobes, iii) diffuse sulphide mineralization at the metabasite-marble contact, iv) small interfingering of metabasite protruding within the marble resembling a fluidification of the hostrock, v) crosscutting of the dykes, vi) parallel tabular structures with geometry not related to any metamorphic event thus resembling dykes, vii) contact band characterized by mixing of phases suggesting a widespread mixing at the protoliths interface.

The seven described structures, all found in the MML, resemble those of a basalt intrusion within a carbonatic sediment only partially lithified.

Major, trace and REE elements of *Musso* and *Lugano-Val Grande Fault Zone* (LGFZ) metabasites, analyzed in this study, are compared to other metabasite and volcanics of the Southern Alps available in the literature: I) metabasites with and without cummingtonite from the *Piona Peninsula (DOZ)*, II) metabasites from *the Strona Ceneri Border Zone (SCBZ)* and III) *Triassic* basaltic volcanics of the central Southern Alps.

The *LGFZ* sample have very similar geochemical characteristics to *SCBZ* that allow to suppose a common origin. *Musso* samples show an in-between composition: they have similar Ba, Na, Al content to the *SCBZ*, *LGFZ*, and *Triassic* volcanics but have TiO2, Zr, Nb, MgO and SiO2 content similar to *Anisian* (a group belonging to the Triassic set) and part of the *DOZ*. This could be due to a partial metamorphic imprint with elements depletion, or a different volcano-tectonic origin, more similar to that of the *Anisian* basalts.

Genetic diagrams, from literature, confirm the division between the DOZ and the SCBZ. SCBZ and LVGZ appear as a compact group with a MORB to tholeiitic composition. The Musso samples belong to intraplate products with alkali-basalt to tholeiitic composition.

These data are only partially sufficient to suppose a particular role of the Musso marble lenses and the included metabasites but definitely testify the existence of this tectonic structure since at least Variscan age (Devonian-Early Carboniferous).

In Chapter 3, the ductile and brittle structures mapped along the Musso Fault Zone (MFZ) are described and a hypothesis for the Musso fault evolution is presented, touching the following main stages:

1) Marble lenses (Musso marble) are boudinaged along the MFZ and represent the oldest rocks characterizing it. Their age is still not determined, but the included metabasites have unique geochemical characteristics that do not allow to attribute them nor to DOZ nor the Strona Ceneri Border Zone amphibolite suites. We speculate a Devonian perhaps to Early Carboniferous age for the marble and the included metabasites.
2) Geochronological and thermal data from literature shows that the Northern Lake Como region experienced a Triassic thermal peak and development of intra-basement shear zones, thinning the Adriatic crust. In this context the oldest structures directly and incontrovertibly connected to the MFZ are the Fe-carbonate veins, of Early Triassic age, which are preserved also boudinaged within the Musso mylonites. The same can be said also for the LGFZ, as demonstrated by extensive siderite mineralization presence in the Gaeta mine and Val Cavargna.

3) Fe-mineralized veins are found in similar extensional context in all the Southern Alps, along faults bordering Permo-Triassic continental basins. Therefore it is possible that also the MFZ was bordering a small basin to the N, nonetheless justifying the presence of the sedimentary Monte Pozzuolo and Sasso Pelo. In the Lake Como area continental extension started in the Norian and continued to Liassic.
4) The mylonites of the MFZ possibly developed after the Early Triassic thermal peak when temperature dropped to around 250-350°C allowing crystallization of quartz-albite-chlorite-sericite associations, before the emplacement of the 220Ma old Piona's pegmatites which do not show mylonitization even near the MFZ.
5) From the Liassic to the onset of the Alpine compressive stage there is a long inactivity time span, with no records for the MFZ.
6) Alpine N-S contraction brought into a steep south dipping position the Paleozoic to Mesozoic rocks and lineaments and caused upper and middle crust to detach from their substratum along the MFZ. This contraction was responsible of the ductile-brittle deformation observed along the MFZ with development of widespread and abundant pseudotachylytes. Similar structures dated along the Orobic and Porcile thrusts yielded two sets of ages: an older Late Cretaceous and a younger Eocene ages.
7) Widespread distensive cataclastic bands along the Musso and contiguous faults, possibly indicating a distensive to transpressive stage, by correlation with nearby data of Val Morobbia, may belong to Oligocene.
8) Finally, right strike-slip dextral brittle deformation took place, visible along the largest fault planes, most probably driven by the Insubric Line.

Introduction and scope of the research

The first step that lead to the present study was my Bachelor Thesis that focused on the iron mineralization along the Musso Fault, their hosting rocks and the important and historical Dongo mines and. It was a research based mostly on geochemical analysis and field observations of local geology and historical conditions of the mines. During the PhD, this study was extended to several similar mineralizations of the Southern Alps, from the Lake Como area to the Dolomites. This brought us to publish an article whose title is "Iron mineralization in the Southern Alps: a signal of the Permo-Triassic rifting?" where a common origin for all the Fe-carbonate mineralizations in the Southern Alps, and a clear relationship with the Permo-Triassic rifting-related faults are proposed. This work constitutes the first chapter of this thesis and it is presented as the article currently submitted to the Lithos journal.

The work on the iron mineralizations and the tectonic features that we found in the Musso area for the first time, lead us to the conclusions that the Musso Fault is a very important regional tectonic structure, poorly constrained, that played a role in the central Southern Alpine basement evolution, similar to that of the Lugano-Val Grande Line and the Orobic Thrust. We found and mapped, beside the already cited Fe-mineralization, marble lenses, diffuse mylonitic rocks, pseudotachylytes of metric length, hundred meters long fault walls and cataclastic bands. The second part of this thesis is dedicated to the study of the Musso Fault rocks and the surrounding basement, it is split in two chapters. Chapter 2 describes the Musso marble and the included metabasites from a geochemical and structural point of view. The alignment of marble lenses, including the main Musso lens, appear as a Variscan structure that divide two different basements. The main evidences that lead us to this conclusion are that the metabasites included in the marble still preserve some of the original emplacement structures, and a geochemical similarity to the metabasites of the Early Carboniferous, Strona-Ceneri Border Zone.

In chapter 3, we describe and present the summary of the ductile and brittle structures mapped along the Musso Fault, such as schistosity, folds, mylonites, pseudotachylytes and faults planes. Based on that, and a deep and extensive study of the previous works in the region (El Tahlawi, 1965, Fumasoli, 1974, Bertotti, 1993, Schumacher, 1997, Spalla et al., 2002 and other cited in the chapter), few thematic maps including geochemical and geochronological data are proposed. In this chapter is presented an hypothesis for the Musso fault evolution, touching the following main stages: i) Silurian-Early Carboniferous (?) sedimentation of the marble protoliths and syn-sedimentary intrusion of basic dykes, ii) Variscan orogeny metamorphism ii) reactivation in Early-Permian in a rifting tectonic, marked first from emplacement of the Fe-mineralization,

followed by a green schists mylonitic stage, iii) Middle Triassic HT-LP event with emplacement of pegmatites, iv) the analysis of brittle structures that we found widely consistent with the t Alpine tectonics.

Author biography

Carlo Montorfano started to work on the geochemical characterization of the Musso Fe-mineralization in 2008 during his Bachelor Thesis at the Insubria University, Environmental Science course. The study continued and expanded to the Musso Fault during the 2010 Master thesis of the same course. After graduation he started working for TESMEC Spa, an earth moving machinery manufacture, where he covers a multidisciplinary role in the TESMEC Research and Development Department, as geologist, geotechnical laboratory technician, sales advisory and estimator for contracting. He specialized in the performances and cost estimation for pipelines, mining and civil construction jobsites and followed projects in several countries such as Qatar, Saudi Arabia, Indonesia, Russia, China, India, Chile and France.

Meanwhile, starting in fall 2010, together with Prof. Luigina Vezzoli of the Insubria University and Prof. Silvana Martin of the Padua University, he continued the researches on the Musso Fault in a non-paid PhD position that lead to the present thesis.

Acknowledgments

I gratefully acknowledge the support of my parents, Adriano and Jolanda, while I pursued this project. I also want to thank TESMEC Spa for allowing me to conclude this project.

The authors thanks Prof. Luciano Secco, Giuseppe Cassinis, Andrea Pozzi, Sandro Recchia, Gabriele Carugati, Pietro Frizzo, Simone Tumiati, Gilberto Masciocchi, Daria Pasqual, Luca Toffolo, Ilaria Conconi, Marcello Marelli and Stefano Zanchetta for the helpful reviews and support in the analytical laboratory.

1 Siderite mineralization in the Southern Alps: a signal of the Permo—Triassic rifting?

Abstract

Siderite mineralizations are distributed along the Southern Alps between Lake Como and Eastern Dolomites, mostly along major faults as Orobic, Val Trompia and Valsugana lineaments. They are dominantly unconformable veins in the Southalpine basement of Lake Como (Dongo, Val Cavargna) and Val Trompia (Torgola and Pinetto) and in Late Permian rocks of the Orobic Alps (Lorio and Torsolazzo), or as stratiform conformable ore bodies within Lower Triassic Servino Fm carbonatic rocks (Manina, Fusio, Fura, San Vittore) (Cassinis et al., 1997; Brigo & Venerandi, 2005). Similar setting is described for siderite veins and strata bounds mineralization in the Eastern Dolomites (Santa Lucia, Transacqua and Valle del Mis). Several publications describe the setting and the characteristics of the siderite, because the mining activity for iron extraction has been active since XV. This work aims to define structural, stratigraphical and geochemical correlations among the siderite mineralizations of the Southern Alps that support a common time and process of genesis. The composition of the siderite is rather homogeneous, but it is enriched in Mn when it forms strata-bounds in carbonatic rocks, whereas it is enriched in Mg when it forms veins cutting the basement. According to Frizzo & Scudeler Bacelle (1983), siderite appears to have invaded the carbonatic rocks and impregnate them more or less extensively. The origin of Fe and Mg of the siderite remains unclear. Hydrothermal solutions charged of Fe and Mg, at presumed low temperature (≈200°C), traveled across the upper crust in a large portion of the Southern Alps, mostly where extension faults were active since Early Permian and some basins (e.g. Collio) were locally opening. A specific time range, spanning from Late Permian to Early Triassic in Lombardy and in the Dolomites is recorded. The time of siderite impregnation ended with the beginning of the Triassic magmatism in Lombardy and Venetian regions. The siderite mineralizations are a geodynamic indicator in the Southern Alps, possibly in relation to the Permo-Triassic rifting process.

Keywords: siderite mineralization; REE; metasomatism; Southern Alps; Permian; Early-Trias; alpine rifting.

1.1 Introduction

Massive siderite mineralizations are widespread in the Italian Southern Alps, from the Lake Como area to the Dolomites. They are found within the crystalline basement and the Upper Carboniferous, Permian and Lower Triassic sediments (Brigo & Venerandi, 2005) with different modes of occurrence (relationship with the host rocks) and sizes. The modes of occurrence are stockworks of veins and stratiform-stratabound orebodies. The basement and cover sequences are described with large detail, pointing out the paleofault activity and the relations with the mineralizations, based on the new Italian geological maps 1:50.000 scale and literature (Cassinis et al., 1997; Brigo & Venerandi, 2005).

The siderite mineralizations of the Southern Alps were mined since Middle Age until XIX century also due to the valuable Mn enrichment that improved the quality of the steel (Frumento 1952). Several authors studied the mineralizations and published giacimentological maps, major elements data (in particular Fe, Mn and Mg), O^{18} and C^{13} data, mineralogical composition and texture observations (Frizzo, 1970; Frizzo & Omenetto, 1974; Frizzo & Scudeler Baccelle 1983; Cortecci & Frizzo, 1993; Rodeghiero & Zuffardi 1985; Cassinis et al., 1997, Brigo & Venerandi, 2005). An hydrothermal origin for the siderite veins was suggested by Cortecci & Frizzo (1993). The main limits of the previous studies are the limited geographical extension of the observations, the scarcity of geochemical data and the few tectonic data usually limited to specific areas. Because the mineralized rocks are associated to large quantity of sterile host rocks and the territory is mostly mountainous, nowadays there is not an economical interest towards these ores. Therefore until now it has not been drawn a wide-ranging and concluding framework of the Southern Alps siderite mineralizations which we try to give in this work.

This work is based on geochemical-mineralogical data (REE, microchemical analysis) of 21 siderite mineralization sites from 4 mining areas located in the Lombardian and Venetian Alps, and a tectono-stratigraphical review.

REE were analyzed since they characterize the mineralizations and can inform about the fluid forming imprint-origin and the fluid-rock interaction (Bau and Moller, 1992). In addition, major elements, detected at microprobe on siderite crystals, vary due to two processes as metasomatism of the host carbonatic rock and precipitation (Cassinis et al., 1997).

1.2 Geological overview

The Southern Alps derives from the Mesozoic passive margin of the Adria promontory (Africa plate), after the closure of the Tethys Ocean (Ligure-Piedmont branch) during the collision of the African and European plates (Laubscher, 1974). The Southern Alps are bounded to the N by the

Insubric Line and to the S they dip under younger Po Plain deposits. To the W the Southern Alps includes the *Ivrea-Verbano Zone,* a high grade basement with a Permian intrusive mafic complex. The central Southern Alps are composed of amphibolite to greenschist basement, including several metamorphic units (Strona-Ceneri, Scisti dei Laghi, Val Colla, Orobic; Colombo & Tunesi, 1990; Di Paola et al., 2000, Spalla et al., 2002); the eastern Southern Alps include the Agordo, Trento and Recoaro greenschist basements of the Dolomites. At regional scale, the main tectono-metamorphic event is Variscan (Siletto et al., 1993, Di Paola et al., 2000). After the Variscan event, the basement rocks were exhumed developing a retrograde metamorphic assemblage older then 312Ma in the central Southern Alps (Diella et al., 1992, Spalla et al., 2002). A low pressure-high temperature tectono-metamorphic event, recorded between 290 and 180Ma (Mottana et al., 1985) was followed by a rifting stage. The extension of the Southern Alps basement (Serie dei Laghi) evolved into the rifting of the Ligure-Piedmont Ocean (Ferrara & Innocenti, 1974; Lardeaux & Spalla, 1991). Some Late Variscan to Triassic ductile to brittle deformation bands, (Val Colla fault, Porcile Line) are present in this basement. Structural and petrological data suggest that a continuous extensional deformation affected the Southern Alps from Permian to Jurassic (Brodie & Rutter, 1987; Brodie et al., 1989; Bertotti, 1991). In the Val Colla basement, a late Triassic thermal anomaly developed as indicated by occurrence of sillimanite, andalusite and intrusion of pegmatites (Sanders et al., 1996). Subsidence following the rifting lead to the deposition of continental sediments (Conglomerato Basale, Collio and Verrucano Lombardo Fms). At early Triassic time (Induan-Olenekian) marine transgressions lead to the marine sedimentary sequences of the Servino Fm in Lombardy and Werfen Fm in the Venetian Dolomites (Sciunnach et al., 1999). These formations show features typical of shallow-water marine sediments, with carbonatic and terrigenous deposition under high-energy (bar, open lagoon) to tidal-flat and sabkha conditions (Frizzo & Scudeler Baccelle, l983). The orebodies in the Servino Fm are thin when crossing the terrigenous lithotypes and thick when intersecting carbonatic layers.

The massive siderite mineralizations are found in the basement and Permian—Triassic sequence up to the Olenekian, which represents the highest stratigraphic position in the Lombardian and Venetian Alps.

The basement and the Permo—Mesozoic sequence have been largely thrusted and folded by the Alpine tectonics. Permo—Liassic extensive faults have been reactivated as thrusts, like the Orobic and Porcile thrusts in the Lombardian and the Valsugana thrust in the Venetian Alps (Doglioni 1992). Evaporitic sequences of Late Permian and Early Triassic accommodate alpine thrusting from Cretaceous (Schumacher 1997). Late E-W strike-slip, mainly driven by the

Insubric Line, fragmented some of the Alpine thrusts and reactivated some others like the Musso Fault as transcurrent fault.

Beside the difficulties of interpretation, a syntethic tectonic scheme of Lombardy and Venetian Dolomites can be traced as follow for Permian—Trassic time range:

- from E to W there was a variation in thickness of the Early Triassic sequence in the graben-horst systems already subsidizing since middle Permian, with the eastern side deeper. The main basins at this stage were the Collio, Boario and Orobic to the W with the Servino sedimentation; and the Tione, Tregiovo and Belluno basins to the E with Werfen sedimentation (Bernoulli, 2007);
- the main extensional faults at Early Triassic were: Lugano-Val Grande, Porcile, Sellero, Gallinera Lines to the W (El Tahlawi, 1965, Bertotti et al., 1993; Bernoulli, 2007, Gosso et al., 2012, Boriani, 2012); and Valsugana, Antelao Lines to the E (Doglioni, 1992);
- there is no record of Early Triassic (Olenekian) volcanic activity in these regions.

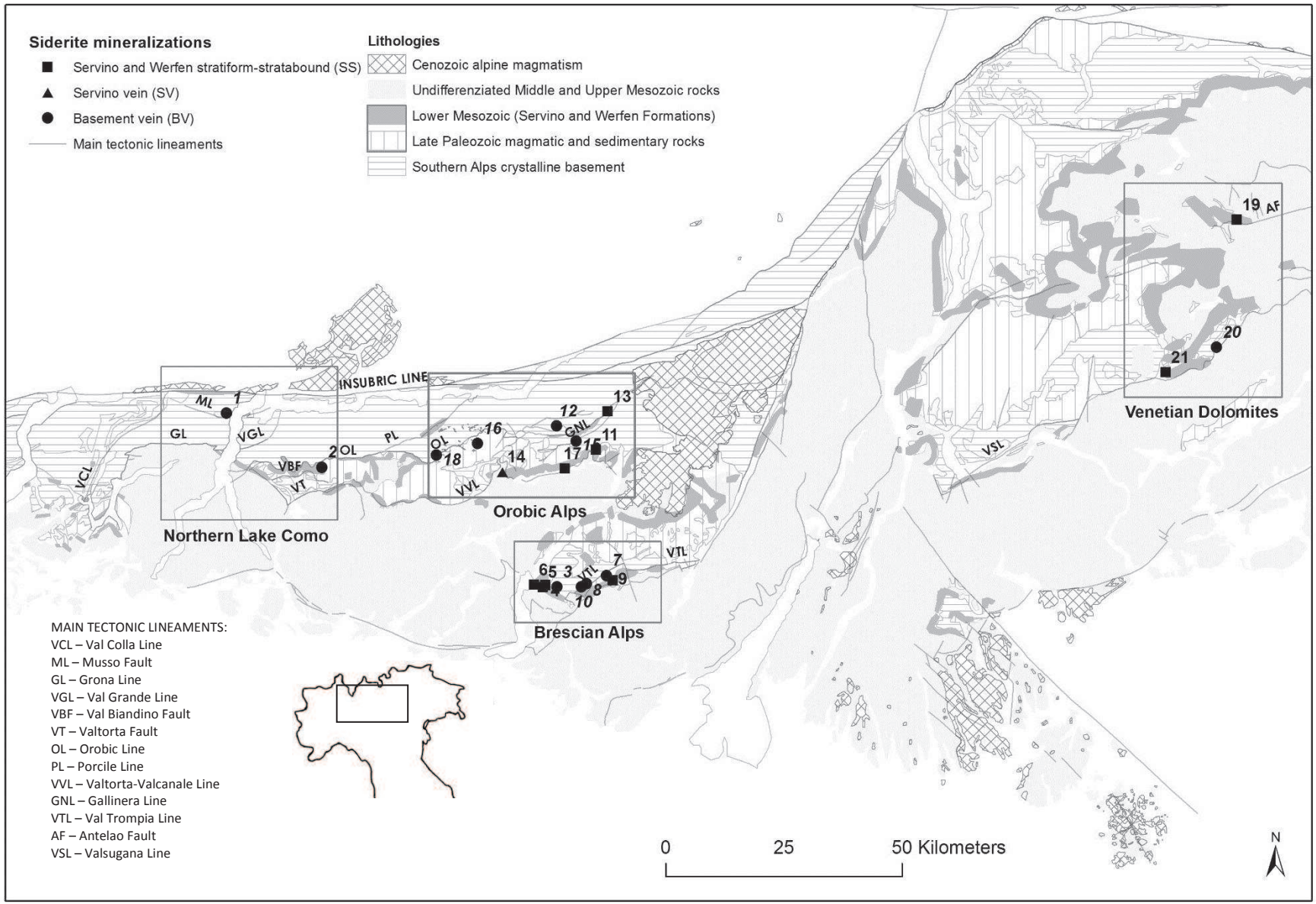

Fig. 1. Structural map of the Southern Alps with siderite mineralization. Squares refer to main interest areas described in the text. Black points indicate the mineralized sites. The mine's numbers refer to georeferenced mining sites. See table 1. Mineralization symbols: BV → basement vein, SS → Servino and Werfen stratiform stratabound, SV →Servino and Werfen veins. (After: Bernoulli, 1976, Servino and Werfen Fms after De Zanche & Farabegoli, 1981, Bigi et al., 1992, Montorfano et al., 2008).

1.3 Siderite mineralizations

The 21 studied siderite mineralizations are grouped geographically in 4 mining areas as indicated in Fig. 1 and Table 1. The mineralizations occur in three typical geometric settings in respect to the host rock. These are described below:

a) *Veins in the basement and pre-Triassic terrains (indicated as BV).* They are generally tabular or sheet-like bodies occupying fracture sets. The size of the veins range from centimeter to meter in thickness. Swells are diffuse and generally they are the mined orebodies. Major veins can also include large portions of host rock completely cemented by the mineralization. Seldom millimeter veinlets be tens of meters long.
b) *Veins in the Servino and Werfen (SV)*. They are similar to those in the basement but emplaced along faults within Servino and Werfen Fms. They may also include large quantities of brecciated host rock. (i.e. Manina Pass mineralization).
c) *Stratiform-stratabound in the Servino and Werfen* (SS). They are bodies that show lateral and vertical transitions, both gentle and sudden, with calcareous host rocks. The paragenesis is composed of massive and coarse-grained siderite and ankerite, and variable quantity of quartz. The mineralizations can generally be identified with originally stratoid or lens shaped oolitic—bioclastic carbonatic bodies largely replaced by siderite and ankerite.

The mineralizations are dominantly composed of siderite±ankerite±sulphides, however they can include considerable quantity of ankerite. Often these mineralizations are cut by late generations of veins, which can contain sulphides, quartz, barite or fluorite. The settings and mineral paragenesis were not well characterized in the past, and often all the minerals were attributed to a unique crystallization event. This may also be due to several stages of fracturation and cementation (Fig.2A, B and E).

The mineralizations are not closely associated to the master faults, but they appear associated to minor structures that belong to the same system.

*Table 1. Studied sites *Type of mineralization: BV → basement vein, SS→ Servino and Werfen stratiform stratabound, SV→Servino and Werfen vein*

#	Mineralized site	Mineralization setting*	Host rock	Mineral association	References	Mining area as per Fig. 1
1	Dongo	BV	Val Colla basement	Siderite ± chalcopyrite, pyrite	Montorfano, 2008	Northern Lake Como area
2	Lago Inferno	BV	Collio and Verrucano Lombardo Fms	Siderite, late hematite, barite, sulphides	This study	
3	Duadello - Pisogne	BV	Maniva basement	Siderite, chalcopyrite, bismutite, native Bi, pyrite, sphlerite, blenda, molibdenite	This study	Brescian Alps
4	Fura - Pisogne	SS	Servino Fm	Siderite, ankerite and sulphides		
5	San Vittore – Pisogne	SS				
6	Fusio - Pisogne	SS		Siderite and late barite	Cortecci & Frizzo 1993	
7	Torgola – Collio	BV	Late Variscan granodiorite	Siderite, late fluorite, quartz , sfalerite,		
8	Pinetto - Bovegno	BV	Maniva basement	Siderite		
9	Carlo Tessara – Bovegno	SS	Servino Fm	Siderite		
10	Regina – Bovegno	BV	Maniva basement	Siderite, quartz and later pyrite, cassiterite, wolframite		
11	Garzetto - Passo Tenerle	SS	Servino Fm	Siderite	This study	
12	Monte Lorio	BV	Gallinera basement	Siderite	Cortecci & Frizzo 1993	Orobic Alps area
13	Lava - Malonno	SS	Servino Fm	Siderite, ankerite, pyrite and chalcopyrite; late quartz, hematite		
14	Manina Pass and Lizzola– Val Seriana	SV	Servino Fm	Siderite; late quartz and ankerite		
15	Torsoleto Lake	BV	Gallinera basement	Siderite; late ankerite and siderite	Cortecci & Frizzo 1993	
16	Scaletta	BV	Collio Fm			
17	Gaffiona and Val Gaffione - Schilpario	SS	Servino Fm	Siderite late barite	This study	
18	Masoni Mt - Publino Lake	BV	Gneiss chiari Gallinera basement	Siderite, ankerite		
19	Colle Santa Lucia	SS	Bellerophon – Werfen Fms	Siderite, ankerite	This study	Dolomites area
20	Valle del Mis	BV	Agordo basement	Siderite		
21	Transacqua and Valle Uneda	SS	Bellerophon– Werfen Fms	Siderite, ankerite		

1.3.1 Northern Lake Como

This area covers approximately 700 km^2 and extend from the Insubric Line to the N, to the Orobic and Grona Lines to the S.

The mineralization of Dongo (1 in Fig. 1) belongs to Val Colla basement. The orebodies are massive veins that cut the regional schistosity (Spalla et al., 2002). In the Dongo area, these are located along NE-SO trending decametric faults. The mineralization is spathic siderite in cm-to-m thick and a few hundreds m long stockwork veins (Fig. 2A). The siderite crystal sizes range from < 1mm to approximately 1 cm. Often the veins are cataclastic and cemented by secondary siderite. Sulphides (mostly chalcopyrite and pyrite) are widespread; it is possible to identify both late veins up to 5-10 cm thick and spread-out impregnations. Fumasoli, 1974 signaled the occurrence of Verrucano Lombardo and Servino Fms outcrops, hundreds of meters long, along the Insubric Line near the Dongo mine.

The Dongo veins (1 in Fig. 1) occur discontinuously in E-W direction over several kilometers to the N of the Musso Fault. The Musso Fault is E-W directed almost vertical and cuts the Val Colla basement. Near Dongo the fault is constituted by two fault planes that bound at N and S the kilometric size Musso marble lens. The fault is normal and belongs to the Lugano-Val Grande fault system referred to the rifting stage (Bertotti et al., 1999).

The mineralization of Lago Inferno (2 in Fig. 1) is composed of veins and stratiform bodies within the Permian Verrucano Lombardo and Upper Collio Fms. The Upper Collio Member of Early Permian age is constituted of continental sandstones, siltstone and volcanics. To the E of Lake Como the Collio is in contact with the Orobic crystalline basement and the Val Biandino quartzdiorite. The Middle to Upper Permian Verrucano Lombardo Fm is composed of massive conglomerates, sandstones and siltstones, below in unconformable contact with the crystalline basement or with the Collio Fm and above in contact with the Servino Fm. In the Northern Lake Como district, the Verrucano Lombardo crops out from E to W, as a thin band located along the Orobic lineament. Near Introbio its thickness becomes approximately 600m and decreases to few meters to the W of Como Lake near Gaeta (Gaetani et al., 1986). In the SE area the Inferno lake mineralization is near the Orobic Line (now Orobic Thrust). This takes in contact the basement to the N with the Collio, Verrucano and Servino Fms to the S. The Orobic Line is an alignment of S-verging, low angle cataclastic and mylonitic bands (Schonborn, 1992).

To the W of the Lake Como area, the main tectonic lineament is the Grona Line. Along it, near the shore of the lake, the Servino Fm includes the Gaeta Mine. This is a mainly limonitic mineralization with late crosscutting pyrite veins that occurs within the fault zone of the Grona Line, associated to a dolomitic lithotype. Near Gaeta, the Servino Fm includes sandstone, siltstone and dolostone. The Servino thickness increases from W to the E of the lake, from ca 35m to ca 200m, due to tectonic activity and associated subsidence (Bernoulli, 1964). The Grona Line is interpreted by Bertotti et al. (1999) as part of the Lugano-Val Grande Fault, a several hundred meters thick, steeply south dipping fault with mylonites to the N and cataclasites to S (El Tahlawi 1965; Bertotti, 1991; Bertotti et al., 1993). To the W of Lake Como, the Lugano-Val Grande Fault is the tectonic contact between the Val Colla basement and the Late Permian to Liassic sediments. E of Lake Como, the deepest part of the Lugano-Val Grande fault is exposed, separating the Monte Muggio basement with its Upper Permian to Lower Triassic sedimentary cover from the Dervio-Olgiasca zone cover-free (El Tahlawi,1965; Diella et al., 1992). The Lugano-Val Grande Line is interpreted as an extensive listric fault of Permian age. From a tectonic point of view, the North Lake Como area had a two-stage evolution (Bally et al., 1981; Bertotti, 1991): a Middle Permian to Liassic extension along N-S trending, E- dipping normal

faults as the Lugano-Val Grande followed lately by the Alpine N-S contraction (Bernoulli, 1964).

1.3.2 Brescian Alps

This area is approximately 150 km^2 and extends from W to E, between Pisogne and the northern Val Trompia area, along the Val Trompia Line (Fig. 1). This ENE-WSW directed, N dipping fault takes in contact the basement (Maniva unit) and the Permo-Mesozoic cover. The Val Trompia Line is interpreted as an alpine regional thrust and the basement is extensively exposed to the N of it. However, the presence of the Collio Fm to the N and its absence to the S demonstrates that the Val Trompia Line was active during pre-alpine time as a distensive fault, and it is interpreted as the southern limit of the Permian Collio basin (Cassinis et al., 2011, Forcella et al., 2012).

The mineralizations of Duadello, Pinetto and Regina (respectively 3-8-10 in figure 1) are located within this basement. They are stockworks of veins constituted of spathic siderite, sometime cataclastic and cemented by secondary siderite and quartz. Late pyrite, chalcopyrite and tetrahedrite are widespread. The Torgola mineralization (7 in figure 1) is emplaced within the Permian granodiorite of Val Torgola-Val Navazze, intruded in the Maniva basement (Frizzo, 1970; Cortecci & Frizzo 1993; De Capitani et al., 2007). Two superimposed mineralizations fillings fractures crosscut the plutons: the older mineralization is a siderite breccia cemented by late fluorite, quartz and Pb-Zn sulphides. The veins vary in thickness from 0,5 to 5,0 m and in length from 20 to more than 1000 m. The Torgola –Val Navazze granodiorite has a cooling age of about 271 Ma (De Capitani et al., 1994), almost coeval with the Collio Fm volcanics (mainly ignimbrites and pyroclastites) dated, from zircons, at 283.1±0.6 Ma for the 'Lower Ignimbrites', and 279.8±1.1 Ma for uppermost ignimbrites (Auccia Volcanics) (Schaltegger & Brack, 2007). The Navazze-Torgola intrusive complex and the surrounding basement are covered by the Upper Permian Verrucano Fm. The mineralizations of Fura, San Vittore, Fusio, Carlo Tassara and Garzetto (respectively n 4,5,6,9 and 11 in Fig. 1) are emplaced within the Servino Fm. These mineralizations are meters size subvertical veins and tens of meters size, stratiform-stratabound bodies. The stratiform-stratabound bodies show both gentle and sudden transition with the host rock. All siderite veins within the basement and the sedimentary cover are emplaced along N-S trending fractures.

1.3.3 Orobic Alps

This area extends from W to E, over approximately 40 km^2, along the eastern Orobic and the western Gallinera Lines.

The mineralizations of Mt Lorio, Torsoleto Lake and Mt Masoni (respectively n. 12, 15 and 18 of Fig. 1) are located within an amphibolite facies basement. Mt Lorio and Torsoleto Lake are located in the basement of the Cavalcafiche Pass (Gosso et al., 2012) while the Mt Masoni mineralization is hosted is the Gneiss Chiari of Corno Stella. The Gneiss Chiari derived from intrusive bodies of Ordovician age (Gosso et al., 2012). The Scaletta mineralization (16 in Fig. 1) is hosted in the Collio Upper Member constituted of conglomerates, siltstones and claystones (Collio Fm chapter from Cassinis in Cita Sironi et al., 2006). The mineralizations are emplaced within N-S directed veins and are composed of spathic siderite locally cataclastic and cemented by late siderite, quartz and ankerite. There are minor and widespread sulphide veins.

The Malonno, Manina Pass-Lizzola and Schilpario mineralizations are emplaced within the Servino Fm (respectively 13, 14 and 17 of figure 1). These mineralizations are stratiform-stratabound and veins. The texture of the mineralization is spathic but can be also cataclastic and cemented by veins of late siderite and ankerite. Pyrite and chalcopyrite are widespread.

The Porcile Line is within the basement but several lenses of Permian to Lower Triassic rocks outcrop along it. The Orobic Line crosscuts the area in the western part and takes in contact the basement to the N with the Permian rocks to the S. It is a low angle south vergent thrust within the basement, the Verrucano Lombardo and Servino Fms (Schonborn, 1992). Several lenses of Servino Fm are located along it. Other Alpine thrusts (Sellero, Gallinera and Valtorta-Valcanale; Laubscher, 1985) show an inherited tectono-sedimentary setting similar to the Orobic Line. The Valtorta-Valcanale shows Middle-Upper Triassic rocks at the hangingwall and Permo-Lower Triassic rocks at the footwall, with a normal fault geometry. Therefore it is interpreted as a blind alpine thrust. The main tectonic lineaments of this area have approximate E-W direction. The oldest sediments outcrop to the N and the age decrease toward S. The faults acted as main thrust during the alpine age (Boriani et al., 2012) to accommodate with slightly different local geometries the compressive stage. It is possible to find lenses of sedimentary rock, mainly Permian to Lower Triassic, suggesting a possible paleo-extensional stage.

1.3.4 Venetian Dolomites

The Valle del Mis mineralizations (20 in Fig. 1) occur within the Agordo greenschist facies basement in the upper part of Imperina Valley bordered to the S by the Valsugana thrust of Alpine age. The basement overthrusts the Jurassic sequence of the Belluno area (Monte del Sole) (Poli & Zanferrari, 1992). The siderite mineralization is mainly present as veins cutting the schistosity in the metapelites, associated to quartz and sulphides.

The Santa Lucia and Transacqua-Val Uneda mineralizations (respectively 19 and 21 in Fig. 1) are emplaced within the folded and faulted sedimentary cover of the Agordo basements,

Bellerophon and Werfen Fms (Baccelle Scudeler et al., 1969; Brondi et al., 1977; Braga et al., 1971). The Transacqua and Val Uneda mineralizations are located in the southern part of the Pale di San Martino dolomitic massif, while the Santa Lucia is in Val Fiorentina, inside the Venetian Dolomites. The host rock is mainly represented by carbonatic with minor pelitic layers. The mineralized veins include dominant spathic siderite associated to barite forming coarse and fibrous aggregates locally deformed and minor late Ag-rich galena. The mineralization occur partly along paleo-faults and partly along the stratigraphic surfaces.

The main tectonic lineaments of this area are the Valsugana and the Antelao thrusts. The Valsugana thrust is a regional fault, approximately 50 km in length mainly NE to SW directed active during late alpine time in ductile conditions presumably reactivating a pre-alpine lineament (Braga et al., 1971, Poli & Zanferrari, 1992). In the later stage it has been reactivated in brittle conditions as high angle fault. The Antelao Fault is a 30 km long lineament, E to W oriented, active as an Alpine thrust in brittle conditions but it also presumably reactivated a pre-alpine lineament (Doglioni, 1987).

Fig. 2. Mineralized samples.

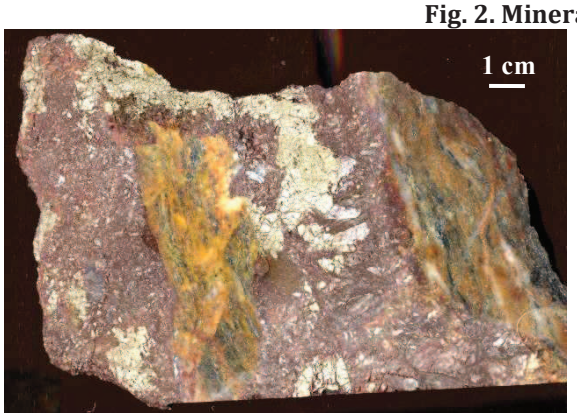

Fig. 2A: Large siderite vein, with abundant sulphides (mainly chalcopyrite) and large clasts of hostrock (micaschists), Dongo, Northern Lake Como

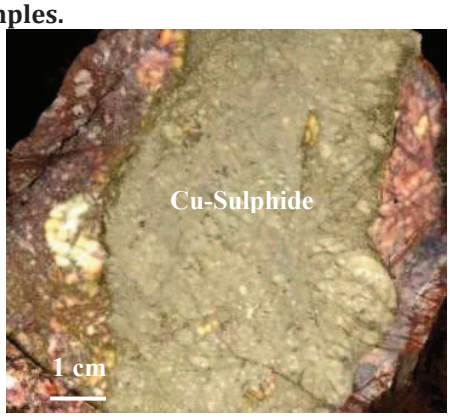

Fig. 2B: Siderite cm-sized vein intruded by a late Cu-sulphide vein. Cataclastic siderite cemented by later siderite, Dongo, Northern Lake Como

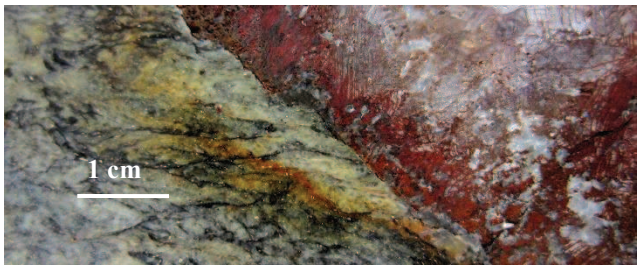

Fig. 2C: Contact between host-micaschist and siderite vein with abundant quartz, Dongo, Northern Lake Como

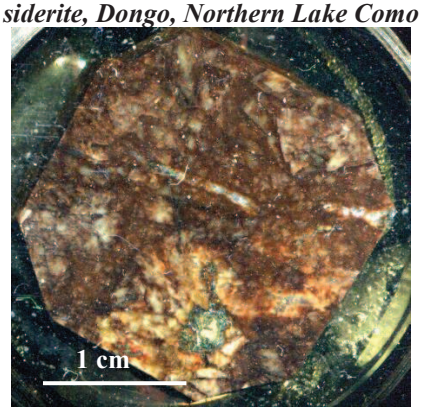

Fig. 2D: Vein mineralization from the basement Regina site (sample REG6), Brescian Alps

Fig. 2E: Stratiform mineralization in Servino Fm from the Carlo Tassara site (sample CT4), Brescian Alps

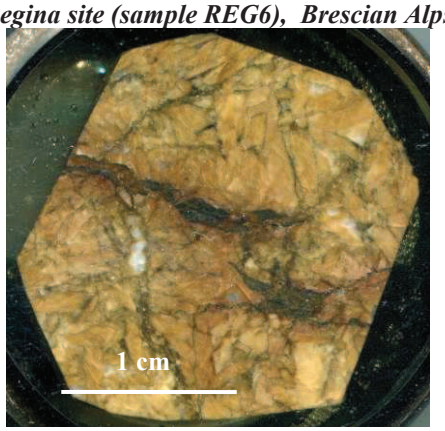

Fig. 2E: Vein mineralization from the Collio Fm, Scaletta site (SC2), Orobic Alps

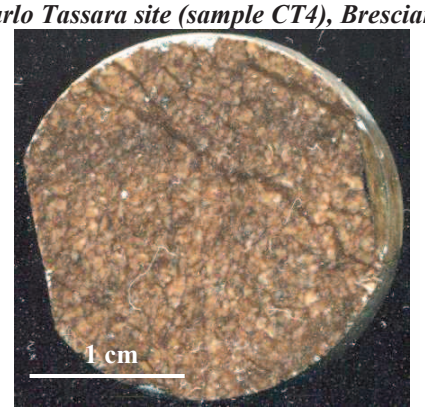

Fig. 2G: Stratiform mineralization from the Servino Fm, Lava site (LAV36) , Orobic Alps

1.4 Material and method

The mineralized samples were studied for determination of major elements of siderite with the EMPA methodology and for determination of REE elements of siderite with the ICP-MS methodology. Details about the methodology are reported below:

Major elements analysis

The chemical microanalysis were performed in the laboratory of CNR, Department of Geosciences, University of Padua, by means of the electron microprobe CAMECA Camebax microbeam 799. It has been used a current of 10 mA and a ΔV of 15 kV; the maximum error is 2% for major and 5% for minor elements. CO_2 is calculated to 100% by difference with the main cations.

Rare Earth Elements (REE)

Approximately 20 mg of pulverized selected sample were accurately weighted inside a pressure-resistant vessel (100 mL), and they were digested with 1 mL of 69% concentrated ultrapure nitric acid and 3 mL of 36% concentrated ultrapure hydrochloric acid. The reactor was closed, starting the digestion procedure in a microwave oven following the program: step 1 – 250 W for 2 min; step 2 – 0 W for 1 min; step 3 – 250 W for 2 min; step 4 – 400 W for 2 min; step 5 – 500 W for 5 min; step 6 – 0W for 1 min; step 7 – 600 W for 5 min; step 8 – oven ventilation for 6 min. After cooling the vessels to room temperature, sample was diluted to 30 mL in a LDPE container with ultrapure water produced by a Millipore MilliQ Gradient A10 system. The solution obtained was analysed directly by ICP-MS (Thermo, XSeriesII) for the determination of REE.

REE were determined by Inductively Coupled Plasma-Mass Spectrometry (Thermo Elemental, mod. X-Series^{II}). Optimisation of the instrumental parameters was performed to achieve best sensitivity, low levels of oxides (CeO^+/Ce^+ <2%). Mass calibration of the quadrupole was also performed. Major instrumental parameters are as follows: plasma power 1.4 kW; gas flows: nebuliser 0.97 L/min, cool 13 L/min and auxiliary 1.0 L/min. Multistandard solutions of REE were prepared by adequate dilution of the ICP multi-element standard solution for MS (Merck, 29 elements 10 mg L^{-1} and 7 elements 100 mg L^{-1}) and REE multi-element standard solution (Carlo Erba Reagenti, 17 elements 10 mg L^{-1}) and acidified with HNO_3 to a final 2% nitric acid concentration.

1.5 Geochemical analysis results

1.5.1 Major elements

The microanalysis by EMPA method were carried out on a set of siderites considered representative of the investigated mineralized bodies. From the oxide weight % indicated in

Table 2 were obtained the molecules % for the construction of the ternary diagram $MnCO_3$-$MgCO_3$-$FeCO_3$ reported in Fig. 3A. The analyzed siderites have a high $FeCO_3$ content (> 70%) independent of their typology (SS, BV, SV). The SS and BV siderites differ in the $MnCO_3$ %, which is generally higher in SS siderites (> 8%); same time, the BV siderites are generally depleted in $MgCO_3$ (from 28% to less than 5%) increasing the $FeCO_3$ %, while SS siderites are characterized by the lowest $MgCO_3$ contents (Mn enrichment). We can therefore say that BV siderites are characterized by Mg → Fe substitution, while SS siderites have a marked Mn enrichment to the detriment of Mg, irrespective of the Fe content.

The SV siderites tend to overlap with BV siderites, at low Mn and high Mg contents.

1.5.2 REE

For interpretation, we used shale normalization according to Bau and Moller 1992, Hein 1993, Fernandez-Nieto et al., 2003, Bolhar et al., 2005. Between the crust compositions we choose to normalize to PAAS (Pourmand et al., 2012) (Fig 4A B,C,D). However the REE patterns of studied siderite are more similar to chondrites (Nakamura, 1974).

PAAS, compared to siderite data, are generally enriched in REE with the LREE strongly higher than the HREE (PAASLa is generally 10 times higher than the sideriteLa). The only exception is PAAS Eu, which is similar in concentration to analyzed samples, resulting in a PAASEu/sideriteEu ≈ 1, with the exception of samples from the Venetian Dolomites (Fig 4 D) which are clearly richer in Eu. Eu concentration is almost 10 times higher than PAASEu. Because of the PAAS normalization, siderite patterns have $HREE_{SN}$ generally higher than $LREE_{SN}$. The plots show that BV are generally richer in $HREE_{SN}$ while SS are poorer in $HREE_{SN}$. In Fig 4E, Er and Ho among the REE better show the correlation with the type of mineralization and confirm what seen in the Fig. 4A, 4B, 4C and 4D. SV samples show REE affinities with both the BV and SS.

Fig. 3 Microprobe data of the siderite samples.

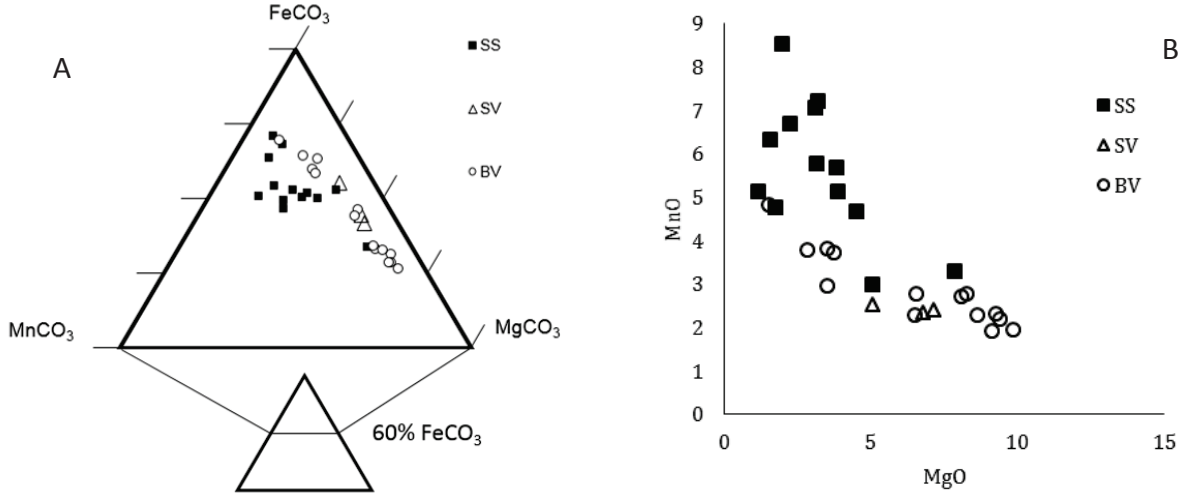

Fig. 4: REE data: Fig. A, B, C and D normalized to PAAS (Pourmand et al., 2012). PAAS normalized REE data (REE$_{SN}$) are shown in Fig. 4A for North Lake Como, 4B for Brescian Alps, 4C for Orobic Alps and 4D for Venetian Dolomites. Fig. E show Er vs Ho of siderite: from stratabound SS (black squares) to veins in the basement BV (circles)

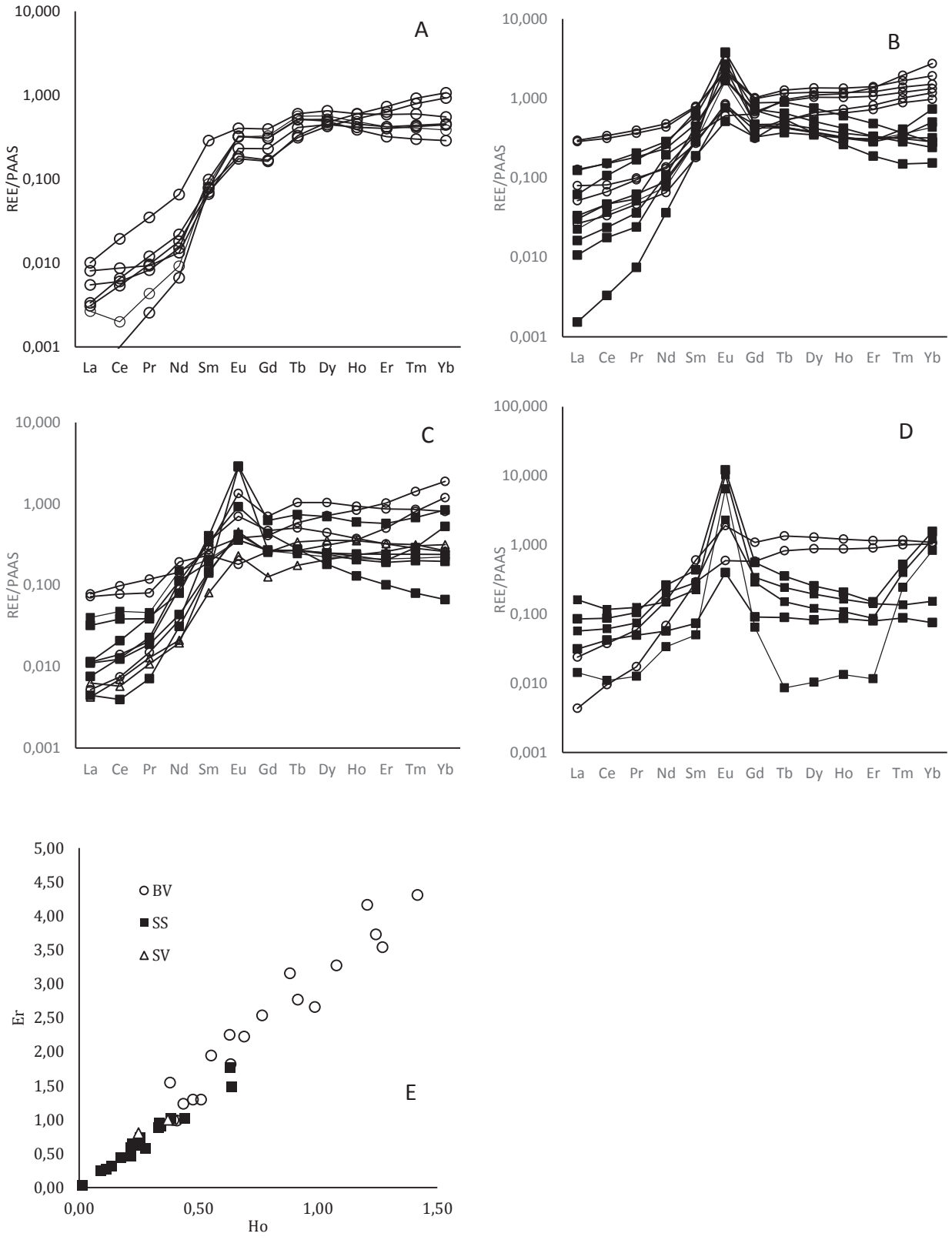

Table 2. Microprobe analysis data – siderite (order per mining district – Location, refer to the map in fig.2)

Mineralized site	*Sample*	*MgO*	*CaO*	*MnO*	*FeO*	*CO_2*	*$MgCO_3$*	*$FeCO_3$*	*$MnCO_3$*	*CaCO3*	*Tot*	*Type of mineralization*
1	N6	9,38	0,40	2,21	47,16	40,84	25,09	70,75	3,36	0,76	99,96	BV
2	INF 1	8,26	0,43	2,78	47,92	40,49	22,25	72,39	4,25	0,84	99,73	BV
2	INF9	8,10	0,51	2,71	48,16	40,45	21,85	72,86	4,16	0,98	99,86	BV
4	FA 2F	1,98	1,15	8,51	49,57	38,73	5,58	78,33	13,63	2,33	99,87	SS
4	FA 2G	3,09	1,05	7,07	49,68	39,04	8,64	77,86	11,23	2,10	99,83	SS
5	SVITT 3	3,82	0,74	5,67	50,50	39,21	10,62	78,81	8,96	1,48	99,88	SS
6	FS 5	1,72	0,79	4,77	54,05	38,59	4,85	85,69	7,65	1,60	99,79	SS
6	FS 6a	3,17	2,83	7,20	47,39	39,24	8,81	73,81	11,36	5,65	99,62	SS
7	T 5	3,72	1,03	3,74	52,15	39,19	10,33	81,30	5,90	2,06	99,59	BV
8	PIN 11	3,51	0,64	2,96	53,70	39,10	9,80	84,03	4,70	1,28	99,81	BV
8	PIN 6	3,52	0,57	3,81	52,86	39,09	9,81	82,65	6,03	1,14	99,63	BV
9	CT 4	1,13	0,58	5,12	54,71	38,40	3,21	87,20	8,26	1,19	99,86	SS
9	CT13	1,53	1,21	6,32	53,61	39,40	4,41	86,39	10,32	2,50	103,62	SS
10	REG 11	1,49	0,78	4,83	54,28	38,52	4,22	86,20	7,77	1,58	99,77	BV
11	GZ 7	4,48	0,59	4,67	50,77	39,39	12,40	78,84	7,35	1,17	99,77	SS
12	LOR 1	6,49	0,50	2,28	50,66	39,97	17,72	77,55	3,54	0,99	99,80	BV
12	LOR 11	9,82	0,61	1,94	46,55	40,97	26,15	69,50	2,93	1,18	99,76	BV
12	LOR12	9,13	0,45	1,91	47,74	40,77	24,45	71,74	2,90	0,87	99,96	BV
13	LAV 15	5,04	0,53	3,01	51,73	39,53	13,89	79,97	4,71	1,04	99,61	SS
13	LAV 36	7,86	0,31	3,29	48,04	40,36	21,24	72,80	5,05	0,60	99,70	SS
14	MAN 1	6,77	0,33	2,34	50,40	40,03	18,43	76,98	3,62	0,65	99,68	SV
14	MAN 13	7,14	0,39	2,42	49,87	40,16	19,40	76,04	3,74	0,77	99,95	SV
14	MAN 9	5,02	0,23	2,53	52,59	39,51	13,87	81,42	3,97	0,46	99,71	SV
15	TOR 4	9,24	0,53	2,33	46,95	40,80	24,68	70,37	3,54	1,03	99,62	BV
16	SC 9	8,62	0,52	2,28	47,92	40,60	23,15	72,23	3,47	1,00	99,85	BV
18	MP1-10	6,53	0,42	2,79	50,23	40,02	17,84	76,92	4,33	0,83	99,92	BV
19	SL123-9	3,85	1,09	5,14	50,62	39,30	10,71	78,94	8,11	2,18	99,94	SS
20	VM26	2,81	1,12	3,79	53,27	38,96	7,88	83,72	6,04	2,26	99,89	BV
21	TR36C	3,13	2,56	5,78	49,26	39,24	8,70	76,90	9,14	5,13	99,87	SS
21	TR36S	2,24	4,08	6,70	47,86	39,11	6,24	74,94	10,63	8,19	100,00	SS

Tab. 3: ICP-MS data used for principal component analysis. Concentration in ppm.

Mineralized site	*Sample*	*La*	*Ce*	*Pr*	*Nd*	*Sm*	*Eu*	*Gd*	*Tb*	*Dy*	*Ho*	*Er*	*Tm*	*Yb*	*Lu*	*Type of mineralization*
1	2F3	0,12	0,18	0,04	0,34	0,60	0,39	1,97	0,50	3,01	0,51	1,30	0,18	1,16	0,15	BV
1	4Fverde	0,02	0,09	0,03	0,25	0,53	0,40	1,86	0,46	2,61	0,41	0,99	0,13	0,86	0,12	BV
1	M3alfa	0,24	0,53	0,08	0,56	0,68	0,39	1,86	0,46	2,74	0,48	1,29	0,20	1,37	0,19	BV
1	M3beta	0,36	0,77	0,09	0,49	0,46	0,28	1,39	0,37	2,38	0,44	1,23	0,19	1,34	0,18	BV
1	N4alfa	0,14	0,47	0,10	0,68	0,48	0,21	0,99	0,29	2,53	0,63	2,25	0,42	3,23	0,48	BV
1	N4beta	0,15	0,58	0,12	0,82	0,55	0,23	1,02	0,28	2,27	0,55	1,94	0,36	2,79	0,42	BV
2	INFX	0,45	1,71	0,35	2,45	1,99	0,49	2,39	0,54	3,48	0,63	1,82	0,27	1,66	0,20	BV
3	D11	2,30	5,91	0,96	5,10	2,44	0,73	3,85	0,86	5,87	1,21	4,16	0,88	8,29	1,25	BV
4	FA2(i)	1,01	3,22	0,52	2,88	1,97	2,02	2,56	0,38	1,96	0,34	0,93	0,16	1,30	0,27	SS
4	FA4	1,35	4,12	0,55	7,25	2,43	2,90	2,86	0,39	1,99	0,33	0,88	0,15	1,51	0,39	SS
4	FA4b	1,49	4,10	0,63	3,36	1,96	4,55	2,70	0,38	2,01	0,34	0,90	0,18	2,20	0,63	SS
5	S.VITT.1	0,48	1,56	0,25	3,61	2,03	0,92	2,83	0,42	2,23	0,39	1,02	0,14	0,86	0,11	SS
6	FS19	0,72	2,09	0,37	4,05	3,07	2,11	4,28	0,49	1,94	0,28	0,58	0,07	0,46	0,08	SS
6	FS20	0,07	0,29	0,08	1,35	1,30	0,62	1,96	0,33	1,84	0,33	0,95	0,14	0,96	0,13	SS
7	T1	3,55	7,18	1,01	4,86	1,87	1,04	2,38	0,48	3,27	0,69	2,22	0,40	2,95	0,44	BV
7	T10	5,69	13,25	1,86	8,75	3,29	2,06	4,09	0,82	5,50	1,08	3,27	0,54	3,98	0,56	BV
8	PIN4	13,24	29,96	4,02	17,80	5,47	2,56	5,97	1,03	6,36	1,24	3,73	0,62	4,55	0,65	BV
8	PIN7	12,74	27,65	3,70	16,27	5,28	2,73	6,18	1,13	7,21	1,42	4,31	0,75	5,77	0,84	BV
9	CT18	2,76	9,45	1,71	9,94	4,75	4,63	5,31	0,80	4,03	0,64	1,48	0,17	0,84	0,10	SS
9	CT7	5,53	13,48	2,07	10,64	4,18	3,26	4,39	0,58	2,74	0,44	1,02	0,13	0,73	0,10	SS
10	REG6	1,18	2,95	0,47	2,43	1,24	0,99	1,90	0,46	3,50	0,77	2,54	0,46	3,53	0,51	BV
11	GZ6	0,49	1,09	0,19	1,63	1,02	0,51	1,59	0,24	1,28	0,22	0,59	0,09	0,59	0,08	SS
12	LOR12	3,49	8,71	1,20	5,38	1,89	0,46	2,46	0,52	3,81	0,88	3,16	0,64	5,71	0,86	BV
13	LAV1	0,34	1,13	0,23	4,16	2,36	1,12	2,62	0,25	0,96	0,14	0,31	0,04	0,20	0,03	SS
13	LAV30	1,43	3,39	0,39	4,24	1,33	0,44	1,64	0,24	1,33	0,26	0,74	0,11	0,72	0,10	SS
13	LAV8	1,79	4,23	0,47	5,63	1,44	0,44	1,60	0,22	1,19	0,22	0,65	0,10	0,67	0,09	SS
14	MAN13	0,28	0,51	0,11	0,73	0,98	0,55	1,53	0,30	1,91	0,37	1,00	0,14	0,80	0,10	SV
14	MAN9	0,19	0,61	0,13	0,79	0,56	0,28	0,77	0,16	1,10	0,25	0,80	0,14	0,95	0,14	SV
15	TOR2	0,23	0,66	0,15	1,39	2,09	1,64	4,25	0,92	5,54	0,99	2,66	0,38	2,43	0,34	BV
16	SC2	0,51	1,25	0,21	3,41	2,38	0,85	2,84	0,45	2,37	0,40	0,99	0,13	0,78	0,10	BV
17	SCH1	0,51	1,84	0,41	2,99	2,79	3,55	3,79	0,66	3,73	0,63	1,76	0,31	2,54	0,48	SS
17	SCH2	0,20	0,35	0,07	1,17	0,98	3,46	1,62	0,24	1,33	0,24	0,62	0,13	1,59	0,49	SS
18	MP1	3,24	6,88	0,82	7,22	1,61	0,22	1,57	0,24	1,66	0,38	1,54	0,36	3,61	0,59	BV
19	SL122	1,39	3,71	0,50	2,11	0,50	0,48	0,55	0,08	0,44	0,09	0,25	0,04	0,23	0,04	SS
19	SL123	0,63	0,96	0,13	1,25	0,34	7,81	0,39	0,01	0,05	0,01	0,04	0,11	2,51	0,94	SS
20	VM21	1,06	3,30	0,60	5,76	4,16	2,32	6,59	1,20	6,86	1,27	3,54	0,53	3,29	0,38	BV
20	VM26	0,19	0,84	0,18	2,54	2,01	0,72	3,51	0,74	4,68	0,92	2,77	0,45	3,11	0,39	BV
21	TR36	3,78	7,67	1,06	9,78	2,99	14,71	3,37	0,31	1,36	0,22	0,46	0,23	4,72	1,71	SS
21	VU13	2,54	5,41	0,76	7,48	1,96	2,80	2,06	0,22	1,03	0,17	0,43	0,06	0,46	0,10	SS
21	VU17	7,15	10,30	1,27	5,58	1,55	12,47	1,75	0,13	0,64	0,11	0,27	0,18	3,65	1,33	SS

1.6 Discussion

The hydrothermal siderite system in the light of the geological and structural relationship is a directional flow from the mineralization in the basement (BV), to be considered as a former crystallization stage, to the metasomatic crystallization in the cover i.e. the Servino-Werfen stratiform-stratabound (SS) orebodies. On the base of this principle, the composition of the siderite in the BV can be seen as originated from a primordial fluid whereas the SS siderite composition is the result of a more evolved fluid that interacted with the carbonate host rock. Therefore, in the studied hydrothermal system, it is possible to observe three types of geometric settings (BV, SV and SS) corresponding to three crystallization environments and two type of processes: precipitation in the BV and SV and metasomatism of host rock in the SS. In Fig. 5A we give a schematic view of the siderite hydrothermal system.

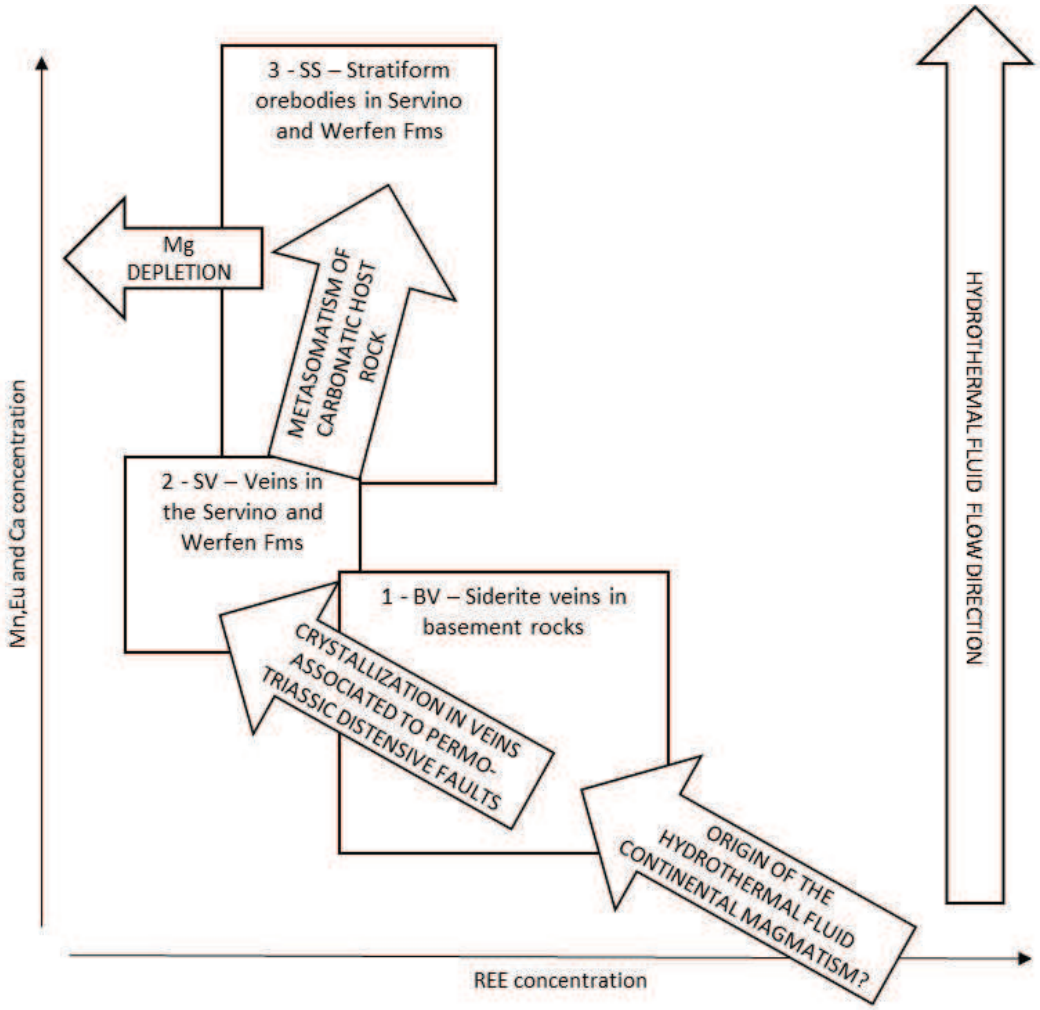

Fig.5A: Model of the Southern Alps siderite mineralization system with the crystallization method and environments, and the most important elements

Major elements of siderite

Between the major elements, Mn better discriminates the genetic environments of siderite. The SS siderite have Mn enrichment and Mg depletion (Fig. 3) compared to BV and SV. Mn enrichment is possible in a high temperature hydrothermal environment (i.e. about 200°C) where Mn is more compatible with siderite. On the contrary, in an epigenetic environment Mn-poor siderites occur as a consequence of the temperatures lower than 140°C like in the Bohemian Massif Central (Zimak et al., 2002). Hydrothermal fluid, when in contact with the dolomitic limestone of the Servino and Werfen Fms, tends to dissolve the calcite instead of the dolomite (Cortecci & Frizzo, 1993). Large quantity of Ca^{2+} enter in the hydrothermal solution and brings to precipitation of Mn-rich siderite while the Mg+Ca elements remain in the fluid.

REE as a result of crystal-chemical or fluid evolution

Two main events concurred to originate the siderite REE patterns: one is the crystal-chemical control, which is driven by the ionic radius compatibility between the REE^{3+} and the main cations, and the second is the fluid/host-rock interaction (Bau & Moller, 1992, Morgan & Wandless, 1980).

Crystal-chemical control

Due to the differences in the ionic radius between Fe^{2+} (0,73Å) and REE^{3+}, (the smallest REE is Lu^{3+}>0,86 Å), the siderite has a greater compatibility with the HREE than LREE (and Eu^{2+})(ionic radii after Shannon, 1976). This can be the main reason of the flat REE pattern of the siderite compared to the average crustal composition. This can be considered the main control in the BV and SV because there is only slight to none interaction with the wall rock and therefore the REE trend in the siderite would depend only from its crystal-chemical compatibility with the REE. In the SS due to the metasomatic process it is possible an exchange of REE with the host carbonates. This find it justification in the Eu positive anomaly found in the SS.

The most important parameter in $Eu^{3+/}Eu^{2+}$ redox potential in aqueous solutions is temperature (Bau and Moller, 1992). Therefore, the oxidation of Eu^{2+} to Eu^{3+} enables Eu to be incorporated into the carbonate lattice because of the smaller size of the Eu^{+3} ion. At low temperature (exceeding 200°C and P=0,5kbar) Eu^{2+} dominates and Eu^{3+} anomaly is unlikely to develop even in presence of sulfate. However, at high-temperature regime Eu anomaly can develop even under just mildly reducing conditions (Bau and Moller, 1992). BV siderites do not display large Eu anomaly then demonstrating a rather low fluid temperature at crystallization, T≈200°C. SS siderites show a slightly Eu positive anomaly that is due to the higher concentration of Ca in the siderite (up to 3% of CaO) that increases the compatibility of Eu with the carbonates. No data have been found suggesting a high temperature regime, to explain the Eu positive anomaly.

Therefore, in the SS the Eu positive anomaly seems to be due to crystal-chemical processes (Lak Shatanov & Stipp, 2004).

Normalization: siderite versus crust and chondrites

To understand the origin of the hydrothermal fluid we compare the REE trend of the siderite with the continental crust and the chondrites compositions in Fig. 5B and C. We consider, as representative of the continental crust: the PAAS (Pourmand et al., 2012), the European Shale (*Haskin and Haskin, 1966),* the Southern Alpine Permian granitoids (De Capitani et al., 2007), the Northern Lake Como basement (Caironi et al., 2002) in Fig. 5B and the Triassic volcanics in Fig. 5C (Cassinis et al., 2008). For the chondrites, we used the data after Nakamura et al. (1974). As last, we added the typical seawater composition (Elderfield & Greaves, 1982). The plot (Fig. 5B and C) shows that: compared to the siderite, the crust is generally richer in REE with higher LREE, the chondrites have similar trend but slightly depleted and the seawater has the typical marked Ce negative anomaly (Bau & Moller, 1992) that we did not found in our samples.

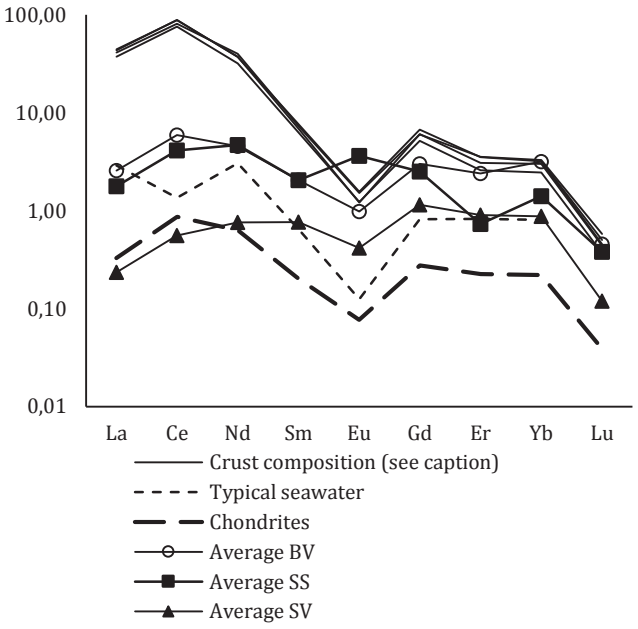

Fig. 5B: Average REE content of siderite mineralization of the Southern Alps compared to: (i) crust composition that includes PAAS (Pourmand et al., 2012), ES (Haskin and Haskin, 1966), Permian granitoids of the Southern Alps (De Capitani et al., 2007), Triassic volcanism of the Brescian Alps (Cassinis et al., 2008) and Northern Lake Como basement (Caironi et al., 2002), (ii) chondrites and (iii) typical seawater

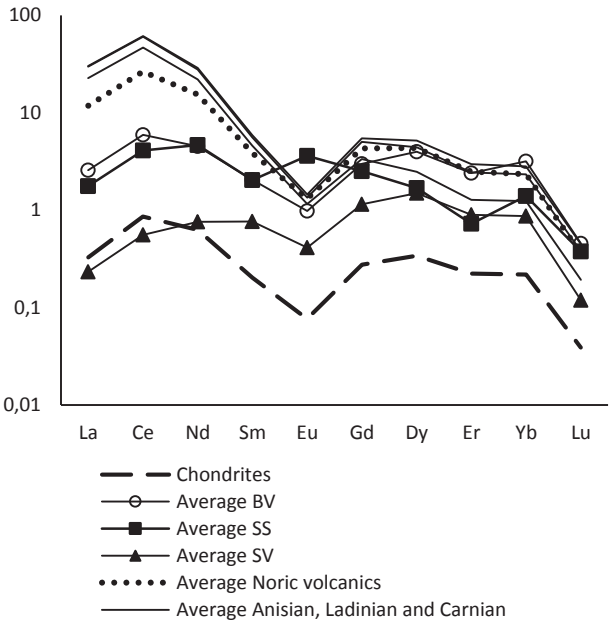

Fig. 5C: Comparison with Triassic volcanics (Cassinis et al., 2008). Anisian, Ladinian and Carnian average includes 19 samples: five trachites, one andesite, three basalts and one dolerite. Norian average includes four dolerites.

Geological evidences

From a tectonic point of view, the revision of the literature and the new observations of the studied sites, show that the siderite mineralizations are associated to tectonic structures of Permo-Triassic age or to rifting of the basement and opening of intra continental basin. This process had different rates and characteristics in the Southern Alpine Domain, but it is clear that the main extensional faults had N to S direction (Doglioni, 1987; Bernoulli, 2007), and the basement reached a thermic peak. The relationships between the mineralized sites and the main tectonic lineaments are not always clearly visible because the old distensive structures were partly or entirely reactivated during the Alpine orogeny in younger E to W trending structures. For example in the Northern Lake Como, the Dongo mineralizations are associated to the Musso Fault: these are emplaced within a few kilometers long band at northern side of this regional fault. The Musso Fault is mostly recognizable thank to the Alpine reactivation in ductile-brittle conditions and dextral transprensive regime. Remnants of Middle Triassic sediments are also found along the Musso Fault, at its southern boundary. Nonetheless ductile fault rocks testify the deeper origin and in a possibly extensional regime similar to that of the Lugano-Val Grande Fault. Another example of similar fault evolution is the Valsugana Fault, that in the area of Valsugana near Pergine, separates the Mesozoic sequences from the basement as described by Sally, 1998 and thereafter interpreted as a Permo—Triassic extensional. Similar conditions are found also for all the other mineralized sites.

From a stratigraphic point of view, the siderite mineralizations are associated to the Lower Triassic age Fms and underline Permian and basement. During Early Triassic time, the sedimentation was typical of shallow-water marine sediments, with carbonatic and terrigenous deposition under high-energy to tidal-flat and sabkha conditions (Frizzo & Scudeler Baccelle, l983). Sediments show progressive deepening due to the activity of Permo-Mesozoic faults that bordered the sedimentary basins (Monte Generoso Basin, Collio Basin and the Dolomite basins). Lower Triassic sediments (Servino in Lombardy and Werfen in the Dolomites) do not include magmatic rocks.

This opens the question about the source of the hydrothermal fluids: the possible origin in relation with the Early Permian magmatism or in relation to incipient events related to the Middle Triassic magmatism. The Permian magmatism is mostly of felsic composition and it is related to thinning of the Variscan crust. This event is widespread in the Adria Domain (e.g. the Lugano volcanics and Biandino plutons to the W in Lombardy and the Bolzano volcanics and Cima d'Asta, Bressanone plutons to the E in the Dolomites) (i.e. Barth et al., 1993; De Capitani et al., 2007). Younger Ladinian Fms include volcanic rocks (Crisci & Ferrara, 1984; Sloman,

1989; Cassinis et al., 2008). The Triassic magmatism is mostly from basic to ultrabasic composition in the Dolomites (Rossi et al., 1974; Pisa et al., 1980) and it is related to a mantle source in an extensional to transpressional context (Castellarin et al., 1980) and it is of basic to andesitic composition in the eastern Lombardy (Cassinis et al., 2008).

1.7 Conclusions

The siderite mineralizations, even if distributed over 300 km from W to E, from a stratigraphic point of view belong to the Early Triassic age. They can be found as veins in the basement and covers (BV and SV) but also as stratiform-stratabound metasomatic orebodies in the carbonatic lithologies (SS). The common paragenesis includes siderite±ankerite±sulphides.

The mineralization is associated to Permo—Triassic and Early Triassic extensional faults, generally reactivated during the Alpine Orogeny in a compressive regime. These faults are associated to the Permo—Mesozoic rifting that brought the continental crust to thinning and to the related thermal peak. Alpine reactivation overprinted partly the old Permo—Triassic and Lower Triassic structures that are only poorly recognizable.

Siderite has homogenous composition with Mg and Mn content correlated to different types of host-rock. Mg concentration decreases in the metasomatic orebodies probably due to the replacement processes in the carbonatic rocks (Werfen and Servino Fms). Mg tend to be more compatible with the dolomite-ankerite phases than the siderite.

REE elements in the siderite samples show a crystal-chemical driven fractionation. In respect to siderite, both older Permian and younger Ladinian volcanics, have different REE patterns, much richer in REE and very similar to the average continental crust composition. Since currently there are no evidences of a possible deeper source of the fluids (mantle or lower crust related?) it is only possible to confirm that the conditions of the crystallization supported a crystal-chemical fractionation related to the REE^{3+} ionic radii compatibility with the siderite lattice. REE trends show slight variation related to the type of host-rock. The variation is a depletion in REE and a slight enrichment in Eu in the metasomatic orebodies. This can be possibly explained with a change in the fluid composition that favored the assimilation of the REE by other phases. The Eu positive peaks seem to be correlated to the enrichment in Ca of the siderite and consequent increase of the siderite crystal-chemical compatibility.

2 Metabasites in the Musso Marble

Marble lenses including metabasites are located in the Northern Lake Como crystalline basement along the Musso Fault (Mottana et al., 1985, Spalla et al., 2002). These marble bodies are poorly studied but in the past, at least since the Roman Age, they were of much interest due to quarrying for extraction of the marble. Quarrying of the Musso marble ended in the second half of the last century (Balzarini et al., 2001) and left large portions well visible and uncovered the included metabasites allowing the current study.

2.1 Geological overview and previous data

The Northern Lake Como region is part of the Southern Alpine crystalline basement and it is generally recognized from the authors as part of the Val Colla unit (El Tahlawi, 1965, Bocchio et al., 1980, Mottana et al., 1985, Bertotti, 1993, Schumacher, 1998, Spalla et al., 2002). It is composed of pre-Alpine poly-metamorphic schists originally part of the Mesozoic passive margin of the Adria promontory (Africa plate). The margin gave origin to the Southern Alps during the collision of the African and European plates (Laubscher 1974). The Southern Alps was then deformed (folded, thrusted and faulted) during the Alpine Orogeny under dominant brittle conditions to assume the present setting. The basement and the Mesozoic sequence of the western Southern Alps suffered weakly, and limited to only few parts, alpine metamorphism under high anchigrade to lower greenschist conditions (Crespi et al 1981). The almost absent alpine metamorphism allow to study the pre-Alpine structures and rocks of the Val Colla unit and to distinguishing several pre-Alpine tectono-metamorphic zones that underwent different metamorphic evolutions (Spalla et al., 2002). Within the Val Colla unit, the authors recognize three tectono-metamorphic zones: the Domaso-Cortafò (DCZ), the Dervio-Olgiasca (DOZ) and the Monte Muggio (MMZ). The three tectono-metamorphic zones show similar lithological associations: gneisses and micaschists in greenschist to amphibolite facies, with interlayered amphibolite, quartzite, calcareous schists and metagranitoids; pegmatites occur exclusively In the DOZ and marble do not occur in the DCZ. Relationship with the Carboniferous, Permian and Mesozoic sequences are peculiar for each zone and synthetized in Table 1 and Fig. 1. The three zones are characterized by different P-T-d-t evolution and separated by relvant tectonic structures (Fig. 1) (El Tahlawi, 1974, Spalla and Gosso, 1999; Spalla et al., 2000):

The tectonic structures have pre-alpine origin and are identified as the Musso Fault Zone to the North (from now on MFZ) and the Lugano Val Grande Fault Zone (from now on LGFZ) to the South (Fig. 1). Both are constituted by large bands of green schist facies mylonitic rocks,

cataclastic bands and fault planes. Along them, important brittle Alpine regional faults over-imposed: the Musso dextral fault and the Grona thrust (Bertotti et al., 1993, Schumacher, 1998).
The LGFZ has been interpreted as a low-angle extensional fault, which was subsequently steepened during Alpine thrust tectonics (Bertotti et al., 1993); such fault controlled the evolution of the Mt. Generoso sedimentary basin (Bernoulli, 2007).
The MFZ is characterized by: I) the presence of a >10 kilometers long band of mylonitic rocks in amphibolite facies (micaschists, gneisses, metabites and marble), II) a strategic importance Fe-carbonate mineralizations (Frumento, 1952, chapter 1 of this study), III) a swarm of hundreds of meters long pegmatites and IV) diffuse pseudotachylites (Chapter 3 of this study). It was formerly active at depth, in Early Permian time, as suggested by many authors (Bertotti,1991; Bertotti et al., 1993; Gosso et al., 1997; Siletto,1991; Siletto et al., 1990, Montorfano et al., 2014 submitted) as a greenschist facies mylonitic zone.

Previous studies on metabasites of the central Southern Alps basement are those of: i) Giobbi Mancini et al., 2003 geochemical characterization of the Strona-Ceneri Border Zone; ii) Bocchio et al., 1998 that studied the amphibolites of the Piona Peninsula and Legnone Mount to the South of the Musso Fault Zone, within the DOZ basement and iii) Di Paola and Spalla, 2000 that presented a microstructural and petrological data of the DCZ, DOZ and MMZ metabasites (in table 1B). For comparison we added geochemical data of basaltic Triassic volcanics after Cassinis et al., 2008.

The Strona Ceneri Border Zone (SCBZ) Metabasites

The Val Colla unit is separated from the Serie dei Laghi unit by the Val Colla mylonites (Schumacher, 1997A). The Serie dei Laghi consists of a meta-arenaceous unit (Strona Ceneri Zone, SCZ), which includes coarse- (Cenerigneisses) and fine-grained (Gneiss Minuti) meta-arenites, and a metapelitic unit (Scisti dei Laghi). These two units are separated by a continuous horizon, mainly consisting of banded amphibolites, with lenses of ultramafites, metagabbros and Grt-bearing amphibolites, called the Strona-Ceneri Border Zone (SCBZ) (Giobbi Mancini et al., 2003).
The SCBZ varies from hundred to several hundreds of meters in thickness and consist of banded amphibolites, associated with banded paragneiss, quartzschists and garnet, staurolite-bearing micaschists, with minor lenses of ultramafites, metagabbros and garnet-bearing amphibolites (retrogressed eclogites). Large lenses of metagranitoids (metapegmatite and meta-aplite dykes) of Ordovician age intruded across the SCBZ. The SCBZ is not continuous but rather fragmentary and boudinated especially in the northern part of the Serie dei Laghi which is strongly deformed.

The different segments of the SCBZ have specific lithological associations. The SCBZ was also intruded by the Early Permian metagranitoids. The schist, the paragneiss, the quartzite and the banded amphibolite of the SCBZ recall the LAG that is the Leptino Amphibolite Group in the French Massive Central (Giobbi Origoni et al., 1997, Giobbi Mancini et al., 2003, Giobbi Mancini et al., 2004) studied by Forestier (1963). The LAG is the remnant of the suture belt between the Gondwana and Laurussia of Devonian age that now divides the two main units of the French Massive Central. The composition of the amphibolites is basaltic. Thermo-barometric data from the amphibolites in the SCBZ gave temperatures in the range of 590–690°C and pressures of 6 to 8 kbar for the main metamorphic event (Giobbi Origoni et al., 1997). SHRIMP analyses on the structureless zircon rims from the amphibolites form a single, well-defined, concordant population with a $^{207}Pb=^{206}Pb$ age of 349±13 Ma (Giobbi Mancini et al., 2004). The SCBZ is of main interest for this study because it is one of the most studied amphibolites in the Southern Alps and as such, they can be used as a reference for studying other metabasites. Boriani and Villa, (1997) obtained an Ar/Ar radiometric age of 340 Ma on hornblende from two samples of garnet-bearing amphibolites.

The metabasites of the Piona Peninsula and Monte Legnone (DOZ)

Metabasites are inter-layered in the pelitic schists of the DOZ. They are cummingtonite bearing and cummingtonite free amphibolites. Composition widely range from N-P-type MORB, through a majority of T-type MORB up to alkali basalts (Bocchio et al., 1998). Zoned garnet analysis shows evidences for two main stages of re-equilibration: a predominant stage older than 303Ma of HT-HP ($T \geq 500°C$ and $P \geq$ 5-8kbar) and a younger stage of HT-LP ($T \approx 550°C$ and $P < 4kbar$) coeval to the DOZ Triassic thermal peak and the Piona pegmatite emplacement.

Metabasite of the Lake Como basement (Di Paola & Spalla, 2000)

Petrological and microstructural studies of the metabasites of the Lake Como confirm the subdivision of the Val Colla unit in the three cited tectono-metamorphic units. DCZ and MMZ recording a Variscan subduction collision and subsequent uplift, while the DOZ underwent a higher thermal regime consequent to the Permo-Triassic crustal thinning thus indicating a deeper position.

Triassic volcanics

Triassic basalts and dolerites occur in the central Southern Alps (Cassinis et al., 2008). These volcanics belong to a peculiar geodynamic regime and their time of emplacement ranges from Anisian to Carnian. NW-wards subduction of Palaeotethys led to epicontinental arc/back-arc conditions between Anisian to Carnian times. In particular, the Ladinian-Carnian interval was characterized by a well defined magmatic cycle, with (base to top): (1) fine-grained rhyolitic

tuffs interbedded with limestones; (2) large volumes of acidic high-K calc-alkaline to shoshonitic subvolcanics, rare intermediate dykes and abundant extrusives; (3) high-K calc-alkaline to shoshonitic subaerial volcaniclastic rocks. A marked geodynamic change probably related to late Carnian is suggested by transitional basaltic dykes (217±3 Ma) and lavas. This rifting event preludes the opening of the Neotethys Ocean.

In Fig. 10A shows the Anisian to Norian geodynamic differences: Anisian intra-plate magmatism rich in Ti, Zr, K while the Carnian is connected to the subduction phase with a calc-alkaline composition. The Norian magmatism conneted to the oceanic rifting is dominated by Mg, Ni, Cr and Ca.

Geochronological data

Several authors attempted to date radiometrically the Lake Como basement and to estimate the P-T deformation evolution path. The data are reported in Table 2.

Marble: Rb-Sr ages on calcite-muscovite of one sample of fine grain marble gave an age of approximately 198Ma (Sanders et al., 1996; Bertotti et al., 1999).

Metabasites: dated by Mottana et al., (1985) gave two different results: approximately 254Ma for biotite and 201Ma for whole rock.

These ages are not related to the emplacement of the rocks, but they only constrain the cooling after the Triassic thermal peak from to around 200Ma (Sanders et al., 1996). Western and Eastern side of Lake Como held different Rb-Sr closure ages for biotite: Sanders et al., 1996 215Ma for the Piona Peninsula basement, while Mottana et al., 1985 250Ma for the metabasites in the Musso marble.

Table 1: Northern Lake Como litho-stratigraphic summary

Litho-stratigraphy	Domaso Cortafò Zone DCZ	Musso Fault Zone MFZ	Dervio Olgiasca Zone DOZ	Lugano-Val Grande Fault LGFZ	Monte Muggio Zone MMZ
Mesozoic	Sequences containing Noric dolostone, Servino Fm and Verrucano Lombardo Fm along the Insubric Line. (Fumasoli, 1974)	Monte Pozzuolo Noric dolostone			Mesozoic sequence
Permian		?	Carboniferous and Permian sequence lenses along the Grona Fault		Red beds of the Verrucano Lombardo Fm. non-conformably overlie the metagranitoids and basement
Carboniferous (Westphalian 313-304 Ma)	?			?	
Metamorphic basement (Spalla et al., 2002)	D1 planar fabric - epidote-amphibolite facies conditions. D2 Re-equilibration in intermediate-pressure amphibolite facies D3 growth of greenschist facies minerals The D1-D2 re-equilibration probably represents the thermal record of eo-Variscan subduction and mid-Variscan continental collision; the available K-Ar age of ca. 385 Ma fits this tectonic outline (di Paola and Spalla, 2000; Spalla et al., 2000);	Fine grained phyllonites with Chl, Ms, Ab and ribbon Qtz, locally with ultramylonitic texture. Shear planes and extensional crenulation cleavages widespread. Micaschists with Chl and Ms e defining the mylonitic foliation S3 associated with s-c structures	D1 intermediate-pressure amphibolite-facies conditions ca. 330 Ma age by comparison with MMZ D2 re-equilibrated. Timing of D2 is constrained at ca. 226 Ma (Rb-Sr and K-Ar mineral ages) by syn-D2 pegmatite emplacement, D3 greenschist-facies retrogression may be related to Liassic normal faulting along the LVGFZ (e.g, Gosso et al., 1997).	Mylonitic micaschists and gneisses with qtz, Ab, Ms and Chl underlining S3, with Grt and Bt porphyroclasts; shear zones with s-c strucutres, extensional crenualation cleavages and dark coloured ultramylonites	D1 intermediate-pressure amphibolite facies dated 330Ma (Mottana et al., 1985) D2 re-equilibrated under greenschist facies (Bertotti et al., 1993; Gosso et al., 1997). syn-D2 greenschist retrogression predates deposition of the Verrucano Lombardo sedimentary in Upper Permian times (260 Ma).
Marble	No marble	Coarse to fine grained marbles with locally containing Amp and Px. S2 is a compositional layering		No marble	?

Table 1B: petrographic synthesis of the Lake Como basement metabasites (Spalla et al., 2002)

	Minerals	Pre-D2	D2	D3	Melanocratic metabasites and hornblendites occur as metre-thick layers in marbles, locally amphibole and clinopyroxene, contain silicate-rich layers composed of zoisite, tremolite, talc and chlorite	Pre-D2	D2	D3		
	Amphibole	X(I)	X(II)	X(Act-Tr)		X(I)	X(II)	X(Act)		
	Plagioclase	X	X	X(Ab-rich)		X	X	X(Ab-rich)		
	Clinopyrozene		X							
	Garnet	X				(xI)	X(II)			
	Biotite	(x)	X (I)	X(II)			X			
Metabasites	**Qaurtz**	X	X	X		X	X	X		
	Chlorite			X				X		
	Epidote			X				X		
	White mica			X				X		
	Pumpellyte			X						
	Calcite			X				X		
	Rutile	X	(X)			X	(x)			
	Ilmenite	(x)	X			(x)	X			
	Titanite		(x)	X				X		
	Undifferentiated opaque minerals	X	X	X		X	X	X		

Table 2 Selected geochronological data of metabasites and marble of the Northern Lake Como basement

Author	Location and sample	Rock type and analyzed mineral	Type of analysis	Minerals	Age (Ma)
Bertotti et al., 1999	Piona (ST4)	Marble	Rb-Sr	Ca-Ms	198±2
Sanders et al., 1996	Piona Peninsula very close to the Laghetto pegmatite (ST4)	Fine grain marble	Rb-Sr	Ca-white mica	198±4
Mottana et al., 1985	Musso quarry (DAT-12)	Amphibolite within the marble (Amphibolite with nematoblastic amphibole and with scales of biotite parallel to the lineation. Modal composition: amphibole (68,6), biotite (8,3), quartz (12,9), sphene (4,8), plagioclase (2,9), opaques (1,2), apatite (1,0), calcite (0,3)	K/Ar	Bi	254±8
			K/Ar	WR	201±5

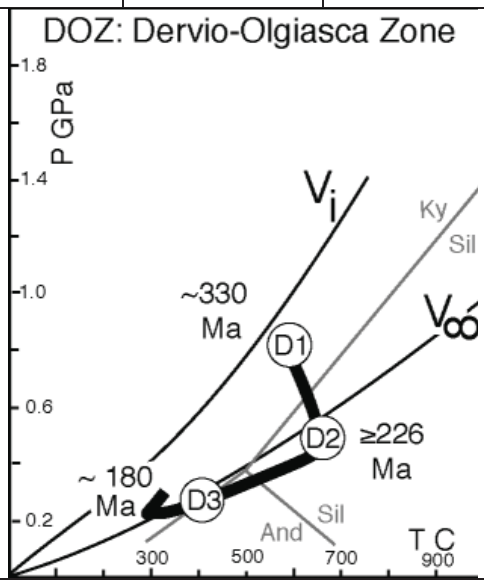

DOZ P-T-t path after Spalla et al., 2002

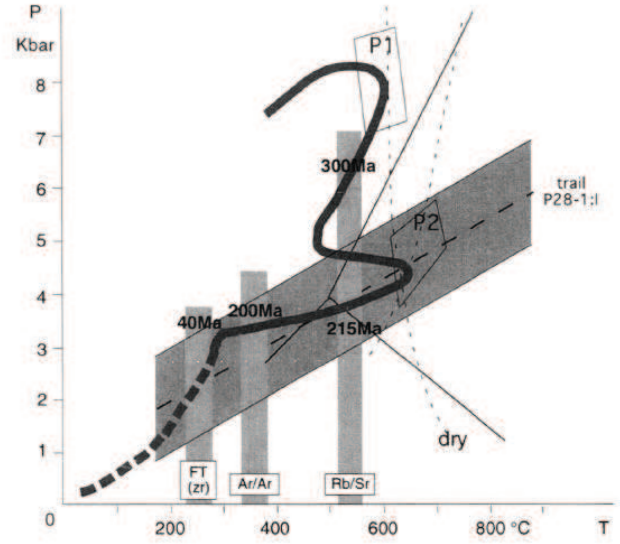

Piona Peninsula basement P-T-t path after Sanders et al., 1996

Fig. 1 Structural sketch northern Lake Como area and its tectono-metamorphic units (Tahlawi, 1965, Fumasoli, 1974, Bertotti 1991, Spalla et al., 2002, Schumacher, 1997A and B)

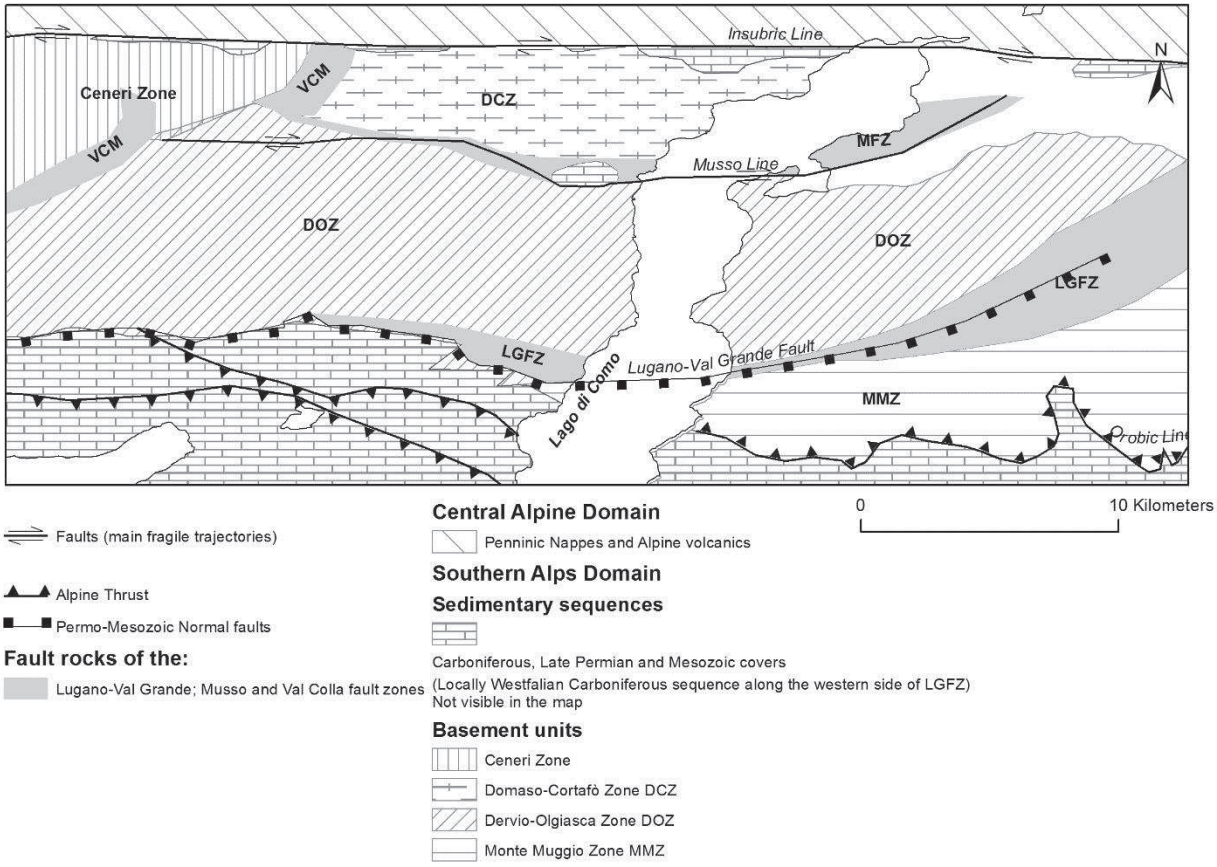

Lithostratigraphic units	Tectono-metamorphic units	Structural boundary
Serie dei Laghi basement	Strona-Ceneri Zone	
		SCBZ - Strona-Ceneri Border Zone
	Scisti dei Laghi	
		VCM – Val Colla Mylonites
Val Colla basement	DCZ – Domaso-Cortafò Zone	
		MFZ – Musso Fault Zone
	DOZ – Dervio-Olgiasca Zone	
		LGFZ – Lugano-Val Grande Fault Zone
	MMZ – Monte Muggio Zone	

2.2 Methods

This research is based on an extensive field investigation to determine lithotypes, the ductile and brittle deformation, the geochemical and petrographic characteristics of the studied rock with ESEM, Microprobe and petrographic microscopy. XRF Geochemical analysis were done to determine major and trace elements of metabasites transposed in the Musso marble and from the Lugano-Val Grande Zone.

2.2.1 Geochemical data XRF (X-Ray Fluorescence) technique

The analysis for the chemical characterization of the samples were carried out at the Department of Mineralogy and Petrology of the University of Padua thanks to the collaboration of the professor Daria Pasqual. The preparation of the samples was done from the following methodology*:*

A - Samples are powdered.

B - Part of the sample is used to determine the Loss on Ignition (L.O.I.) which is the difference in mass due to the loss of H2O and CO2 after heating the powder for 20 minutes at 860° C and for 2 hours at 980° C.

C - Samples are fused adding low temperature melting substance to obtain discs of glass called pearls. Pearls are prepared mixing 0.65 g of powdered sample with 6.5 g of Li2B4O7 and heating the mixture in a melting pot, made of Pt 95%, Au 3%, Rh 2% to facilitate complete recovery of sample, using a Claisse Fluxy machine that can reach a maximum temperature of 1150°C. The heating process last for 10 minutes and gives a pearl ready to be analyzed with XRF.

The fusion allows to eliminate the mineralogical effects. Samples and standards prepared with this techniques have a elevated homogeneity.

D – The determination of FeO is done with the Pratt Washington Method and the result is subtracted from the determination of total Fe done with the XRF to determine Fe_2O. The Pratt Washington Method is a titolation. A known quantity of powder of sample is added to 15 ml of a solution made of one part of deionized water, one part of HF (from a 40% solution) and one part of H_2SO_4 (from a 95% solution). The mixture is then put in a melting pot of Pt and it is heated at 180° C for 8 minutes on a graphite heater. The melting pot is then transferred in a beker of polyethylene with 300 ml of deionized water, 5 ml of H_2SO_4 , and 0.6 g of H_3BO_3 and the solution is stirred with a stick. The solution is then titolated with a solution of KMnO4 to N/10 to give the following reaction:

$2KMnO_4 + 10FeSO_4 + 8\ H_2SO_4 \leftrightarrow K_2SO_4 + 2MnSO_4 + 8H_2O + 5Fe_2(SO_4)3.$

The FeO concentration is determine by this relationship:
%FeO=(ml $KMnO_4$ N/10 x 0.007185 x 100)/mass of sample 0.007185 = g of FeO corresponding to 1 ml of KMnO4 N/10.

The instrumental precision, calculated from repeated analyses on the same sample, is of 0.6% for major elements and of 3% for trace elements. The accuracy of the analytical data is 0.5% for Si, of 3% for the other major elements and of 5% for trace elements.
The limits of detention for the major elements Al, Mg, Na are 0.01%, for Si 0.2%, for Ti, Fe, Mn, Ca, K, P 0.005%. The limits of detention for trace elements are in ppm: Sc=5, V=5, Cr=6, Co=3, Ni=3, Cu=3, Zn=3, Ga=5, Rb=3, Sr=3, Y=3, Zr=3, Nb=3, Ba=10, La=10, Ce=10, Nd=10, Pb=5, Th=3, U=3.
The spectrometer used for these analysis is the WDS Philips PW2400. The software used is the SuperQ for qualitative and quantitative analysis.
Statistic analysis
The major and minor elements data were analyzed using Principal Component Analysis technique (Kovach, 2007). This advanced technique allow to simplify the visualization of the data and to immediately spot the determining variables within the set of data.

2.3 New data (results)

Marble lenses crop out aligned to the Musso Fault with a E to W direction (Fig. 2). The western most lens, few meters in size, is found in the Albano Valley approximately 1 km E from the San Bernardo Church. Proceeding to the E, marble lenses of hundreds of meters are found just W of the San Bernardo Church. The main marble lens (MML) is found between the San Bernardo Church and the western shore of Lake Como. This lens develops for approximately 3 km, tens of meters thick to the West, but approximately 300 m near the lake shore. To the East of the lake, in the Piona Peninsula several marble lenses crop out aligned E to W, with sizes varying from tens to hundreds of meters in length. The eastern most lenses of marble are located in the Forte di Fuentes hill. These are parallel to the Musso Fault.
The marble lenses have sharp contact with the surrounding metapelites (DOZ, fig. 9). Smaller lenses are parallel to the main schistosity of the host rocks. Only the MML shows different kind of contacts with the host rock: to the North is bounded by a subvertical dextral fault concordantly identified by previous authors as the main Musso Fault, to the South it is bounded by a North dipping brittle sinistral fault. This fault is underlined by a 1 to 2 meters thick cataclastic band. To the South the DOZ basement schists dips to the South and to the North the marble mylonitic schistosity dips toward North.

Fig. 2: Structural map of the Musso Fault Zone; (MML – Main Musso marble lens). Black line represent the main trajectory of the fragile Musso fault. The dashed line represent the possible limit of the Musso fault zone, including the phyllonites, mylonites and cataclastic rocks

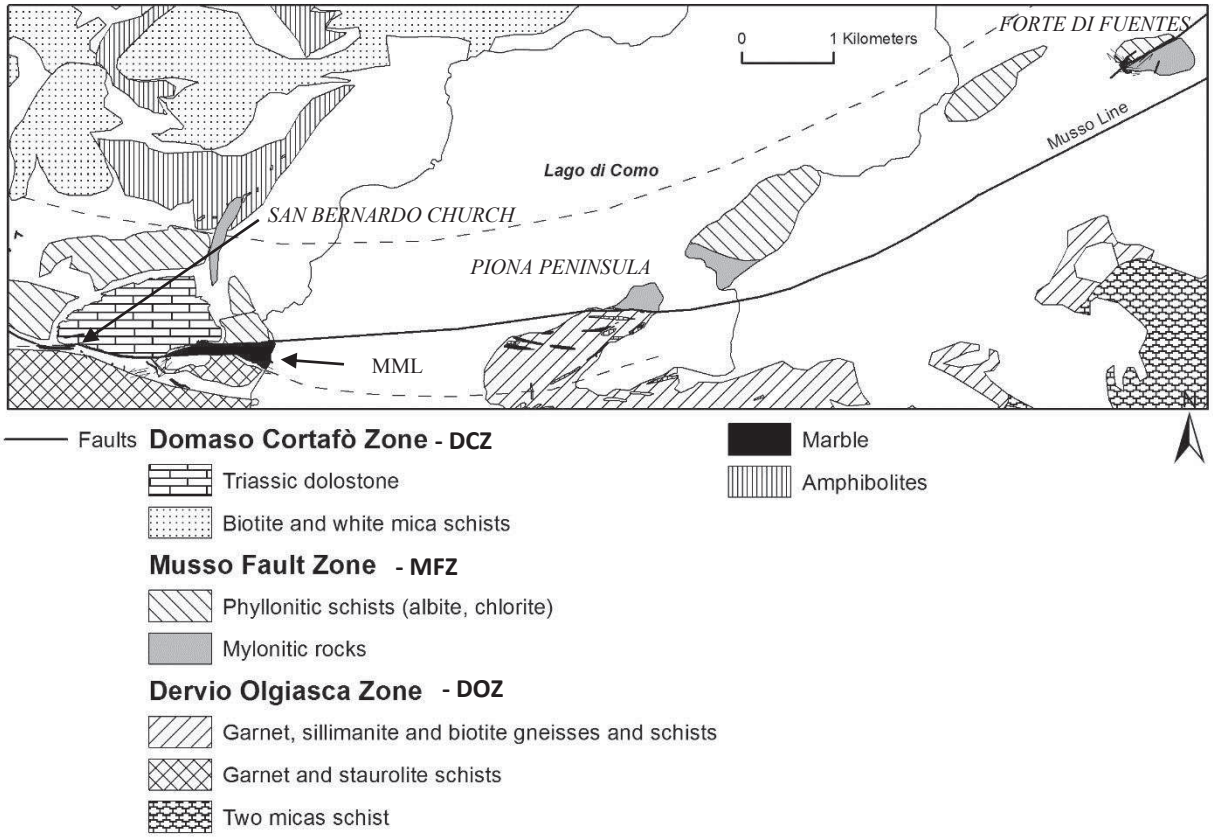

2.3.1 MML lithotypes description

The following description derives from observations of the MML but it applies also to the minor marble lenses. The main differences between the MML and the smallest lenses is due to absence of metabasites in the smaller portions and most limited outcropping volumes.

Within the MML, five different lithotypes are found:

1) Coarse-grained marble
2) Fine-grained marble (mylonitic and cataclastic)
3) Dolomitic marble
4) Fine-grained banded marble
5) Metabasites

1) **Coarse-grained marble - CGM**: It is identifiable in the field thanks to its white to creamy color and large grain size that is averagely >1 cm. It is mostly composed of calcite with lithological layering of quartz, white mica, and sulphides. Actinolite is

widespread as accessory mineral. The following minerals are found in minor quantities: margarite, pyrophillite, chlorite, K-feldspar, goethite, apatite and zircons. Its macroscopic texture is massive. Occasionally the calcite crystals are outlined by rims of very fine-grain calcite neoblasts. Absence of wollastonite and the compositional relation between K-feldspar and albite suggest a low metamorphic temperature probably <350C°.

2) **Fine-grained (mylonitic) marble - FGM**: it composes most of the MML but it also be found to the W in the San Bernardo area and to the E, in the Piona Peninsula and the Forte di Fuentes hill. Its contacts with the CGM is transitional with gradually decreasing grain size bands. Contact bands are composed of large cataclastic grains of calcite of approximately 5 to 10mm bounded by small calcite grains with size <1mm. Dynamic rotation of the larger clasts is visible. FGM is constituted almost totally by small grains size calcite newly formed <2mm. Often relict clast of quartz or calcite can be found. Mineral composition includes calcite and minor quartz, hyalophane, albite, chlorite, muscovite, Ba-muscovite and tremolite.

3) **Dolomitic marble - DM**: large portions of dolomitic marble crop out within the MML and in the San Bernardo church area. In the San Bernardo area the dolomitic marble is identifiable as a compositional layering, underlying an Sx and concordant with the DOZ main schistosity. DM along Lake Como shore is massive and easily recognizable by creamy color, medium size crystals grains (2 to 5mm) and diffuse tremolite veins.

4) **Fine-grained banded marble - FGBM:** The FGBM represent a very subordinate facies in volume. It is found along the major fault planes, near Dongo, close to the entrance of the Merlo Garden, and in the Piona Peninsula. Outcrops are of meter size. The FGBM is composed of alternated white and gray, thin layers of sericite-bearing marble, folded together. (Fig. 3F)

5) **Metabasites:** Boudined lenses of basic rocks, dyke-like bodies, crop out within the MML in the Dongo and Musso quarries. The metabasites have a variety of shapes: globular and tabular, suggesting an original intrusive-sheet emplacement mode. In the Dongo marble quarry, several metabasites are 2-5 m in length and about 1 m in thickness, are parallel to

each other and form E-W direction set recording a "swarm" setting in spite of the deformation. Some bodies are isolated tens of meters away from the other bodies. W of Sant'Eufemia Church, a bigger, globular metabasite body (5-10 m in diameter) is connected to few smaller bodies (1-5 m) (Fig. 6A and B). Metabasites shows variable content of biotite (Fig. 5E and 5F). At outcrop they appear dark green to dark grey with surface alteration of ferruginous color. They show schistosity parallel to that of the surrounding marbles pointed out by green amphiboles (hornblende), chlorite, Na-plagioclase and abundant Fe-epidote indicating transposition.

2.3.2 Metabasite-marble contact

The amphibolite-marble contact was investigates starting from the field observations to distinguish the characteristics. The better-preserved contacts appeared to be those between the hornblende rich metabasites and the coarse grain marble, mostly outcropping in the Musso and Dongo quarries.

Metabasites structures

Metabasites within the MML shows peculiar structures absent in the metabasites of the surrounding basement (DCZ and DOZ):

a) LOCATION: metabasites form a set of discontinues tabular bodies, meter size elongated bodies parallel to each other and slightly boudined. They are visible mainly in the Musso quarry. Larger metabasite lenses with tabular shape appear between the Dongo quarry and to the East of it. Fig. 3C
b) CONTACT: The contact with the marble is sharp and flat can be reactivated in brittle conditions. Fig. 4A, 4B
c) LOBES: metabasites form lobes within the marble that can be interpreted as due to folding or to preserved primary structures. Fig. 6A
d) GRANULATION: Clouds of large amphibole crystals are occasionally are widespread in the marble close to the amphibolite-marble contact.
e) VESICULATION: Locally some field structures record primary vesiculation but the microscopic study has confirmed an evident transposition in the MML Fig 6B.
f) OUTER BAND OF METABASITES: it is constituted mainly of amphiboles, sulphides and calcite. The size of this band vary from less than centimeter to few decimeters. Fig. 7. The band is composed of a microscopic calcite (matrix) with occasionally larger calcite crystals, with plagioclase including hornblende and biotite altered to chlorite. Titanite is widespread while ilmenite is aligned to the contact. Plagioclase shows diffuse

sericitic boundary and the hornblende results rich in Ca. Table 3 synthetize the petrographic composition.

Table 3 Amphibolite-marble contact petrographic summary

	Marble	Marble-metabasites contact band	Metabasites
Calcite	Large grains and Diffuse mylonitic texture	Large grains X	Fracture fillings X
Actinolite	X	X	?
Horneblende	X Large dispersed crystals	X	X
Rutile			X
Ilmenite		X	X
Titanite		X	X
Albite			X
K-feldspar		X	X Pertitic structures
Zircon	X	X	X
Dolomite	X	X	
Clinopyroxene			X
Biotite		X Large crystals with no orientation	X Large lamellae
Phlogopite			X
Quartz	X clasts	X	X
Chlorite	X growth around muscovite	X	X
Muscovite	X		
Hyalophane	X		
Epidote		X	X
Allanite			X
Apatite	X	X	X

2.3.3 Metabasite petrographic analysis

The mineral composition of the metabasite with in the MML shows the presence of amphibole (hornblende and actinolite), K-feldspar, titanite, albite, ilmenite, Fe-chlorite, epidote, Al-Titanite and zircon. The microprobe chemical analysis are shown in detail in the appendix 2. The accessory ilmenite and titanite are widespread. Sulphides are visible and common, with small grain and aggregated, 1-20 mm in size. Sulphides are more common along the contact between metabasite and marble. The metabasite grain size is mostly fine, < 2 mm, but bands of crystals from 0.5 to 1 cm in size are visible in the core of bigger metabasite bodies.

MML metabasite is composed of plagioclase with diffuse pertitic structures with newly formed K-feldspar, have phlogopite and allanite and titanite-ilmenite. MML amphibolite does not display white mica, pumpellyite, garnet nor relicts of it and actinolite is found only within the marble contact band.

2.3.4 Geochemistry

Three amphibolite samples were analyzed: two samples from the Musso marble metabasites (MUSSO4 AND MUSSO5) and one sample from the LGFZ (ANF430). The analyzed metabasites have basaltic composition (Fig. 8C) with the two Musso samples having very similar composition even if sampled from two different lenses. ANF430 results slightly depleted in Fe, but enriched in Al and Mg (Fig. 8A). Minor elements within Musso samples are enriched in Cr, Ni, Cu and Zn and ANF430 (Val Cavargna - LGFZ) richer in Co. ANF430 is depleted in Zr, Nb, La and Ce (Fig. 8B).

Table 5: geochemical data of Musso marble and Grona Line mylonitic Zone metabasites

Provenience	Description	Description	Sample
Musso Fault Zone MFZ	Metabasits from MML Dongo quarry	Metabasites from Musso marble lens (MML)	MUSSO4
			MUSSO5
Lugano-Val Grande Fault Zone LGFZ	Amp of lower Val Cavargna (1km S of SAN BARTOLOMEO) COORDINATES: 511275.83 m E 5102203.09 mN	Fine grain amphibolite from the LGFZ	ANF430

2.3.5 New structural data

The Musso Fault Zone shows a very complex structural layout due to the over imposition of several tectonic events; in this study it is analyzed only the area between the Dongo and Musso villages:

I. S2 is the oldest well recognizable structure in the basement contiguous to the MFZ and within the fault zone. In the marble (MML) it corresponds to a mica and sulphide compositional schistosity well visible in the CGM, generally trending NW-SE and dipping both to NE and SW (Fig. 9A). A schistosity with the same orientation is visible in the other lithologies in the MML (dolomitic marble, metabasites). To the South of the MML in the DOZ, S2 dips to the S. To the N of the MML, in the DCZ, S2 is E-W directed and dips both to the S and N.

II. Mylonitic foliation (Fig 9B)
    a. Within the MML it is mainly visible thank to an associated fracture cleavage; the mylonitic marble generally dip toward E with an almost subvertical 70-80° angle
    b. Very limited portions of FGBM outcrops along the main fault planes. Axial planes dip at 270°/40° (at the entrance of the Merlo Garden) and of 260°/10° – 190°/80° (at the northern entrance of the Musso tunnel).

Fig. 3 Structures in the marble

A: San Bernardo area, coarse grain marble with dolomitic boudins layers (Sx). These structures are parallel to the micaschists S2, dipping South of 50°.

B: Details of A: the silicic layers boudins.

C: Musso quarry: Amphibolite parallel dykes-like structures partly boudined, the Musso Quarry

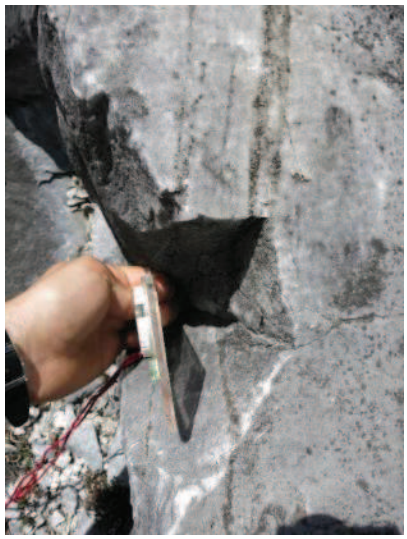

D: Musso quarry: lithological layering composed of white mica and sulphides layers in the coarse grain marble, Musso Quarry

E: Musso quarry: compositional layering (mica and sulfides) showing shear structures in the mylonitic marble

F: Musso fault near Dongo: tightly folded mylonitic marble. Mica-sulphides planes are well visible and preserved. Old state road between Musso and Dongo

Fig. 4 Metabasites contact with the marble and micaschists

A: Musso quarry: Compositional layering (silicic and sulphides) in the marble, follow the amphibolite-marble contact. The metabasites do not cut these planes

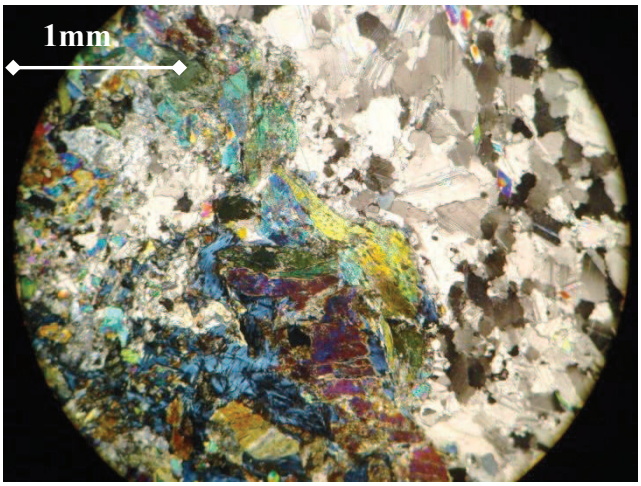

B: Dongo quarry: contact between amphibolite and coarse grain marble; calcitic hornblende along the contact; biotite alteration to chlorite; large calcite crystals along the contact; (50X, NX)

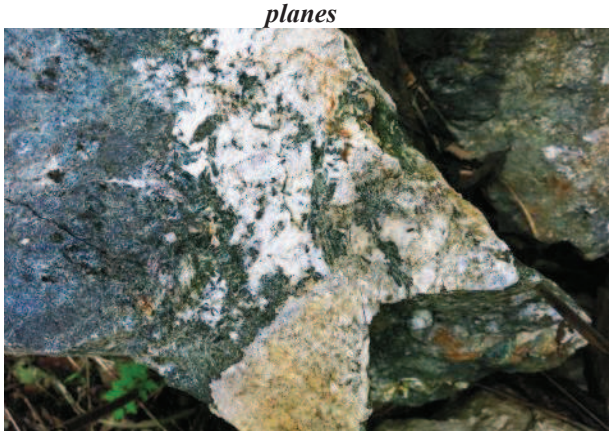

C: Musso quarry: large dolomite-ankerite crystals? at the contact between the amphibolite and dolomitic marble. Large crystals shows isostatic grow. On the right, within the amphibolite large dark crystals of biotite are visible

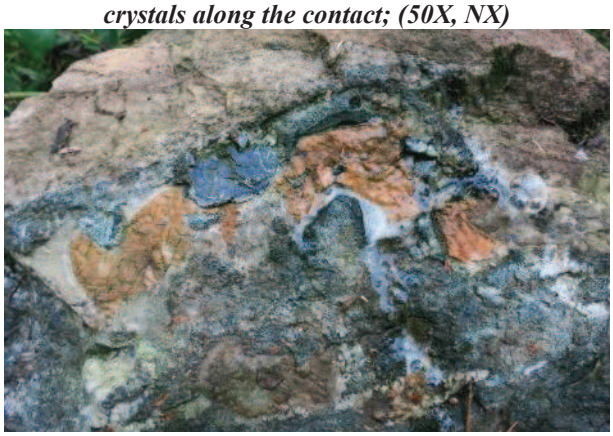

D: Musso quarry: contact between amphibolite and the dolomitic marble display formation of large crystals of dolomite-ankerite? And amphibole?

Fig. 5: Types of metabasite of the Musso fault area

A: Amphibolite from the DOZ (South of the Musso Line): (sample AFM1); (50X , NX)

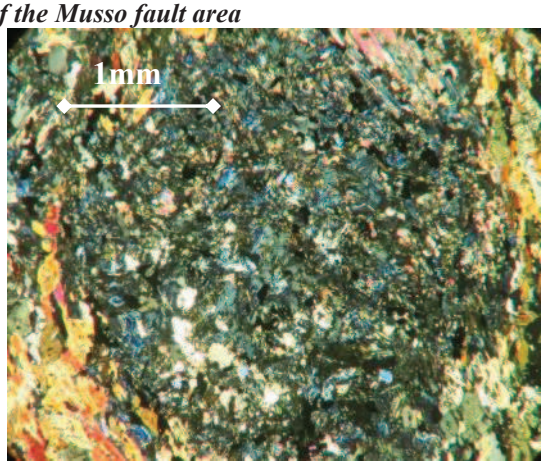

B: Amphibolite from the DOZ (South of the Musso Line): relict of garnet substituted by epidote and ilmenite (sample AFM1); (50X , NX)

C: Amphibolite of the Dongo quarry (Musso fault zone): large crystals are preserved in the central part of the amphibole and do not show alignment;

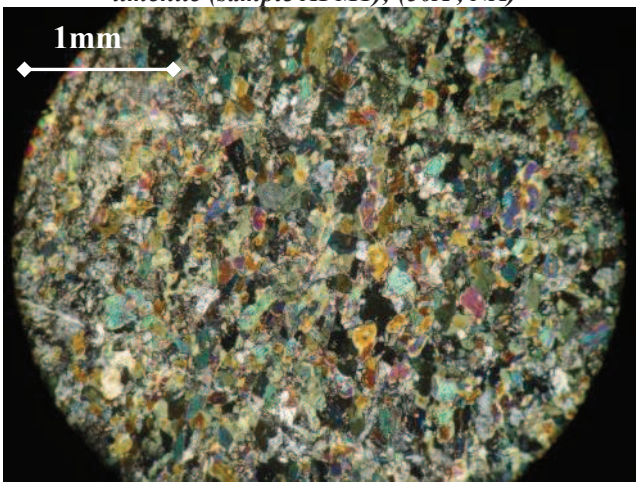

D: Dongo quarry (Musso fault zone); Hornblende amphibolte of the Dongo quarry; (50X , NX, sample MUSSO19)

E: Dongo quarry (Musso fault zone): Biotite rich amphibolite; large biotite crystals do not show alignment probably due to a isostatic growth

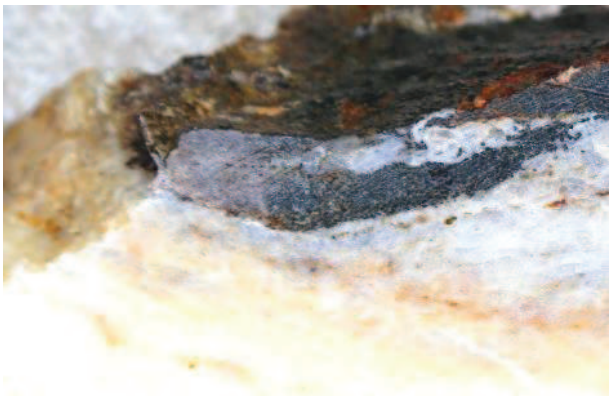

F: Marble-amphibolite contact from the Dongo quarry (Musso fault zone): partial biotitic replacement in the amphibolite underlying fold in the amphibolite; coarse grain marble partially mylonitic;

Fig. 6: Musso amphibolite-marble structures and contact

A: 100m East of the Musso marble quarry: amphibolite lobes. Yellow lines indicate the contact. Red lines highlight the mica and sulphides compositional layering of the marble. Pink area is a quartz lens. Green lines highlight fracturation within the metabasites and marble. Black lines highlight diffuse cleavage of the marble approximately 90/20

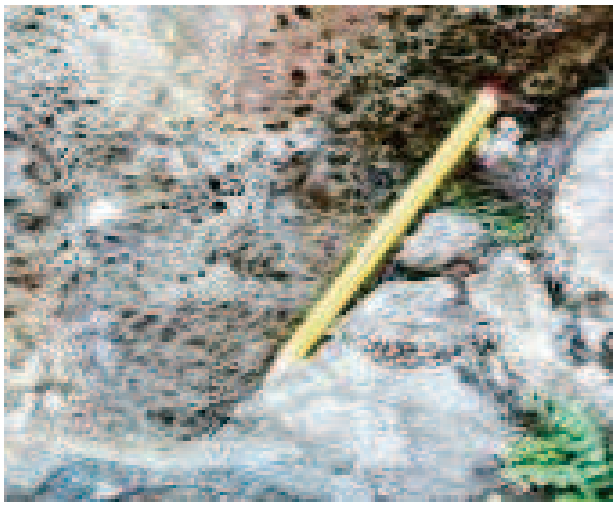

B: 100m East of the Musso marble quarry: vesicular structures within the amphibolite lobes

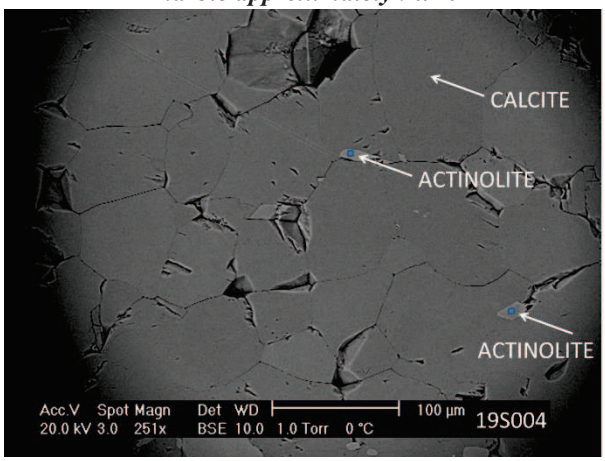

C: Coarse grain marble – CGM: actinolite within the marble

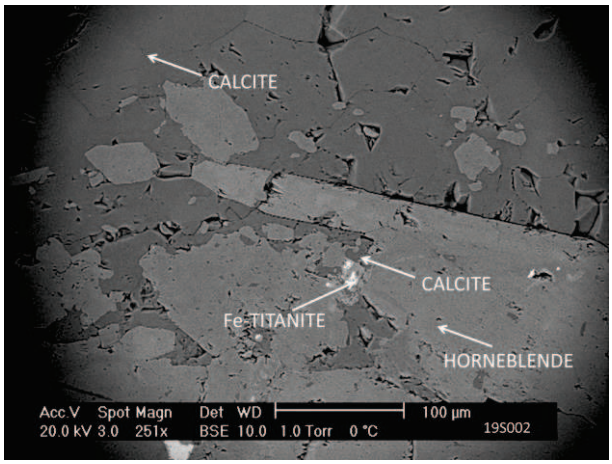

D: Amphibolite –marble contact: contact is underlined by large hornblende crystals.

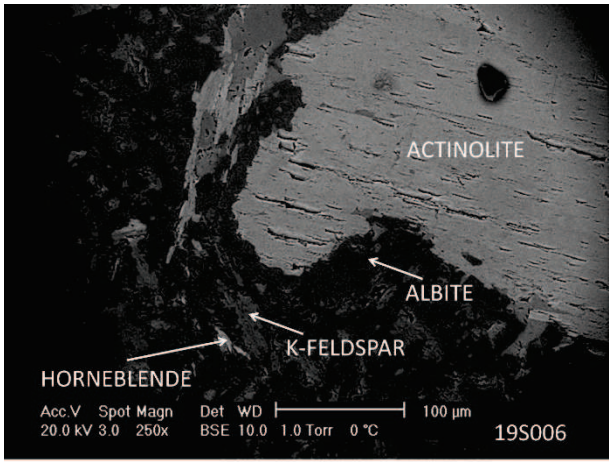

E: Amphibolite –marble contact: Pertitic plagioclase, hornblende and large actinolite

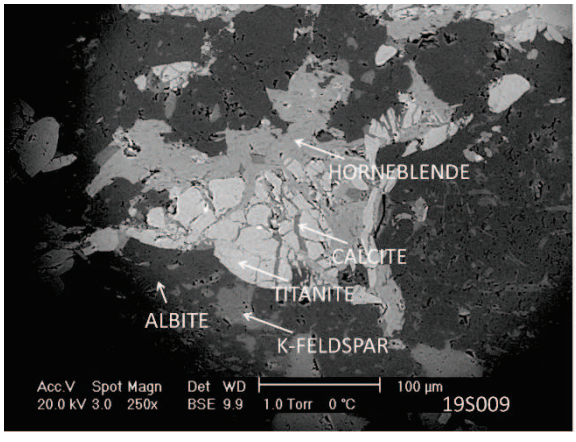

F: Amphibolite –marble contact. Cataclastic titanite with calcite filled veins, hornblende and pertitic plagioclase

Fig. 7: EDX elements map of the Musso marble-amphibolite contact

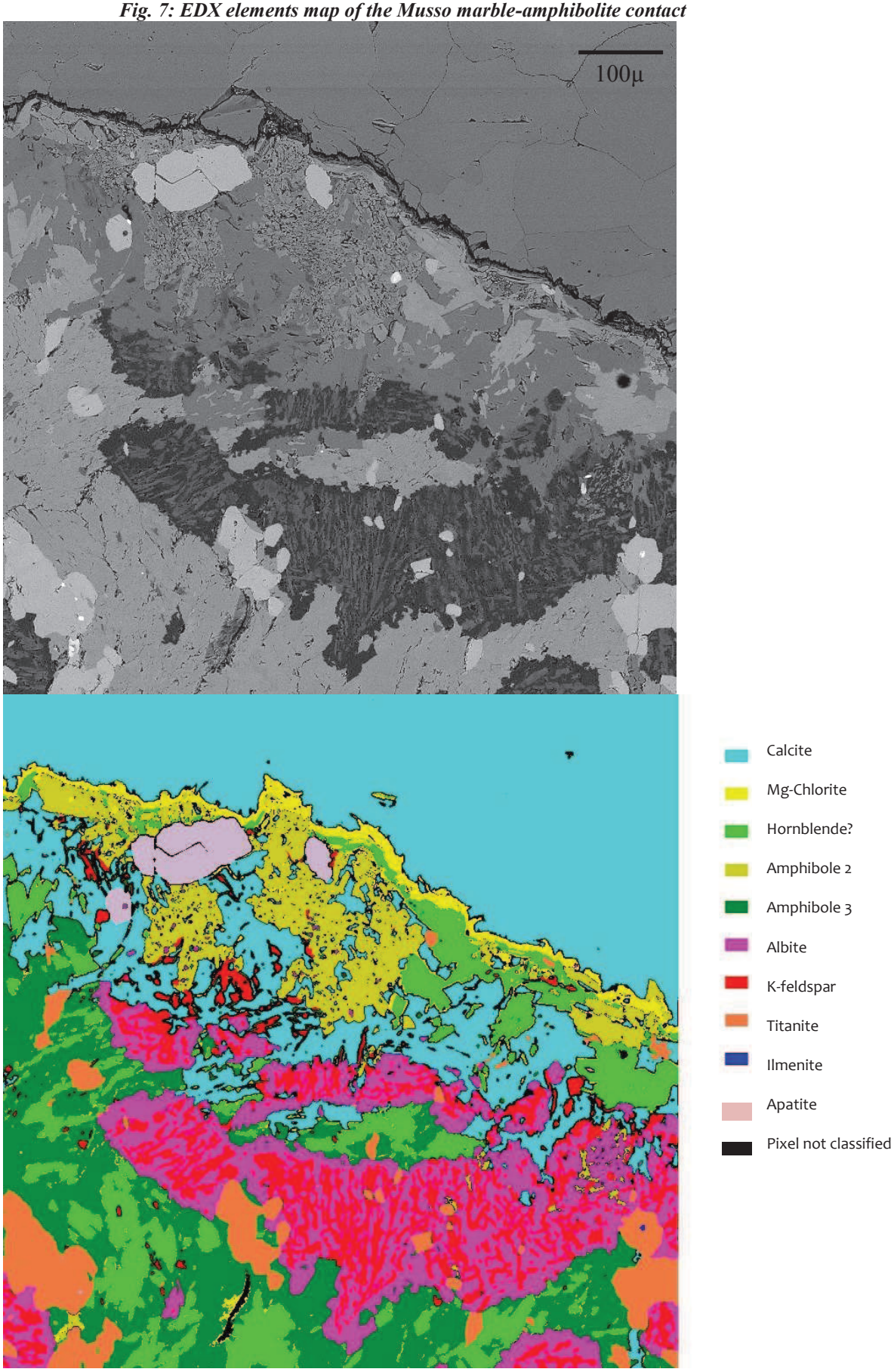

Table 4: Amphibolite petrographic summary

	DCZ NORTH OF THE MUSSO FAULT ZONE (modified after Spalla et al., 2002)			MFZ MUSSO FAULT ZONE			DOZ S OUTH OF THE MUSSO FAULT ZONE (modified after Spalla et al., 2002)		
	Pre-D2	D2	D3	Pre-D2	D2	D3	Pre-D2	D2	D3
Calcite			X			X fracture filling			X
Amphibole	X(I)	X(II)							
Actinolite			X(Act-Tr)			**X (Act)**			**X(Act-Tr)**
Hornblende					X		X(I)	X(II)	
Clinopyroxene		X			X			X	
Rutile	X	(X)					X		
Ilmenite	**(x)**	**X**			**X**		**(x)**	**X**	
Titanite		**(x)**	**X**	**X**				**(x)**	**X**
Garnet	**X**						**X**		
Plagioclase	**X**	**X**	**X(Ab-rich)**	**X**			**X**	**X**	**X(Ab-rich)**
Albite					**X**				
K-feldspar					**(X)**	**X**			
Biotite	(x)	X (I)	X(II)		X		(x)	X (I)	
Phlogopite					**X**				
Quartz	X	X	X			X	X	X	X
Chlorite			X			Fe-X			X
Epidote			X			X		X	X
Allanite						**X**			
White mica			X						X
Pumpellyte			X						X

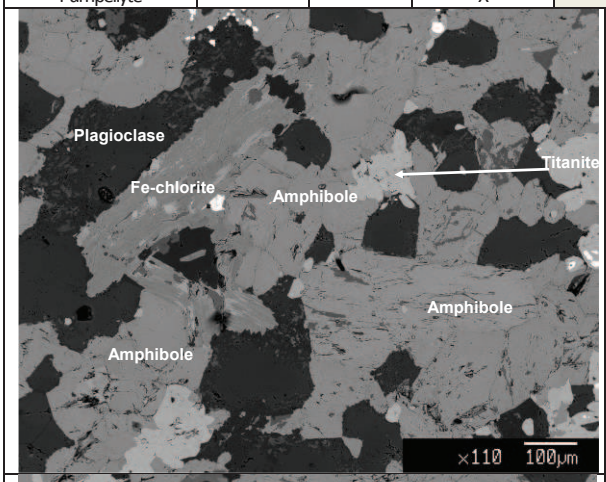

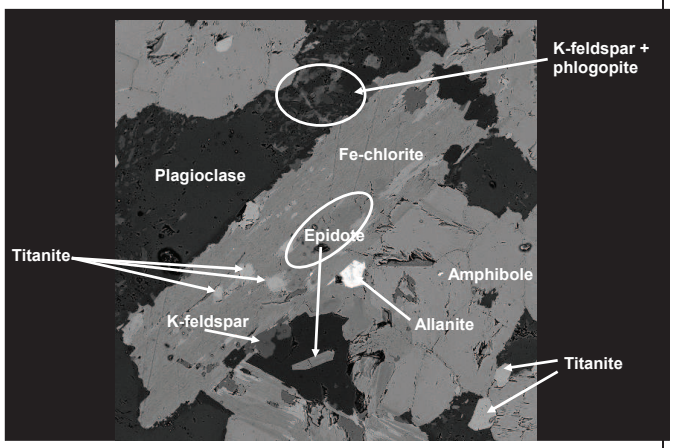

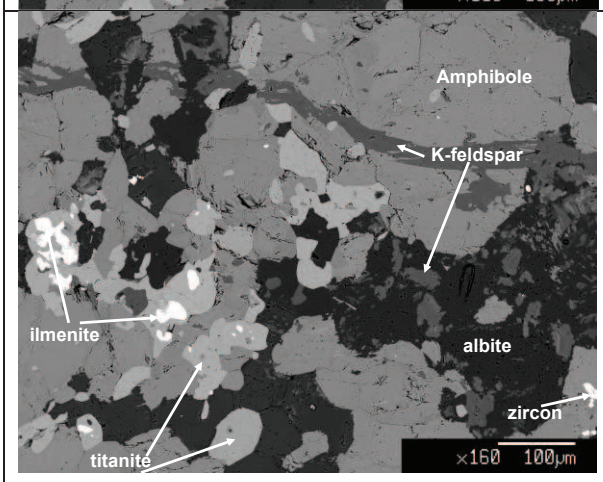

SEM images of the Musso metabasites (sample MUSSO5)

Fig. 8 A and B and C: Major, minor and trace elements of metabasites of the Musso fault zone (MFZ) and the Lugano-Val Grande fault zone (LVZF).

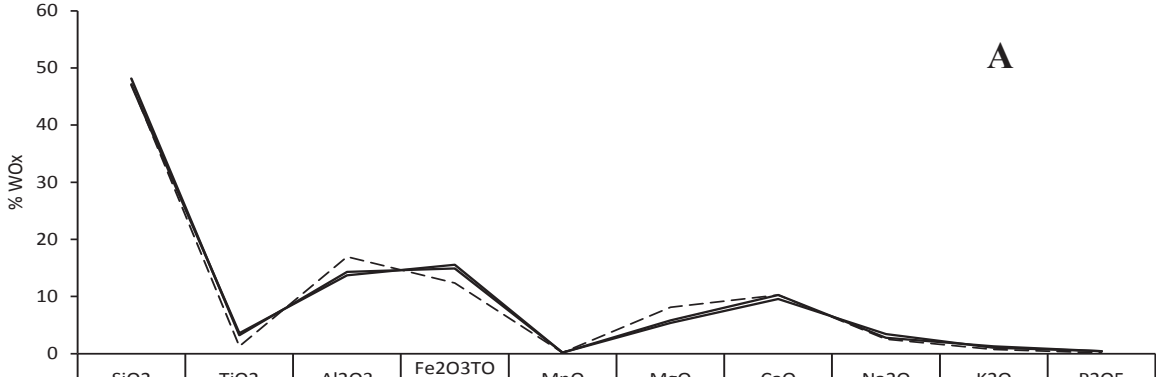

	SiO2	TiO2	Al2O3	Fe2O3TOT	MnO	MgO	CaO	Na2O	K2O	P2O5
MUSSO4	47,04	3,56	13,72	15,6	0,17	5,82	10,28	2,79	1,3	0,46
MUSSO5	48,16	3,25	14,29	14,9	0,18	5,4	9,55	3,43	1,06	0,45
ANF430	47,2	1,31	16,96	12,4	0,19	8,14	10,28	2,56	0,73	0,13

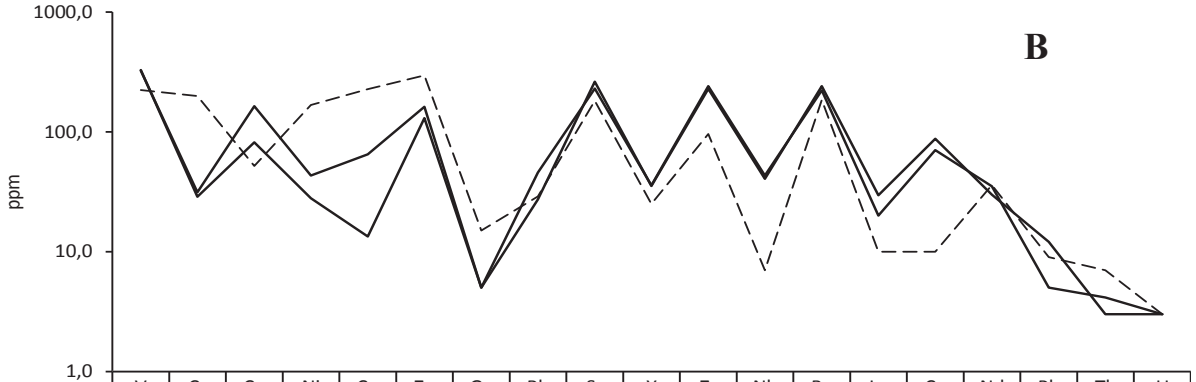

	V	Cr	Co	Ni	Cu	Zn	Ga	Rb	Sr	Y	Zr	Nb	Ba	La	Ce	Nd	Pb	Th	U
MUSSO4	329,5	28,8	81,7	27,9	13,4	130,5	5,0	45,8	229,7	35,8	240,9	43,4	221,9	20,0	70,7	35,2	5,0	4,1	3,0
MUSSO5	325,0	31,3	163,8	43,4	65,1	162,3	5,0	27,3	262,6	35,4	229,0	40,7	241,4	29,6	87,7	30,0	12,1	3,0	3,0
ANF430	224,0	199,0	52,0	168,0	227,0	296,0	15,0	29,0	182,0	25,0	96,0	7,0	185,0	10,0	10,0	36,0	9,0	7,0	3,0

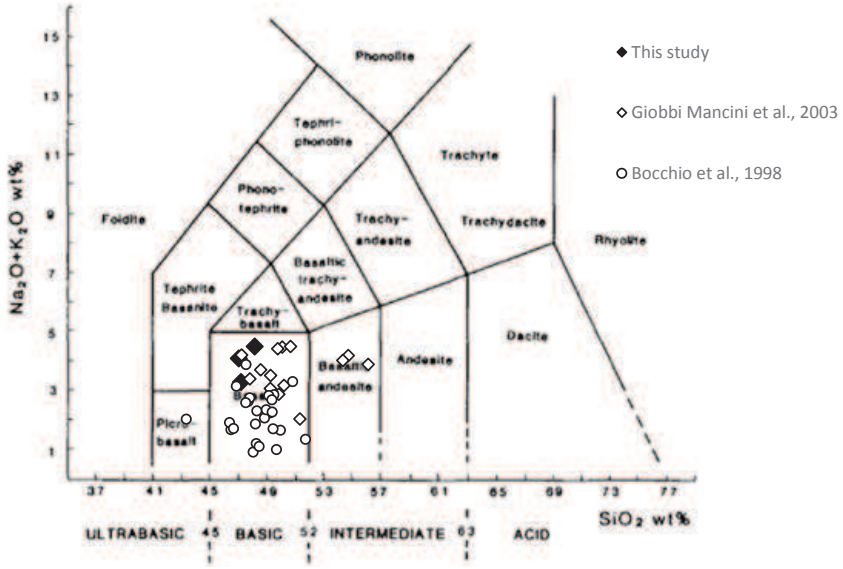

C: TAS diagram of the Southern Alpine metabasites, from selected locations: black marks, MFZ and LGFZ, white circle Strona-Ceneri Border Zone (after Giobbi Mancini et al., 2003), white rhombohedra Piona Peninsula (after Bocchio et al., 1998)

Fig. 9: Structural sketch of the Musso Fault Zone between the villages of Dongo and Musso on the western shore of Lake Como. This area include the main Musso marble lens (MML) and part of the surrounding DCZ and DOZ basements. 9A: main foliation. 9B: mylonitic foliation (T symbol) and associated fracture cleavage (triangle symbol).

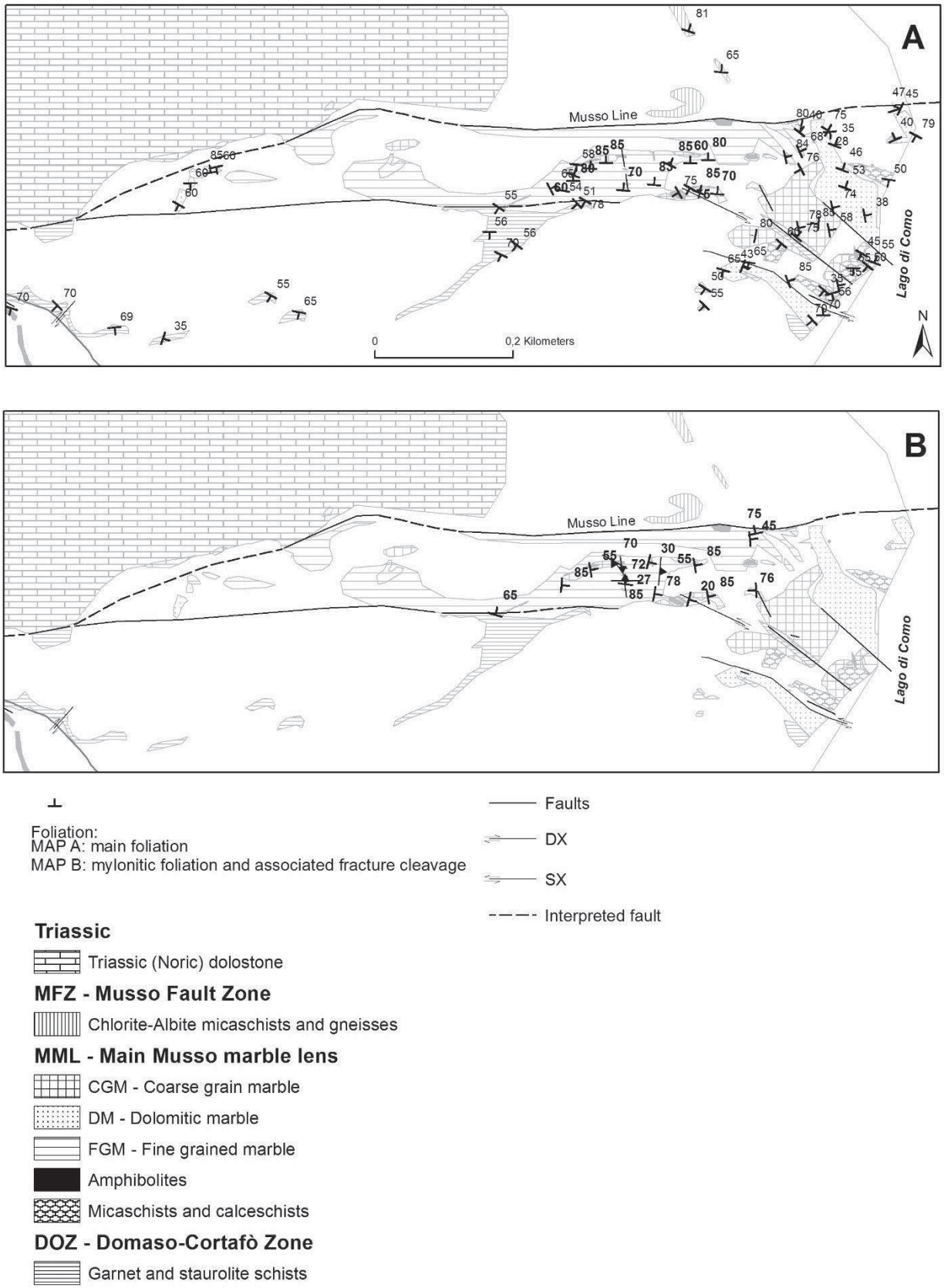

Fig. 9C: Structural data from the Musso Fault Zone

Lithotype	DOZ (South of the Musso Line)	MAIN MUSSO MARBLE LENS (MML)	DCZ (North of the Musso Line)
Micaschists main schistosity S2	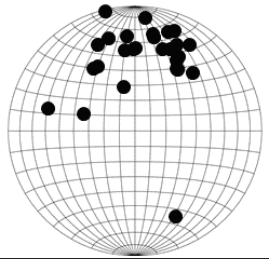	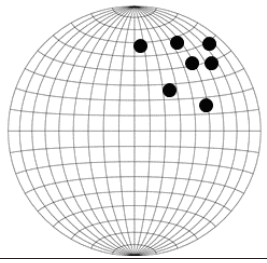	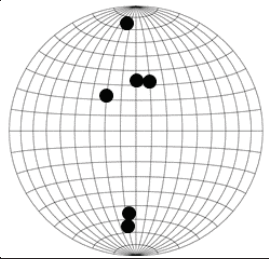
Metabasites main schistosity S2	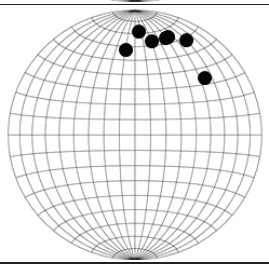	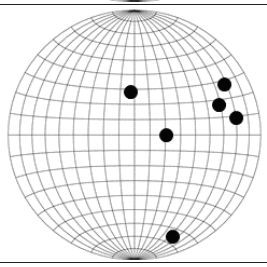	
Marble S2		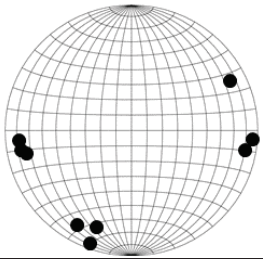	
Dolomitic marble S2	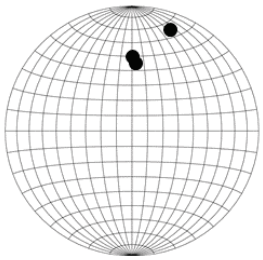	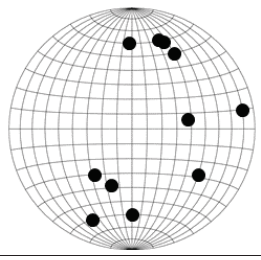	
Mylonites (mylonitic marble for the MML and mylonitic schists for the DOZ) S3	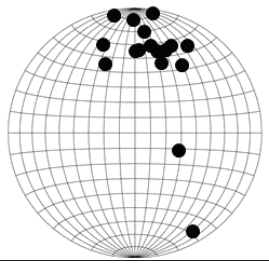	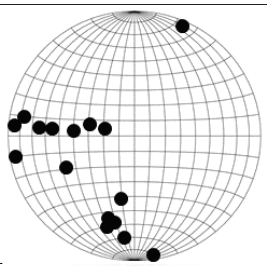	
Mylonites associated to the main faults planes (Fine grain banded marble)		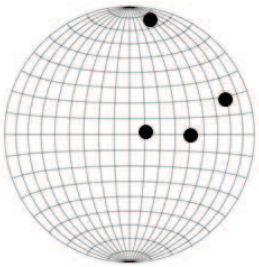 Fold planes	

2.4 Discussion and conclusion

2.4.1 MML marble-metabasite contact interpretation

The marble-amphibolite contact has characteristics that we interpreted as not correlated to the metamorphic evolution but resembling remnants of primary intrusion: i) lobes, ii) compositional layering parallel to the contact of the lobes, iii) diffuse sulphide mineralization at the amphibolite-marble contact, iv) small interfingering of amphibolite protruding within the marble resembling a fluidification of the hostrock, v) crosscutting of the dykes, vi) parallel tubular structures with geometry not related to any metamorphic event thus resembling dykes, vii) contact band characterized by mixing of phases suggesting a widespread mixing at the protoliths interface.

It is also possible to say that partial mixing of the lithotypes can be explained as a consequence of density difference and flowing force of the intrusion in a not totally solidified hostrock while the sulphide mineralization at the basalt-lime interface indicate a quick cooling and a hydrothermal fluids flow probably increased by the host-sediment fluids. The seven described primary contact structures, all found in the MML, resemble those of a basalt intrusion within a carbonatic sediment only partially lithified at time of emplacement.

2.4.2 Structural and petrographic interpretation

The structural analysis of the MML and surrounding basement lead to observe that:

7) The MML is completely bounded by main fragile fault planes and ductile structures.
8) The Sx foliation of the MML is not aligned to the regional S2 foliation neither to the south nor north basements (MML is NW to SE trending compared to the northern and southern basements that are E to W trending)
9) The MML has different N to S trending mylonitic foliation and fracture cleavage compared to S/SW dipping mylonitic foliation found in the southern DOZ basement.
10) The apparent absence of garnet in the MML metabasites suggest a different metamorphic imprint.

These data are only partially sufficient to suppose a particular role of the MML within the Musso fault zone evolution:

1) The MML only partially preserve the pre-D2 HT-HP deformation by contrary to the DOZ basement (epidote). Thus there are not sufficient petrographic data to determine if it belong to the DOZ, DCZ or as more probably to the MFZ.
2) MML reached the same HT-LP regime during D2, developing large static biotite and hornblende. Thus showing a Permo-Triassic thermal peak similar to that of the DOZ.

3) Within the MML, metabasites preserve "primary intrusive" structures.

2.4.3 Regional geochemical correlations

Major, trace and REE elements of Musso and LGFZ metabasites (DOZ-CAV), analyzed in this study, are compared to other metabasite and volcanics of the Southern Alps: I) amphibolites with and without cummingtonite from the Piona Peninsula after Bocchio et al., 1998, II) amphibolites from the Strona Ceneri Border Zone (SCBZ) after Giobbi Mancini et al., 2003 and III) Triassic basaltic volcanics after Cassinis at al., 2008.

All the analyzed data and the eigenvalues of the Principal Components (PC) are reported in APPENDIX 1.

Interpretation:

PC1 (eigenvalue 30%) is correlated to variables (elements) TiO and Zr. These elements seems to be related to the tectonic environment: this is demonstrated by the position of the Triassic samples that form a series with the Norian to the left, the Carnian to the center and Anisian to the right as highlighted by the black arrow in Fig. 10A (the arrow do not represent direction of evolution). The central Southern Alps Triassic volcanic series is well represented and there is no overlapping of samples, thus demonstrating that they belong to different sub-groups with different tectonic meanings within the Triassic volcanics. If we extend the interpretation of the Triassic series to the other series we can say that: DOZ-CUM and DOZ-FREE belong to an almost continuous series divided in two groups overlapping at center, therefore the presence of cummingtonite seems to be related to geochemical composition. SCBZ samples represent a quite homogeneous group overlapping the Carnian and Norian volcanics. The DOZ-CAV of this study falls within the SCBZ and Norian groups. The two MUSSO samples are similar to the Anisian.

PC2 (eigenvalue 22,8%) is correlated to Na2O, Al2O3 and Ba. These elements are plotted separately in Fig. 10C, D, E and F. PC2 splits all the samples in two main groups: DOZ results poorer in the cited elements while SCBZ, Musso, Triassic and DOZ-CAV result richer. Our interpretation is that DOZ amphibolites of the Piona Peninsula have lower Na, Al and Ba content possibly due to metamorphic-loss. The second group did not have elements loss as demonstrated that they well overlap with the un-metamorphosed Triassic samples.

Summary

Triassic un-metamorphosed samples are used in this analysis as a guide to interpret the amphibolite geochemical series, since they belong to well defined tectonic environment while textural relationship and tectonic environments of the metabasites are almost unknown. Triassic samples form an almost continuous series composed of sub-groups, representing different tectonic conditions.

DOZ samples form a well separated group from the others. They are characterized by low Ba, Na Al content and slightly higher Mn, Mg and Ca. They do not overlap with the Triassic, therefore demonstrating a strong geochemical change from a primary volcanic product or a completely different volcanic-tectonic setting.

SCBZ amphibolites form a well constrained group, characterized by slightly higher SiO_2 and overlap with the Norian and Carnian volcanics. Possibly indicating a lower metamorphic imprint-element loss and a similar emplacement environment.

The DOZ-CAV sample have very similar geochemical characteristics to SCBZ. This correlation is found for almost every variable (Fig. 10B,C,D,E,F,G,H) and therefore not deniable even if only one sample was analyzed. We can suppose a common origin for the SCBZ and the DOZ-CAV.

Musso samples show an in-between composition: they have similar Ba, Na, Al content to the SCBZ, DOZ-CAV, and Triassic (Fig. 10B,C,D) but have TiO2, Zr, Nb, MgO and SiO_2 content similar to Anisian and part of the DOZ. This could be due to a partial metamorphic imprint with partial elements depletion (but lower than that of the DOZ), or a different volcano-tectonic origin, more similar to that of the Anisian basalts.

In Fig.10H and 10I we plotted the data on genetic diagram after Mullen 1983 (TiO2-(MnO x 10)-(P_2O_5 x 10) discrimination diagram) and Meschede, 1986 (Nb-Zr-Y discrimination diagram). They confirm the division between the DOZ and the SCBZ. DOZ has a very large range probably due to different ages and tectonic emplacement of the protoliths or to a geochemical change due to metamorphism. In the graph they belong to intraplate volcanism from basalt-alkali to tholeiitic. SCBZ appear as a more compact group with a MORB to tholeiitic composition.

Based on the genetic diagrams, the Musso samples belong to intraplate products with alkali-basalt to tholeiitic composition. The DOZ-CAV confirm its similarity to the SCBZ group.

Fig. 10: Southern Alps amphibolites and Triassic volcanics major, minor and trace elements analyzed by Principal components analysis (MSVP software). Graph A: PC1 vs PC2. Graph B: PC2 vs PC5

Author	Provenience	In the graphs	Type of metabasite	Interpreted origin
Bocchio et al., 1998	from the DOZ and MFZ Piona Peninsula (Eastern side of Lake Como)	DOZ	DOZ-FREE Cummingtonite-free amphibolite	These rock derive mainly from N-P type MORB to T-type MORB and minor alkali-basalts
			DOZ-CUM Amphibolite with cummingtonite	
			DOZ-HOR Horneblendite	
Giobbi Mancini et al., 2003	Serie dei Laghi unit SCBZ	SCBZ	Banded amphibolites	re-sedimented volcanoclastic rocks (tuffites) may represent a remnant of pre-Variscan suture belt
Cassinis et al., 2008	Brescian Alps Collio Basin TRIASSIC VOLCANICS	TRIASSIC	Basalts and dolerites only	Anisian to Carnian volcanic cycle
This study	MML (Musso)	MUSSO	Hornblende rich amphibolites	Intrusive dikes
	DOZ – CAV (LGFZ)	DOZ-CAV	Fine grain amphibolite	?

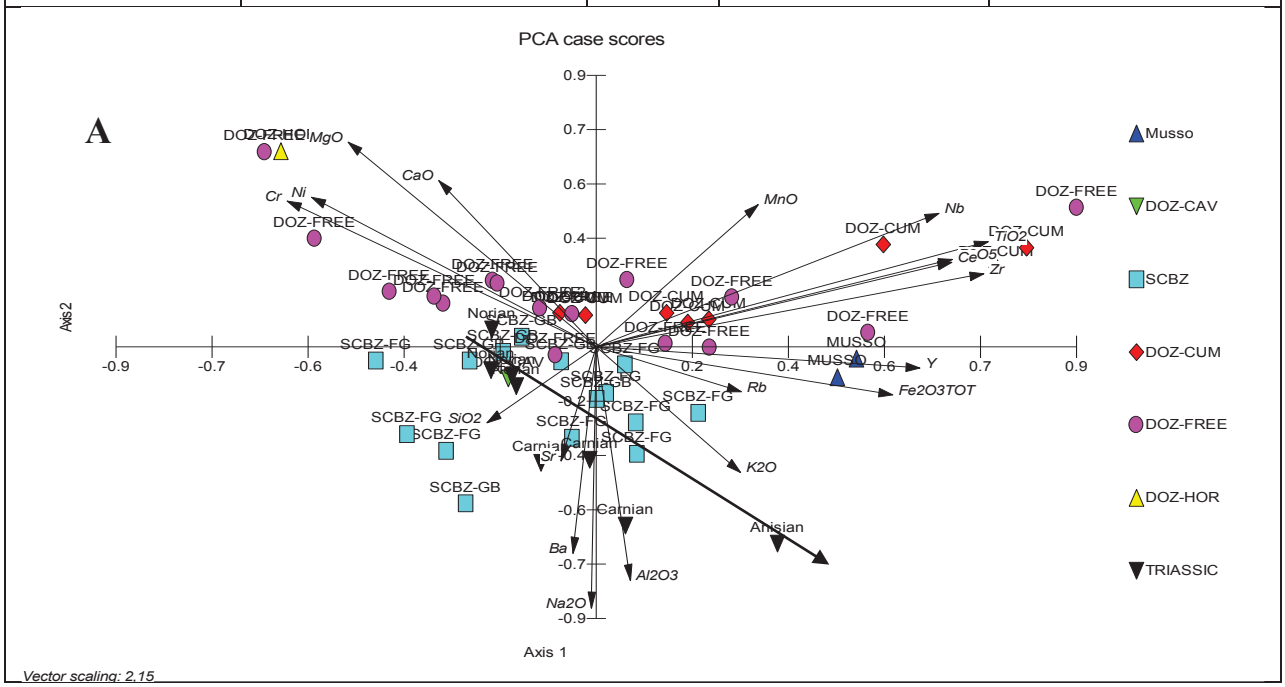

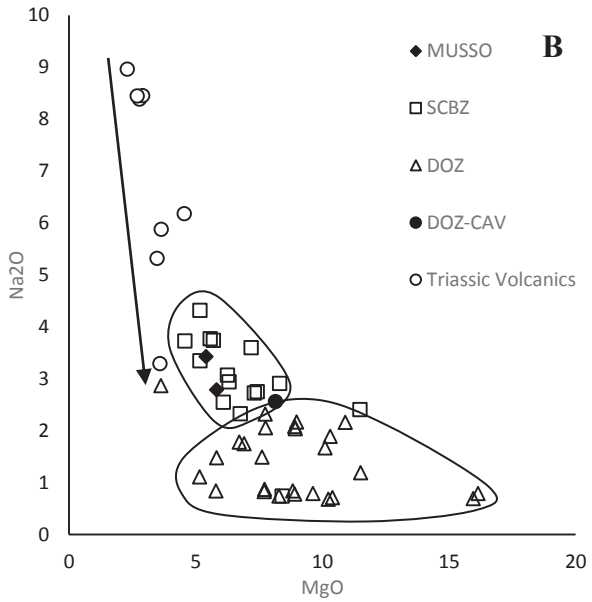

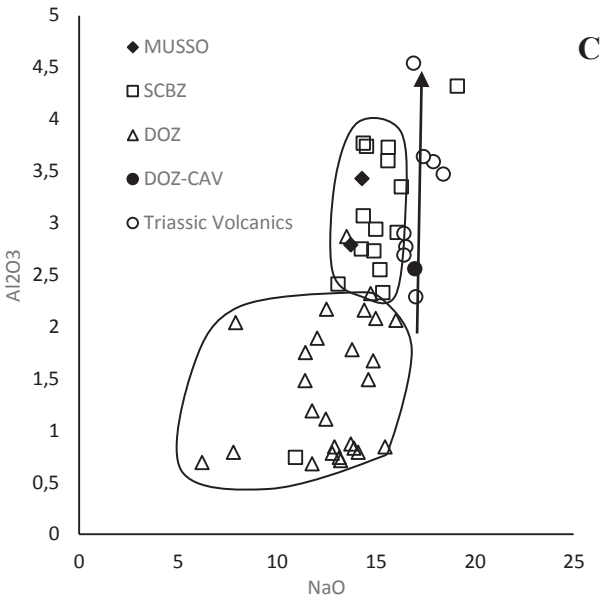

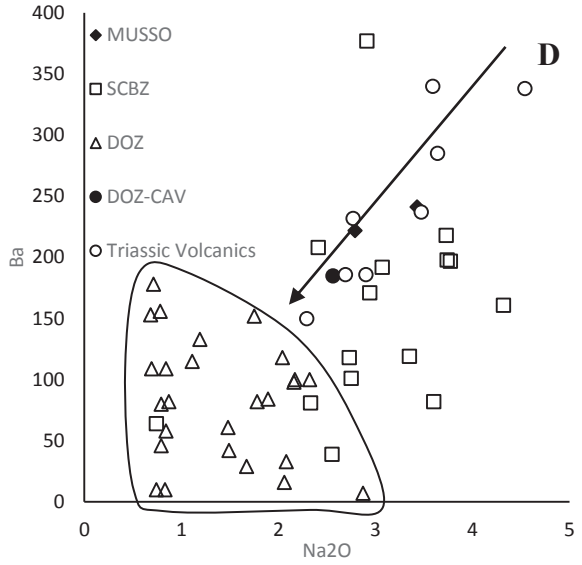

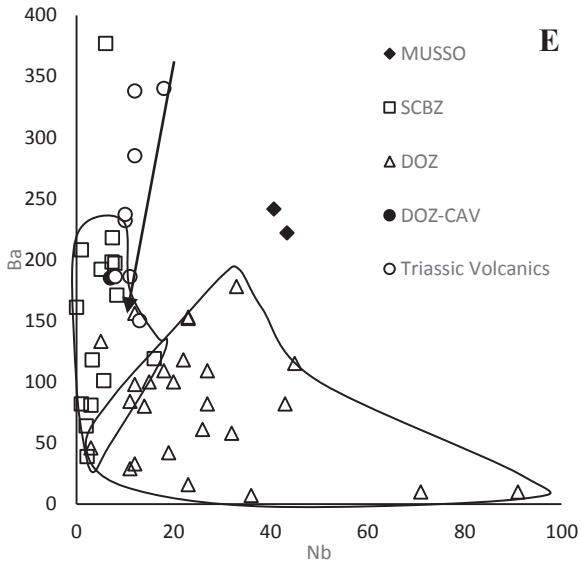

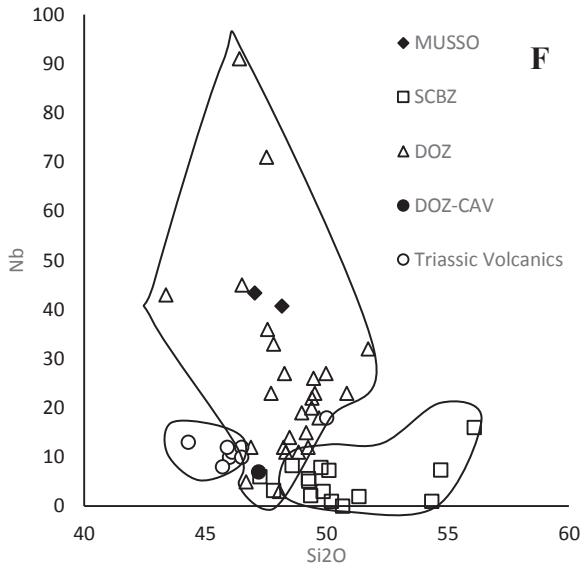

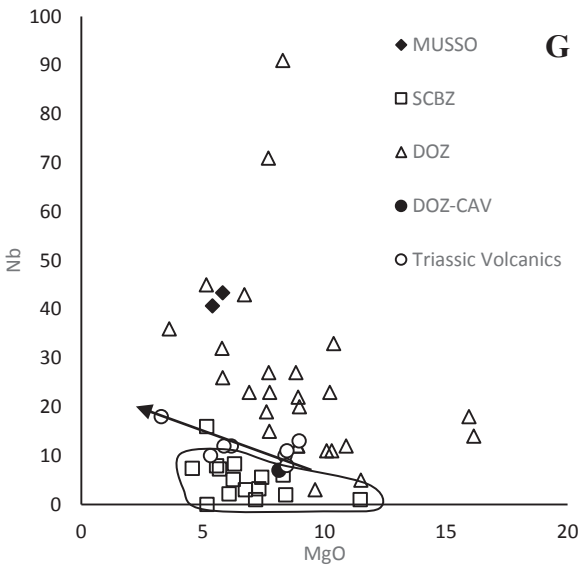

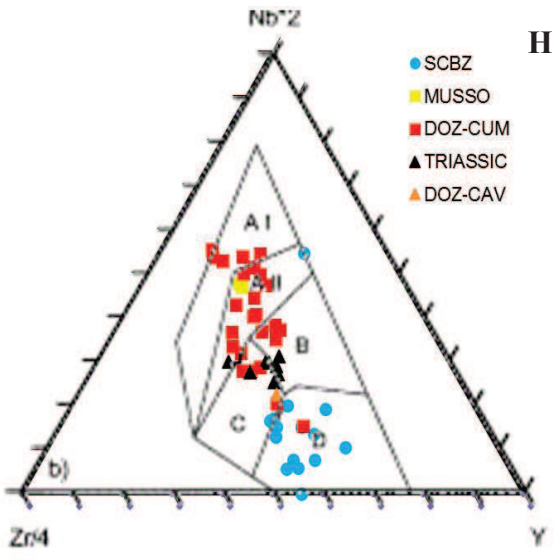

Discrimination (Nb*2)-(Zr/4)-Y diagram (after Meschede, 1986) AI = intraplate alkali basalts; AII = intraplate tholeiites; B = P-type MORB; C = volcanic arc basalts; D = N-type MORB;

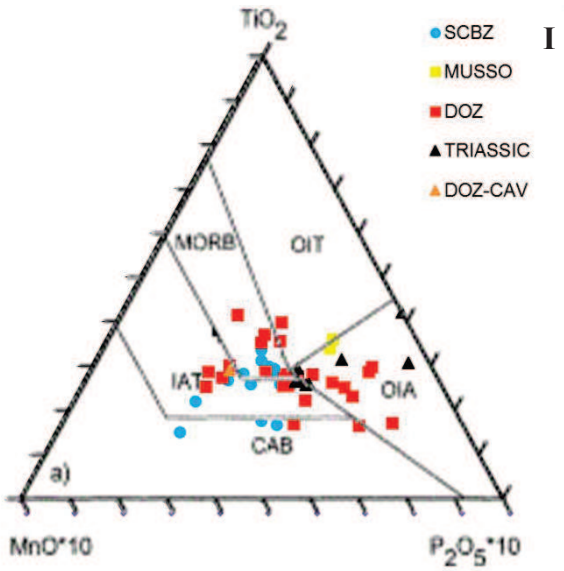

TiO2-(MnO x 10)-(P2O5 x 10) discrimination diagram (after Mullen, 1983). MORB = mid-ocean-ridge basalt, CAB = calc-alkaline basalt, OIT = ocean island tholeiites, OIA = ocean island alkaline basalt, IAT = island arc tholeiites,

2.5 Appendix 1: Amphibolite geochemical data

Geochemical data used in the principal component analysis

Author	*Provenience*	*Description*	*Sample*	*SiO2*	*TiO2*	*Al2O3*	*MnO*	*Fe2O3TOT*	*MgO*	*CaO*	*Na2O*	*K2O*	*P2O5*	*Cr*	*Ni*	*Rb*	*Sr*	*Y*	*Zr*	*Nb*	*Ba*	*Ce*
This study (Musso)	MUSSO	Amp in Musso Marble	MUSSO4	47,04	3,56	13,72	0,17	15,6	5,82	10,28	2,79	1,3	0,46	28,76	27,91	45,84	229,72	35,79	240,93	43,37	221,9	70,65
			MUSSO5	48,16	3,25	14,29	0,18	14,9	5,4	9,55	3,43	1,06	0,45	31,32	43,36	27,31	262,62	35,43	228,97	40,69	241,37	87,66
This study (DOZ)	DOZ-CAV	Amp of lower Val Cavargna (1km S of SAN BARTOLOMEO) 511275.83 m E 5102203.09 m N	ANF430	47,2	1,31	16,96	0,19	12,4	8,14	10,28	2,56	0,73	0,13	199	168	29	182	25	96	7	185	10
Giobbi Mancini et al 2003	SCBZ	Fine-grain amphibolites	MCMA32	56,1	0,36	16,27	0,14	8,8	5,16	8,19	3,35	0,54	0,06	104	33	14	182	17	39	16	119	
			RB12	54,71	1,55	15,62	0,19	10,8	4,57	7,88	3,73	0,46	0,26	40	16	10	312	37	152	7,4	218	38,3
			MCMA20	54,34	0,53	15,6	0,12	7,6	7,18	8,12	3,6	0,42	0,14	242	82	12	438	18	58	1	82	6
			MCMA16	50,2	0,65	13,08	0,15	9,7	11,48	8,97	2,41	0,77	0,15	459	170	30	292	18	64	1	208	
			RB2	50,09	1,82	14,52	0,2	12,6	5,69	8,87	3,74	0,73	0,27	98	30	13	299	36	143	7,3	198	24,2
			VA25	49,77	2,06	14,35	0,23	13,3	5,57	9,3	3,77	0,65	0,25	76	0	16	211	45,4	176	7,9	197	27,6
			RB4	48,58	1,73	14,98	0,19	12,3	6,31	9,9	2,94	0,76	0,19	165	43	16	199	36	125	8,3	171	20,7
			RB15	47,81	2,13	14,88	0,21	13,0	7,31	10,35	2,73	0,67	0,21	181	67	14	207	42	141	3,2	118	19,3
			RB13A	47,25	1,51	16,06	0,21	12,3	8,31	6,57	2,91	1,29	0,17	281	95	41	207	32	75	6	377	17,8
		Garnet-bearing amphibolites	MCMA48	51,33	0,97	10,92	0,23	13,9	8,41	10,08	0,74	1,3	0,11	189	58	89	169	23	47	2	64	-
			EGCA2	50,66	1,02	19,11	0,13	8,9	5,17	9,13	4,32	0,17	0,16	77	33	1	908	21	67	0	161	-
			MCMA53	49,86	1,2	15,34	0,18	11,7	6,76	11,82	2,33	0,55	0,16	262	82	11	131	23	63	3	81	-
			MCMA55	49,35	1,33	15,19	0,16	11,6	6,09	12,49	2,55	0,41	0,18	301	83	7	140	31,3	87	2,2	39	9,36
			MCMA26	49,27	1,63	14,35	0,18	13,0	6,25	10,31	3,07	0,44	0,21	157	22	13	249	34,9	136	5,1	192	18,59
			VA26	49,25	1,36	14,25	0,22	10,2	7,43	11,13	2,75	0,32	0,15	186	0	10	165	35,7	109	5,6	101	18,5
Bocchio et al 1998	DOZ	Cummingtonite bearing amphibolite	LC01	49,24	1,97	14,98	0,25	12,5	8,9	9,02	2,08	0,16	0,32	236	88	2	200	26	146	12	33	29
			LC011	48,85	1,86	14,85	0,23	13,1	10,1	8,59	1,67	0,4	0,31	233	99	14	155	25	128	11	29	11
			LC02	48,97	2,5	14,62	0,2	13,6	7,62	8,45	1,49	0,86	0,54	179	85	39	154	29	190	19	42	22
			LC03	47,71	2,78	16,01	0,25	13,4	7,76	7,97	2,06	0,58	0,46	198	89	27	198	30	202	23	16	31
			LC06	48,22	2,22	12,79	0,36	18,1	8,91	7,57	0,78	1,09	0,19	186	69	47	42	28	129	12	156	17
			LC07	43,37	3,09	13,79	0,4	17,5	6,72	11,1	1,78	0,25	1,15	64	41	8	121	35	189	43	82	49
			LC08	46,51	3,59	12,46	0,3	19,1	5,15	9,35	1,11	0,57	1,43	15	3	13	216	41	202	45	115	91
			LC09	47,81	1,66	13,2	0,14	9,7	10,39	11,53	0,71	2,04	0,41	404	133	63	561	21	144	33	178	37
			LC10	47,53	4,26	13,88	0,2	12,1	7,7	9,36	0,83	1,76	0,86	30	37	53	316	37	364	71	10	128
		Cummingtonite free amphibolites	LC11	46,4	4,65	13,14	0,19	12,4	8,29	10,61	0,74	1,18	0,9	31	44	35	425	39	482	91	10	119
			LC12	49,51	1,89	11,76	0,16	13,1	10,23	7,79	0,68	2,18	0,37	39	30	65	183	25	131	23	153	35
			LC13	51,72	1,65	15,45	0,18	9,6	5,8	13,76	0,84	0,51	0,24	175	60	11	312	24	120	32	58	42
			LC14	50,83	2,05	11,42	0,21	13,5	6,91	9,44	1,75	1,55	0,32	20	22	42	156	30	150	23	152	62
			LC15	47,56	3,27	13,52	0,26	15,4	3,62	9,91	2,87	1,01	0,33	34	21	25	406	36	243	36	7	100
			LC17	49,16	1,66	14,73	0,2	11,5	7,74	10,63	2,32	0,51	0,21	85	49	12	194	24	111	15	100	11
			LC19	49,38	1,8	12,5	0,19	11,6	8,98	12,37	2,17	0,52	0,28	258	95	9	269	26	135	20	100	16
			LC31	49,98	1,49	12,89	0,2	3,2	8,83	11,26	0,84	0,82	0,32	315	118	21	272	10	135	27	109	47
			LC932	46,88	1,46	14,4	0,17	3,4	10,9	10,06	2,16	0,99	0,22	361	242	22	257	21	122	12	98	27
			LC934	48,05	0,99	14,1	0,19	2,7	9,63	13,04	0,79	0,13	0,1	217	68	1	210	19	57	3	46	10
			LC194	46,68	1,17	11,76	0,19	3,7	11,51	12,34	1,19	0,53	0,12	638	378	21	234	20	77	5	133	13

			LC294	48,27	1,03	13,73	0,21	4,7	7,71	14,14	0,87	0,34	0,29	264	76	15	338	21	135	27	82	21
			LC394	49,69	1,64	6,2	0,15	3,7	15,95	12,12	0,69	0,31	0,15	1091	346	6	283	19	85	18	109	25
			LC494	49,46	3,84	11,41	0,25	4,4	5,82	9,13	1,48	0,23	0,33	23	6	8	135	46	169	26	61	25
			LC594	49,4	2,9	7,9	0,24	6,4	8,93	11,96	2,04	0,23	0,25	19	2	14	146	38	147	22	118	11
			LC694	48,31	1,39	12,03	0,19	4,1	10,31	12	1,89	0,42	0,13	243	120	11	307	21	81	11	84	23
		Horneblendite	OR1	48,47	1,7	7,78	0,14	2,9	16,15	12,33	0,79	0,32	0,1	1100	323	2	150	23	90	14	80	37
	Norian	Dolerite	IR-24	44,3	1,606	17	0,09	7,7	8,97	13	2,29	0,41	0,26	426	161	11	255	29	125	13	150	31,7
	Norian	Dolerite	IR-31	46	1,369	16,5	0,15	9,1	8,39	10,8	2,77	1	0,23	342	130	26	402	28	106	10	232	25,7
	Norian	Dolerite	IR-34	46,1	1,392	16,4	0,15	9,0	8,46	11,1	2,9	0,83	0,25	354	128	20	429	28	107	11	186	25,4
Cassinis et al., 2008	Norian	Dolerite	IR-38	45,7	1,335	16,4	0,15	9,1	8,45	11,6	2,69	0,74	0,22	344	122	24	368	24	95	8	186	23,4
	Anisian	basalto	IR-49	50	2,227	17,9	0,03	7,2	3,29	4,42	3,59	5,52	0,47	99	19	55	135	32	213	18	340	49,7
	Carnian	Basalt	IR-53	45,9	1,812	16,9	0	9,9	6,18	6,62	4,54	2,57	0,25	103	43	39	539	28	144	12	338	29,4
	Carnian	Dolerite	IR-55	46,5	1,446	17,4	0,15	9,4	5,88	10,3	3,64	1,31	0,26	120	46	30	615	28	117	12	285	29,5
	Carnian	Basalt	IR-54	46,5	1,382	18,4	0,13	7,8	5,32	11,7	3,47	1,16	0,2	84	33	28	702	23	86	10	237	23,7

Principal component analysis eigenvalues

Eigenvalues					
	Axis 1	Axis 2	Axis 3	Axis 4	Axis 5
Eigenvalues	6,029	4,573	2,346	1,701	1,271
Percentage	30,145	22,866	11,732	8,505	6,353
Cum. Percentage	30,145	53,011	64,743	73,248	79,601

2.6 Appendix 2: microprobe analysis

Samples Am3, An3b, 5 and AM3 were analysed by microprobe. The numbers, drawn on the figures, indicate the chemical analysis as reported down below. The geographical positions of samples are reported on the "Map of samples". The analysis are reported in this appendix following the order of the next table:

Sample	Lithotype	Provenience	Figure
AM3	**Coarse grain marble**	Musso main marble body	1,2,3,4,5,6
An3b	**Fine grain marble**	Piona Peninsula marble lens	7,8,9,10
5	**Amphibolite dike**	Musso quarry	11, 12, 13, 14, 15, 16
AM2	**Amphibolite marble contact**	Musso main marble body	17, 18

Sample AM3

Figure 1

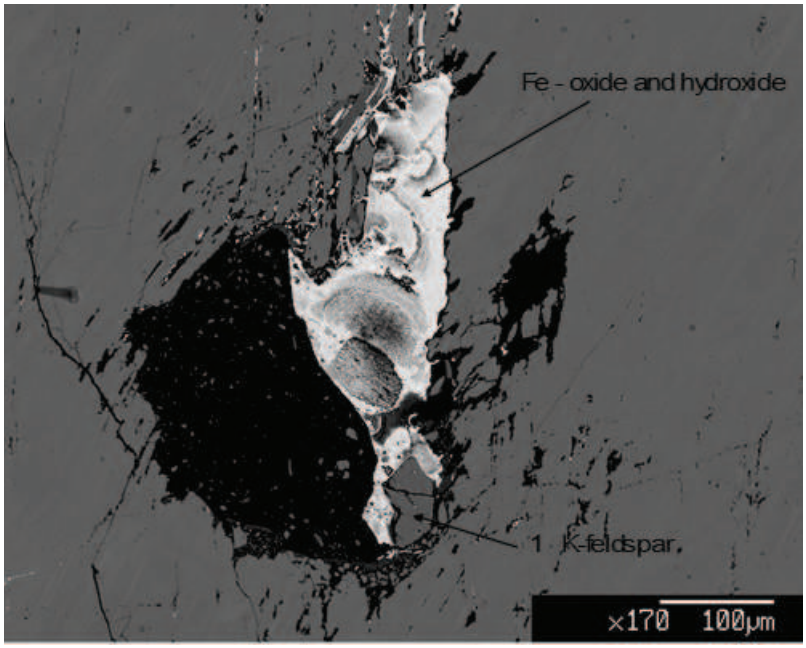

Analysis 1 K-feldspar

Na2O	TiO2	MnO	K2O	MgO	Cr2O3	FeO	CaO	Al2O3	SiO2	NiO	Total
0.3358	0	0.012	16.31	0.0008	0	0.3837	0.0568	18.56	66.46	0.0432	102.1622

Figure 2

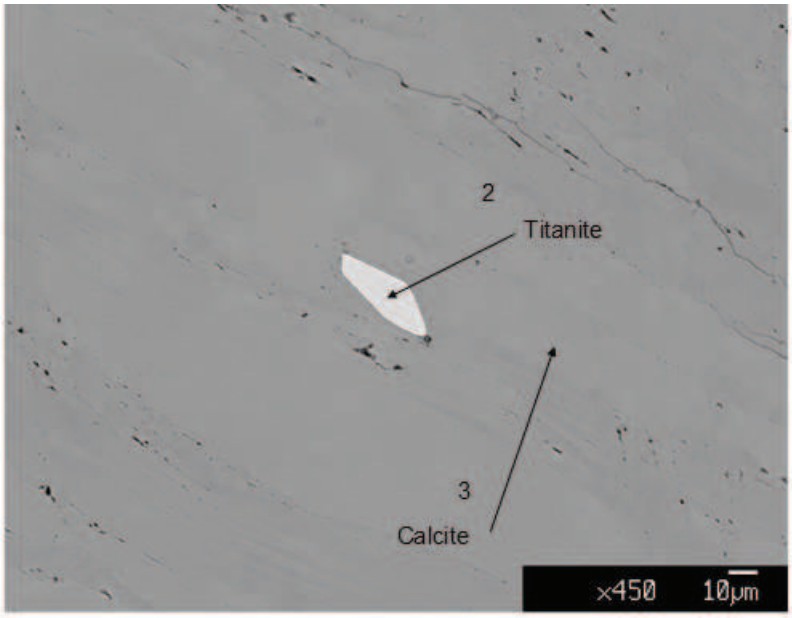

Analysis 2 Titanite

Na2O	TiO2	MnO	K2O	MgO	Cr2O3	FeO	CaO	Al2O3	SiO2	NiO	Total
0.0105	34.07	0.0312	0	0.0164	0.1245	0.0185	29.39	3.85	31.13	0	98.6412

Analysis 3 Calcite

Na2O	TiO2	MnO	K2O	MgO	Cr2O3	FeO	CaO	Al2O3	SiO2	NiO	Total
0.0078	0.0104	0.0532	0	0.3372	0.0315	0.0664	58.28	0	0	0	58.7865

Figure 3

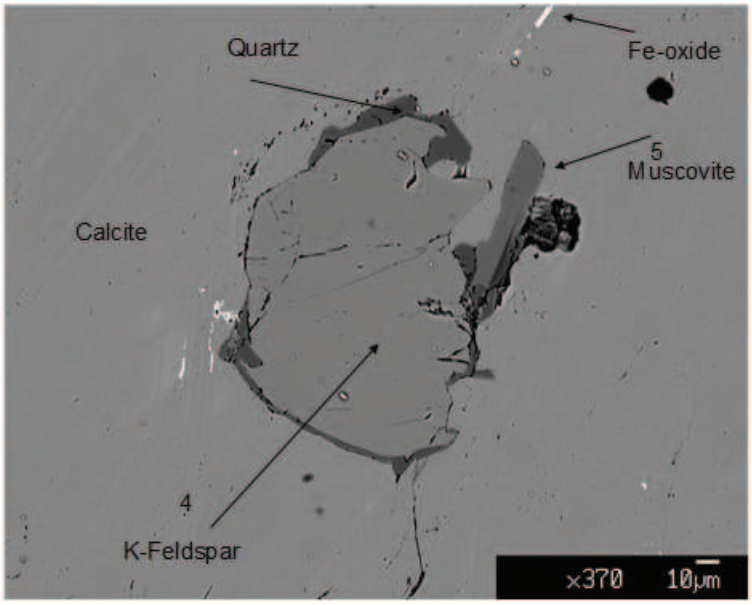

Analysis 4 K-feldspar

Na2O	TiO2	MnO	K2O	MgO	Cr2O3	FeO	CaO	Al2O3	SiO2	NiO	Total
0.2987	0.0184	0	16.27	0	0	0.0106	0.0703	18.56	65.57	0	100.7979

Analysis 5 Muscovite

Na2O	TiO2	MnO	K2O	MgO	Cr2O3	FeO	CaO	Al2O3	SiO2	NiO	Total
0.0485	0.0085	0.0045	10.92	1.0837	0.0444	0.1671	0.2692	36.32	50.6	0	99.466

Figure 4

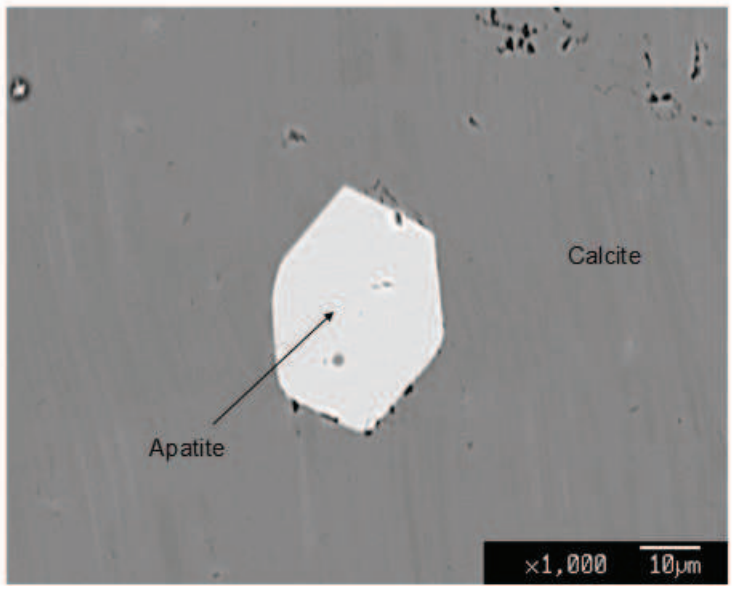

Figure 5

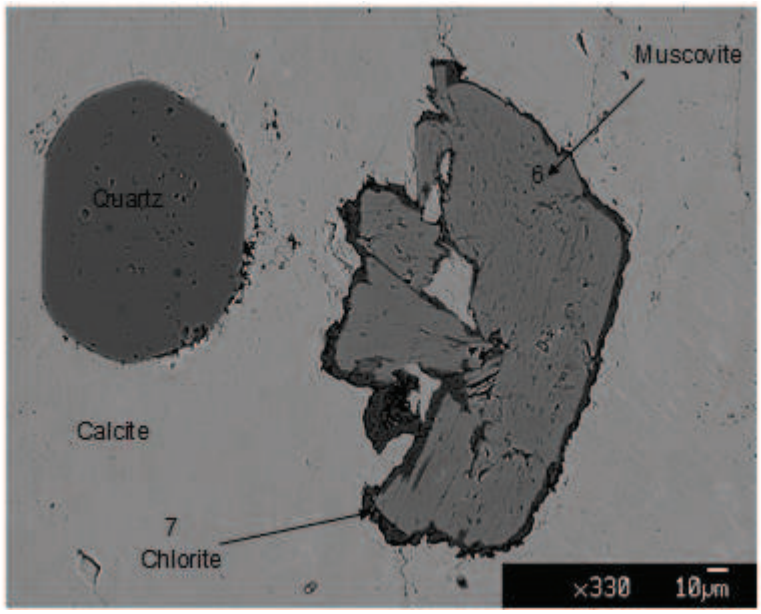

Analysis 6 Muscovite

Na2O	TiO2	MnO	K2O	MgO	Cr2O3	FeO	CaO	Al2O3	SiO2	NiO	Total
0.2158	0.0508	0	10.67	0.1785	0.0066	0.067	0.1775	38.93	48.3	0.0458	98.6421

Analysis 7 Chlorite

Na2O	TiO2	MnO	K2O	MgO	Cr2O3	FeO	CaO	Al2O3	SiO2	NiO	Total
0.0186	0	0.0375	0.1254	13.7	0.0229	0.8465	0.5053	33.44	39.42	0	88.1162

Figure 6

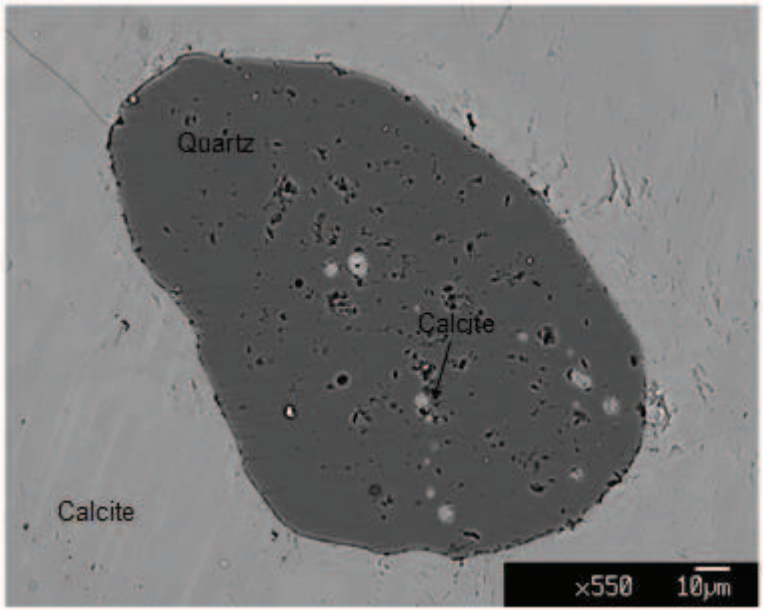

Sample An3b

Figure 7

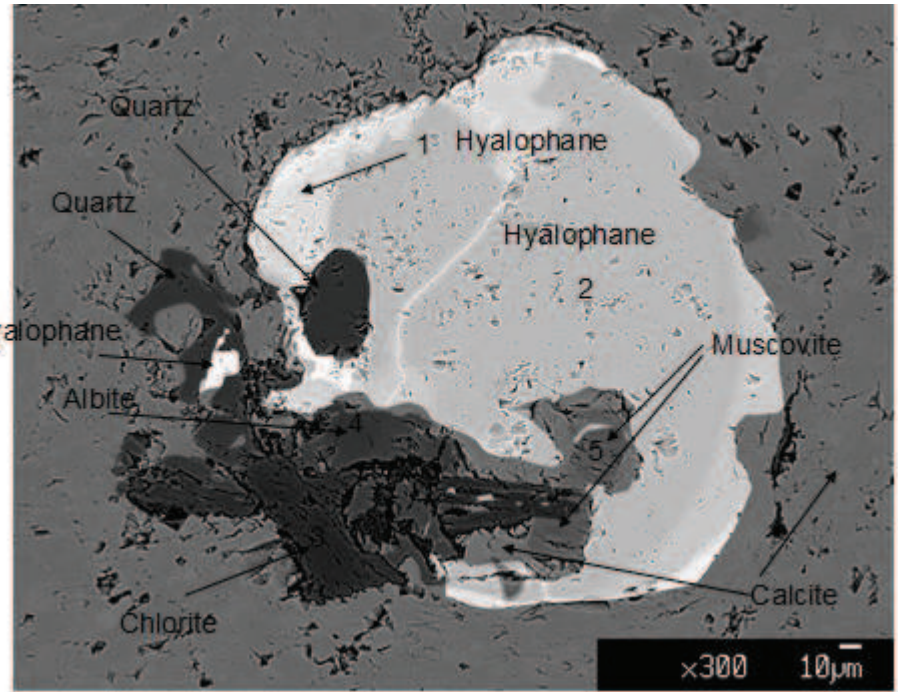

Analysis 1 Hyalophane

Na2O	TiO2	MnO	K2O	MgO	Cr2O3	FeO	CaO	Al2O3	SiO2	BaO	NiO	Total
0.7803	0.2222	0	9.26	0.0152	0.0638	0.0518	0.1163	19.63	50.78	19.06	0.0234	80.9431

Analysis 2 Hyalophane

Na2O	TiO2	MnO	K2O	MgO	Cr2O3	FeO	CaO	Al2O3	SiO2	BaO	NiO	Total
0.8728	0.1587	0	10.71	0.0085	0	0.0513	0.0293	19.32	55.45	13.40	0	86.6007

Analysis 3 Chlorite

Na2O	TiO2	MnO	K2O	MgO	Cr2O3	FeO	CaO	Al2O3	SiO2	NiO	Total
0.0073	0.0014	0.1667	0.0122	30.63	0	3.31	0.178	20.16	31.06	0.0208	85.5464

Analysis 4 Albite

Na2O	TiO2	MnO	K2O	MgO	Cr2O3	FeO	CaO	Al2O3	SiO2	NiO	Total
11.39	0	0.0255	0.0236	0	0	0	0.6271	19.66	68.9	0	100.6262

Analysis 5 Muscovite

Na2O	TiO2	MnO	K2O	MgO	Cr2O3	FeO	CaO	Al2O3	SiO2	NiO	Total
0.1334	0.0084	0.0045	10.29	2.65	0.0519	0.386	0.0815	31.16	50.85	0	95.6158

Figure 8

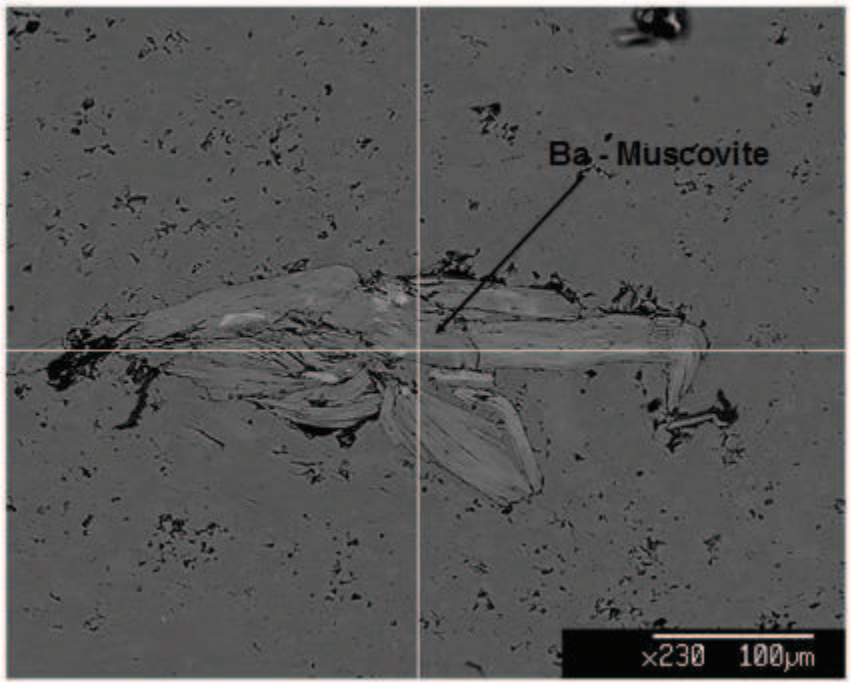

Figure 9

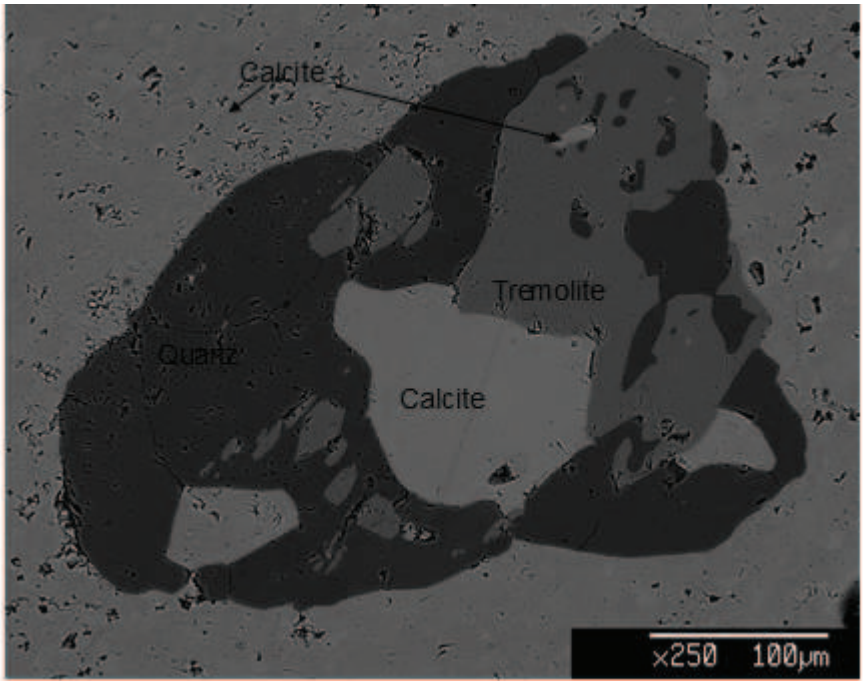

Analysis 9 Tremolite

Na2O	TiO2	MnO	K2O	MgO	Cr2O3	FeO	CaO	Al2O3	SiO2	NiO	Total
0.3956	0	0.1002	0.2907	21.54	0.0112	0.955	13.43	2.24	51.34	0.0335	90.3363

Sample 5

Figure 11

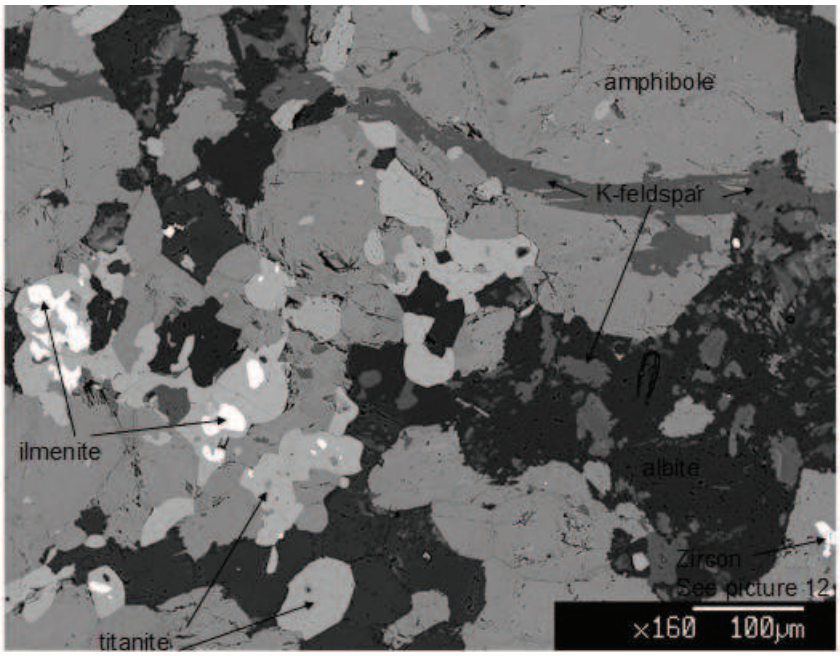

Analysis 1 K-feldspar

Na2O	TiO2	MnO	K2O	MgO	Cr2O3	FeO	CaO	Al2O3	SiO2	NiO	Total
0.2381	0.0328	0.0218	15.99	0.0054	0.008	0.3615	0.0499	18.71	65.66	0	101.0774

Analysis 2 Amphibolite

Na2O	TiO2	MnO	K2O	MgO	Cr2O3	FeO	CaO	Al2O3	SiO2	NiO	Total
1.5	0.7534	0.2841	0.7586	8.34	0.0382	20.41	11.51	10.84	44.04	0	98.4744

Analysis 3 Titanite

Na2O	TiO2	MnO	K2O	MgO	Cr2O3	FeO	CaO	Al2O3	SiO2	NiO	Total
0.0132	38.62	0.067	0.0104	0.0137	0	0.5116	28.76	1.3115	31.35	0.0704	100.7277

Analysis 4 Albite

Na2O	TiO2	MnO	K2O	MgO	Cr2O3	FeO	CaO	Al2O3	SiO2	NiO	Total
11.62	0	0.0263	0.0391	0	0.0308	0.2375	0.1021	19.74	70.1	0.0045	101.9002

Analysis 5 Ilmenite

Na2O	TiO2	MnO	K2O	MgO	Cr2O3	FeO	CaO	Al2O3	SiO2	NiO	Total
0.0269	52.64	4.43	0.0004	0.0241	0	44.68	0.2943	0	0.0002	0.0707	102.1665

Analysis 6 Albite

Na2O	TiO2	MnO	K2O	MgO	Cr2O3	FeO	CaO	Al2O3	SiO2	NiO	Total
8.25	0	0	0.0664	0.0159	0	0.126	5.8	24.19	62.31	0.0127	100.771

Figure 12 Zircons (detail of figure 11)

Figure 13 (the square indicate the detail area in next figure)

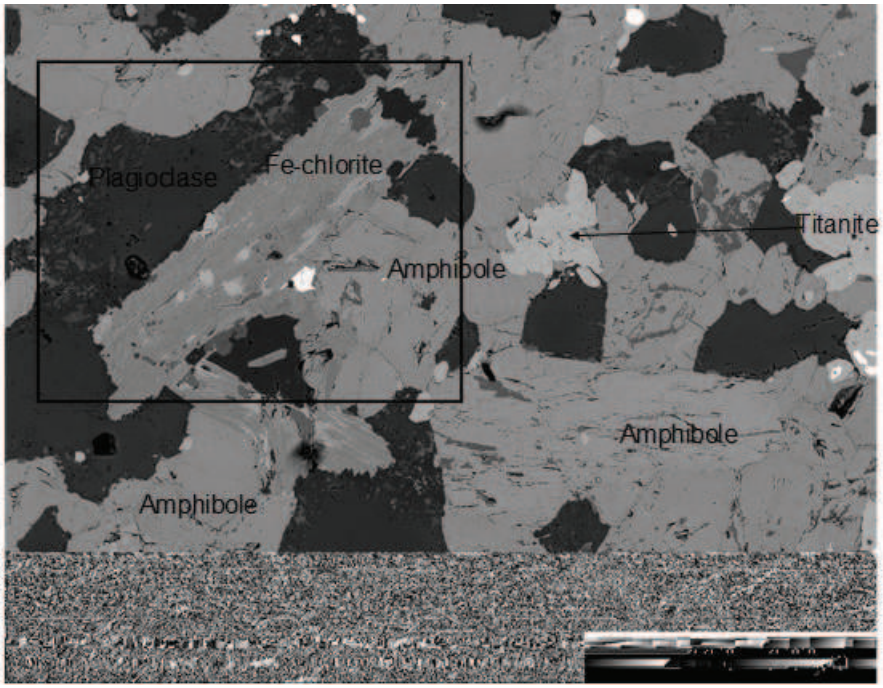

Analysis 7 Fe-chlorite

Na2O	TiO2	MnO	K2O	MgO	Cr2O3	FeO	CaO	Al2O3	SiO2	NiO	Total
0	0.1338	0.2706	0.0108	11.07	0	32.52	0.1638	19.51	26.4	0.0642	90.1433

Analysis 8 Epidote

Na2O	TiO2	MnO	K2O	MgO	Cr2O3	FeO	CaO	Al2O3	SiO2	NiO	Total
0.0027	0.08	0.2354	0	0.0164	0	9.46	23.39	25.74	38.91	0	97.8346

Detail of figure 13

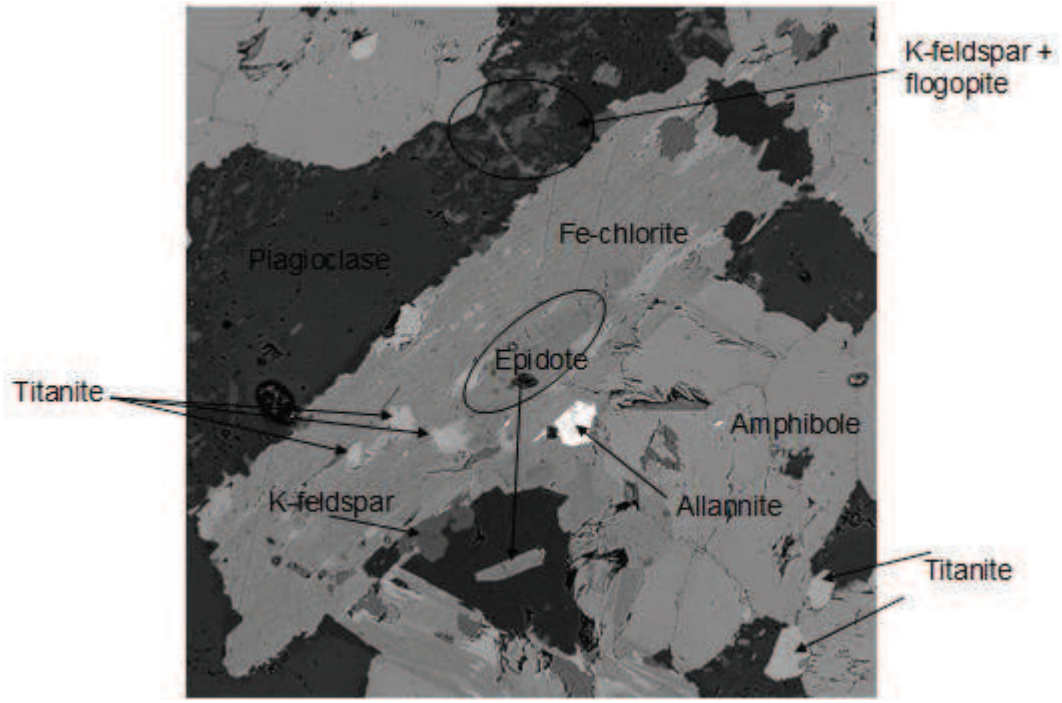

Figure 14 (rectangle in detail in next figure)

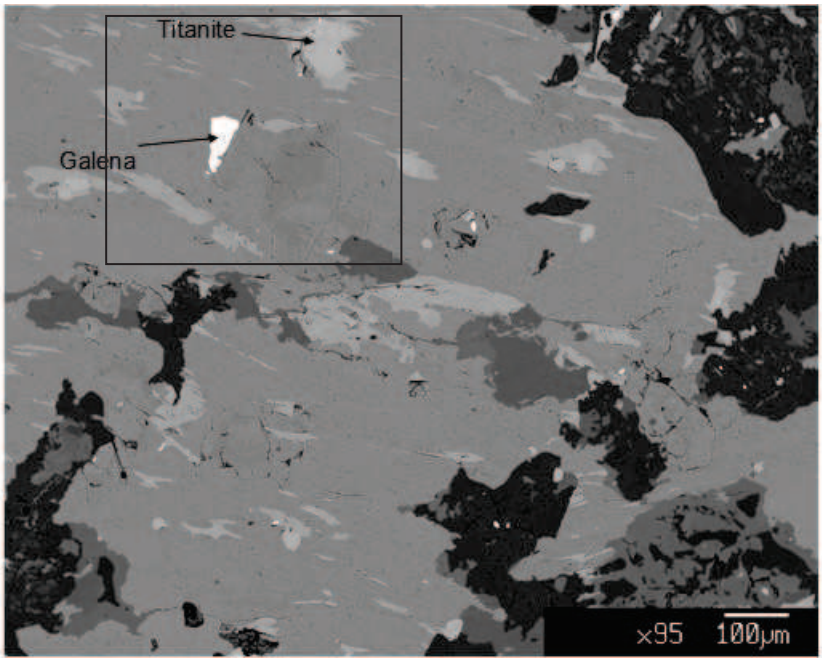

Detail of figure 14

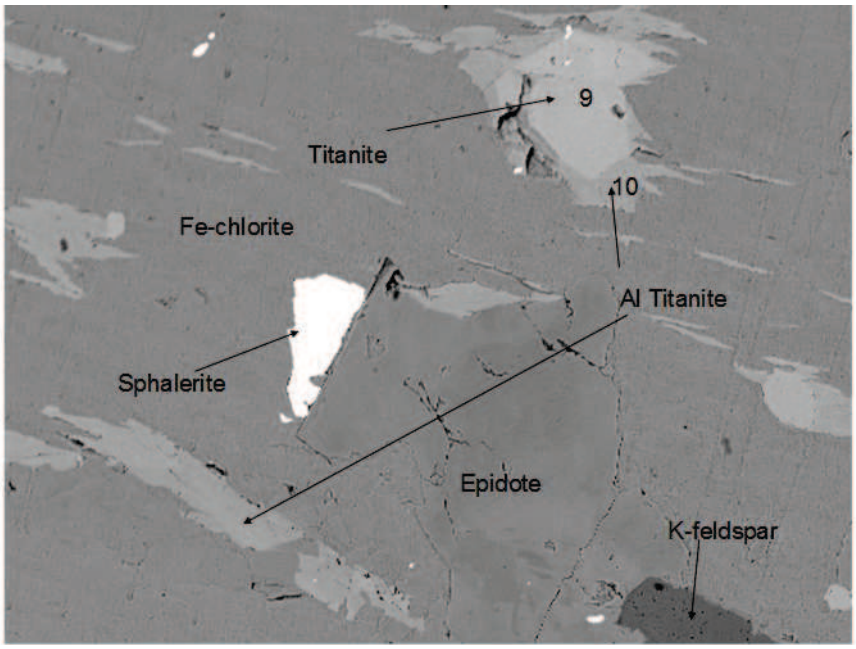

Analysis 9 Titanite

Na2O	TiO2	MnO	K2O	MgO	Cr2O3	FeO	CaO	Al2O3	SiO2	NiO	Total
0	38.47	0.0484	0.0029	0.0227	0	0.4722	28.94	1.156	31.17	0.0115	100.2936

Analysis 10 Al-Titanite

Na2O	TiO2	MnO	K2O	MgO	Cr2O3	FeO	CaO	Al2O3	SiO2	NiO	Total
0.0069	28.62	0.0052	0.0142	0.0764	0.0099	0.6945	29.54	7.49	32.13	0	98.5872

Analysis 11 Epidote

Na2O	TiO2	MnO	K2O	MgO	Cr2O3	FeO	CaO	Al2O3	SiO2	NiO	Total
0	0.0169	0.0864	0.016	0.0103	0.009	7.88	23.54	26.88	39.22	0.0761	97.7348

Figure 15

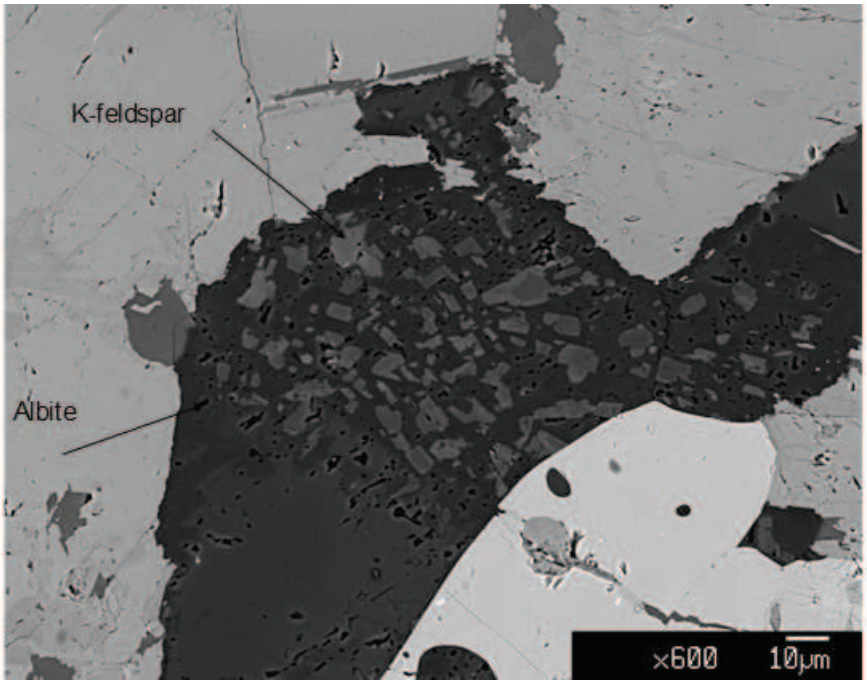

Analysis 12 K-Feldspar

Na2O	TiO2	MnO	K2O	MgO	Cr2O3	FeO	CaO	Al2O3	SiO2	NiO	Total
0.2691	0.0185	0	15.52	0.0085	0.0284	0.2188	0.0483	19.03	67.38	0	102.5215

Analysis 13 Albite

Na2O	TiO2	MnO	K2O	MgO	Cr2O3	FeO	CaO	Al2O3	SiO2	NiO	Total
10.44	0	0	0.1647	0.0062	0	0.1766	1.55	21.03	68.55	0.0009	101.9184

Figure 16

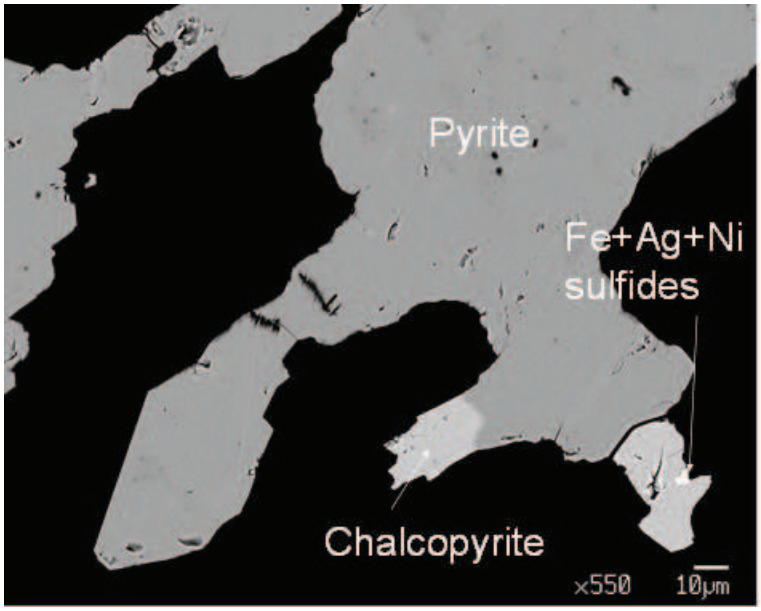

Sample AM2 (Amphibolite – marble contact)

Figure 17 Contact between marble on the right and amphibolite on the left

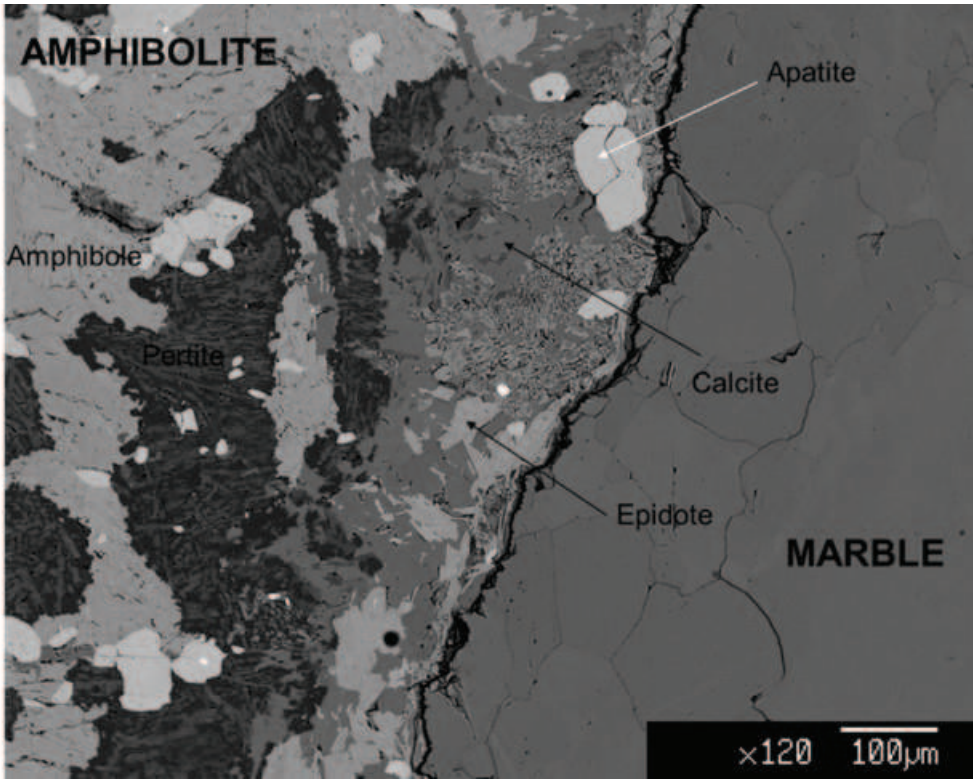

Figure 18

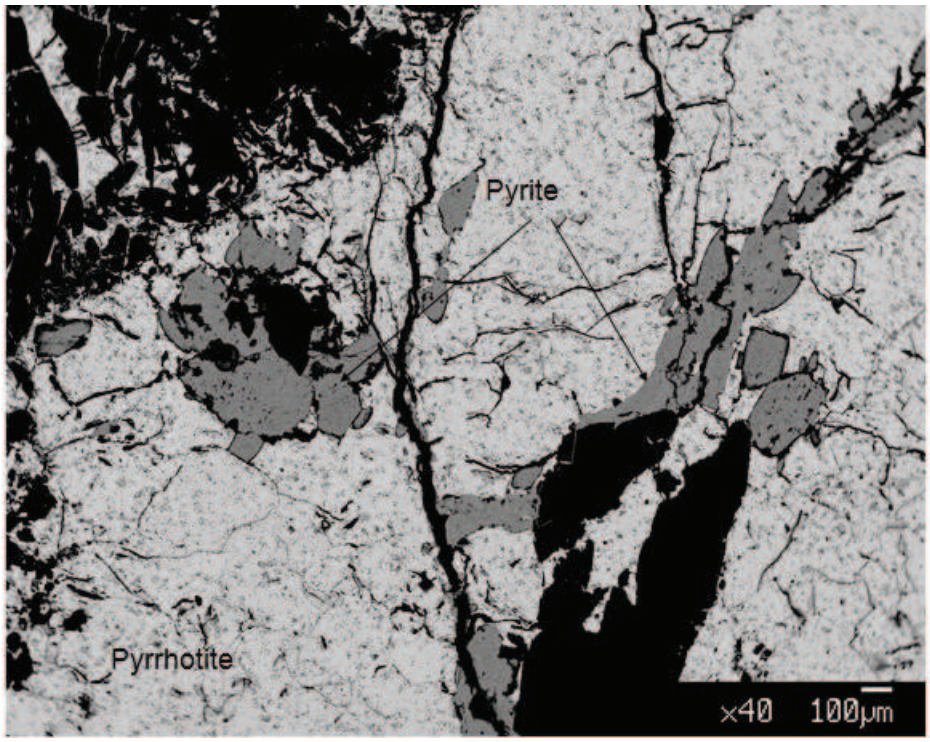

Summary of microprobe analysis

No.	Na2O	TiO2	MnO	K2O	MgO	Cr2O3	FeO	CaO	Al2O3	SiO2	NiO	Total	Comment	Lithotype	
1	0,34	0,00	0,01	16,31	0,00	0,00	0,38	0,06	18,56	66,46	0,04	102,1622	AM3-1	Coarse grain marble	k-feldspar
2	0,01	34,07	0,03	0,00	0,02	0,12	0,02	29,39	3,85	31,13	0,00	98,6412	AM3-2	Coarse grain marble	titanite
3	0,01	0,01	0,05	0,00	0,34	0,03	0,07	58,28	0,00	0,00	0,00	58,7865	AM3-3	Coarse grain marble	Calcite
4	0,30	0,02	0,00	16,27	0,00	0,00	0,01	0,07	18,56	65,57	0,00	100,7979	AM3-4	Coarse grain marble	k-feldspar
5	0,05	0,01	0,00	10,92	1,08	0,04	0,17	0,27	36,32	50,60	0,00	99,466	AM3-5	Coarse grain marble	muscovite
6	0,22	0,05	0,00	10,67	0,18	0,01	0,07	0,18	38,93	48,30	0,05	98,6421	AM3-6	Coarse grain marble	muscovite
7	0,02	0,00	0,04	0,13	13,70	0,02	0,85	0,51	33,44	39,42	0,00	88,1162	AM3-7	Coarse grain marble	Chlorite
8	0,78	0,22	0,00	9,26	0,02	0,06	0,05	0,12	19,63	50,78	0,02	80,9431	AN3B-1	Fine grain marble	Hyalophane
9	0,87	0,16	0,00	10,71	0,01	0,00	0,05	0,03	19,32	55,45	0,00	86,6007	AN3B-2	Fine grain marble	Hyalophane
10	0,01	0,00	0,17	0,01	30,63	0,00	3,31	0,18	20,16	31,06	0,02	85,5464	AN3B-3	Fine grain marble	Chlorite
11	11,39	0,00	0,03	0,02	0,00	0,00	0,00	0,63	19,66	68,90	0,00	100,6262	AN3B-4	Fine grain marble	albite
12	0,13	0,01	0,00	10,29	2,65	0,05	0,39	0,08	31,16	50,85	0,00	95,6158	AN3B-5	Fine grain marble	muscovite
13	0,40	0,00	0,10	0,29	21,54	0,01	0,96	13,43	2,24	51,34	0,03	90,3363	AN3B-6	Fine grain marble	tremolite
14	0,24	0,03	0,02	15,99	0,01	0,01	0,36	0,05	18,71	65,66	0,00	101,0774	Musso5 -1	Amphibolite	k-feldspar
23	0,01	28,62	0,01	0,01	0,08	0,01	0,69	29,54	7,49	32,13	0,00	98,5872	Musso5 -10	Amphibolite	al-titanite
24	0,00	0,02	0,09	0,02	0,01	0,01	7,88	23,54	26,88	39,22	0,08	97,7348	Musso5 -11	Amphibolite	epidote
25	0,27	0,02	0,00	15,52	0,01	0,03	0,22	0,05	19,03	67,38	0,00	102,5215	Musso 5 -12	Amphibolite	k-feldspar
26	10,44	0,00	0,00	0,16	0,01	0,00	0,18	1,55	21,03	68,55	0,00	101,9184	camp 5 -13	Amphibolite	albite
15	1,50	0,75	0,28	0,76	8,34	0,04	20,41	11,51	10,84	44,04	0,00	98,4744	camp 5 -2	Amphibolite	amphibolite
16	0,01	38,62	0,07	0,01	0,01	0,00	0,51	28,76	1,31	31,35	0,07	100,7277	camp 5 -3	Amphibolite	titanite
17	11,62	0,00	0,03	0,04	0,00	0,03	0,24	0,10	19,74	70,10	0,00	101,9002	camp 5 -4	Amphibolite	albite
18	0,03	52,64	4,43	0,00	0,02	0,00	44,68	0,29	0,00	0,00	0,07	102,1665	camp 5 -5	Amphibolite	ilmenite
19	8,25	0,00	0,00	0,07	0,02	0,00	0,13	5,80	24,19	62,31	0,01	100,771	camp 5 -6	Amphibolite	albite
20	0,00	0,13	0,27	0,01	11,07	0,00	32,52	0,16	19,51	26,40	0,06	90,1433	camp 5 -7	Amphibolite	Fe-chlorite
21	0,00	0,08	0,24	0,00	0,02	0,00	9,46	23,39	25,74	38,91	0,00	97,8346	camp 5 -8	Amphibolite	epidote
22	0,00	38,47	0,05	0,00	0,02	0,00	0,47	28,94	1,16	31,17	0,01	100,2936	camp 5 -9	Amphibolite	titanite

Common minerals vs analysis number matrix

Phases	MUSSO5 (Amphibolite)	AM3 (Coarse grain marble)	An3b (Fine grain marble)
albite	**3**		**1**
Al-titanite	1		
amphibolite	1		
calcite		1	
chlorite		**1**	**1**
epidote	2		
Fe-clorite	1		
hyalophane			2
ilmenite	1		
K-feldspar	**2**	**2**	
muscovite		**2**	**1**
titanite	**2**	**1**	
tremolite			1

Mineral phases comparison

Coarse grain marble vs fine grain marble

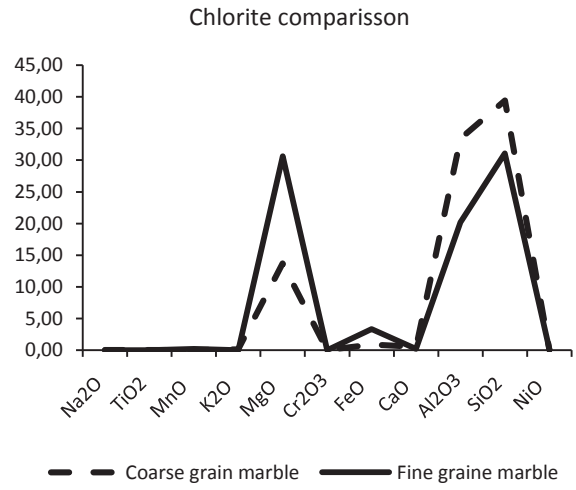

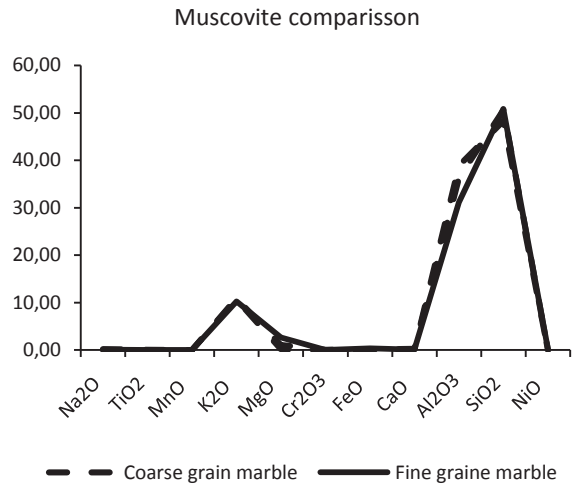

Amphibolite vs coarse grain marble

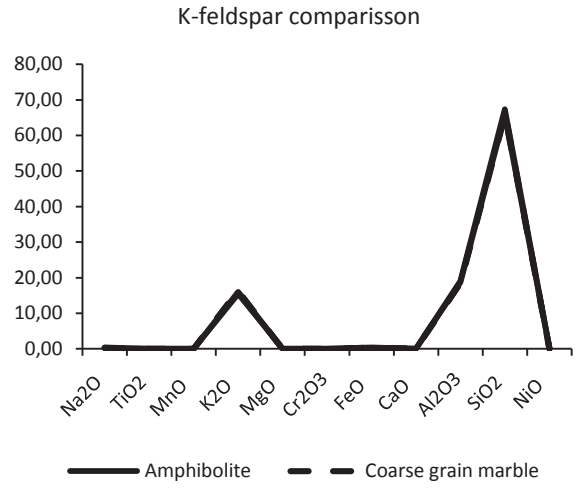

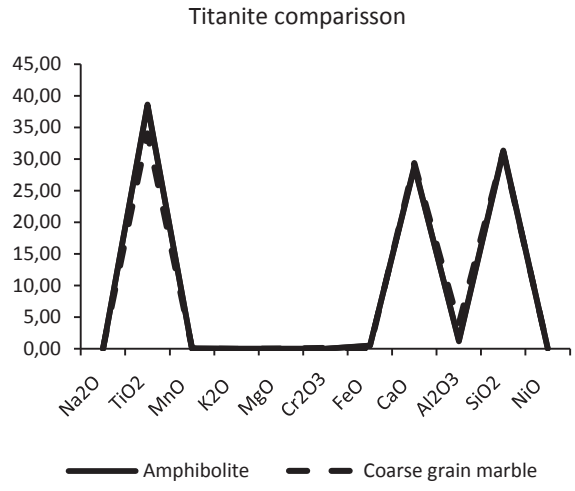

2.7 Appendix 3: Esem images

Micro images of sample 19: amphibolite-marble contact from the Musso quarry

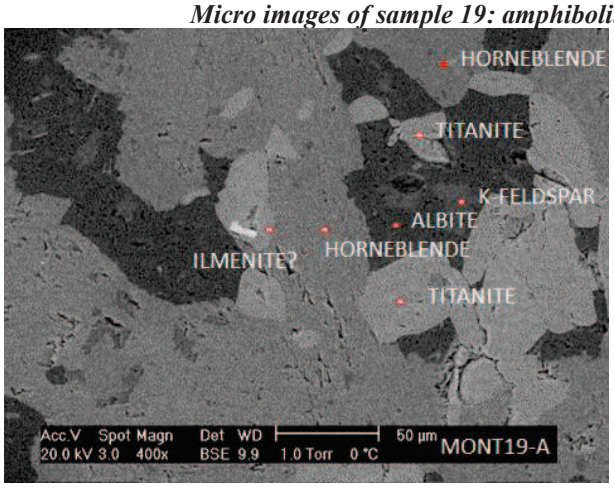

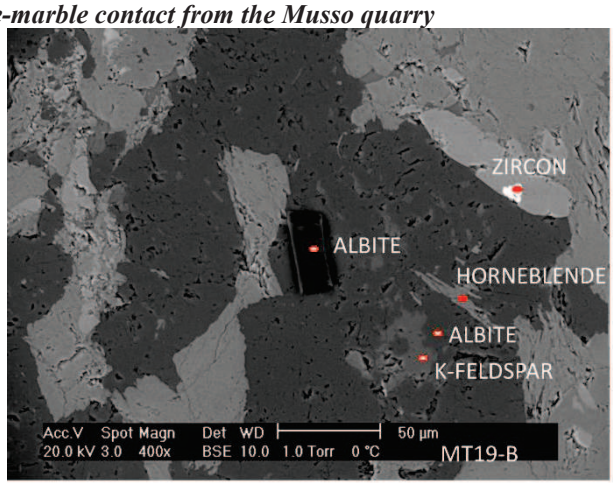

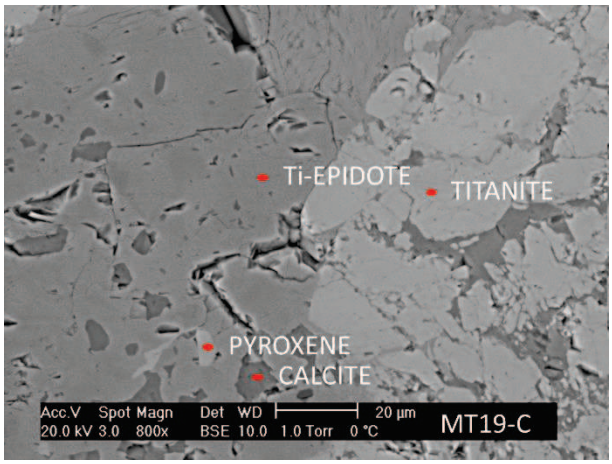

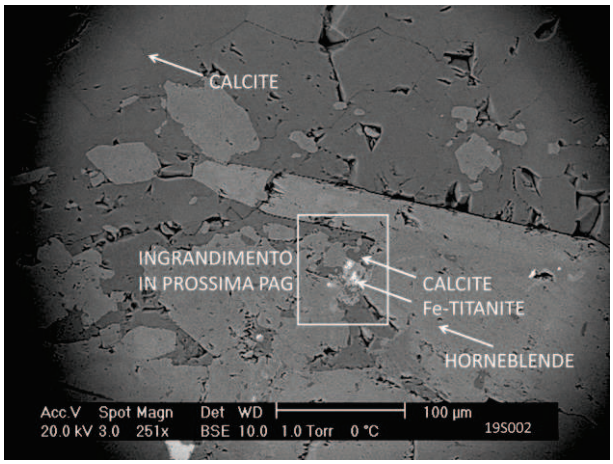

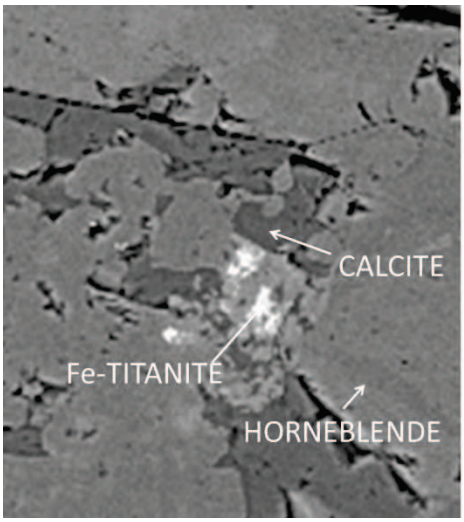

3 Musso Fault Zone evolution

The central Southern Alps, in northern Italy represent a non-metamorphic fold-and-thrust belt formed during the Alpine orogenic events. The age and extent of Alpine deformation, from ductile-brittle to mainly brittle, in this area is a matter of debate (De Sitter & De Sitter-Koomans, 1949; Laubscher, 1985; Gaetani & Jadoul, 1989). The absence of a well recognizable Alpine metamorphism significantly hampers the reconstruction of the timing of the deformation events before the Alpine orogenesis.

In the Lake Como region, a regional fault zone develops from East to West over about 30 km, across the lake, within the central Southern Alps basement. This is characterized by a large band of mylonitic marble including hectometric coarse grained undeformed marble bodies (Marmo di Musso, extensively described in chapter 2 of this work) associated with minor micaschists, metabasites and intruded by pegmatites. This is known as the Musso fault zone (Tahlawi, 1965). On the western side of Lake Como this fault zone runs along the Albano valley, where a recent field survey has revealed extensive occurrences of pseudotachylytes associated to fractures and shear zones cutting the basement.

Pseudotachylites are interpreted to be frictional melting product related to co-seismic slip along faults (Sibson, 1975; Magloughlin and Spray, 1992; Swanson, 1992), as fault plane and/or injection veins (Sibson, 1975). Pseudotachylyte can provide mechanic and time constraints of the fault activity. In particular, in the case of Musso, the dating can constrain the time of activity or reactivation of this intra-basement fault occurring on both sides of Lake Como: was this fault Alpine or pre-Alpine? Which role did it play in the evolution of the central Southern Alps basement?

The Musso fault could have genetic relations with other faults of the central Southern Alps responsible for the Mesozoic extension of the Liguro-Piedmont Ocean, but it could have been easily re-activated during both the Cretaceous-Paleocene orogenesis or during the Tertiary transpression along the Insubric Line.

The peculiarity of the Musso fault zone is the presence of the nearly undeformed rock portions within hectometric lithons (Marmo di Musso exploited since Roman time in the Musso quarries), the strong difference in the texture and mineralogical composition from the surrounding basement rocks (including marbles), the extension of the mylonitic deformation, the presence of siderite veins filling Musso fractures, and the extensive occurrence of pseudotachylytes. The Musso fault was characterized by large fluid circulation, here demonstrated by the presence of

several Fe carbonate- veins filling fractures and by paleo-earthquakes events as demonstrated by the numerous pseudotachylyte veins found in Piona and in the Albano valley.

3.1 Geological overview

The studied area is located in the northern part of Lake Como, Italy (Fig. 1). It is included in the Val Colla basement which is part of the central Southern Alps domain derived from the Mesozoic passive margin of the Adria promontory (Africa plate), after the closure of the Tethys Ocean (Liguro-Piedmont branch) during the collision of the African and European plates (Laubscher, 1974). The central Southern Alps are bounded by the Insubric Line to the north and, to the south, they infill under the Quaternary Po Plain deposits. The central Southern Alps are composed of amphibolite to greenschist basement and Carboniferous, Permian and Mesozoic sedimentary sequences. The basement includes various tectono-metamorphic units: Strona-Ceneri, Scisti dei Laghi, Val Colla, Orobic (Colombo & Tunesi, 1990; Di Paola et al., 2000, Spalla et al., 2002). At the regional scale, in these basement units, the main tectono-metamorphic event was Variscan with retrograde metamorphic assemblage older then 312Ma (Siletto et al., 1993, Di Paola et al., 2000; Diella et al., 1992, Spalla et al., 2002). A low pressure-high temperature tectono-metamorphic event, recorded between 290 and 180Ma (Mottana et al., 1985) was followed by a rifting stage.

Structural and petrological data suggest that a continuous extensional deformation affected the Southern Alps from late Variscan/Permian to Jurassic (Brodie & Rutter, 1987; Brodie et al., 1989; Bertotti, 1991) as demonstrated by ductile to brittle deformation bands present in the basement and in the Permo—Mesozoic cover sequences (Val Colla fault, Lugano-Val Grande Line, Musso fault, Porcile Line) (Fig. 1). As an example, the Lugano-Val Grande fault is interpreted as a low-angle extensional fault which controlled the evolution of the Mt. Generoso sedimentary basin, it was steepened during Alpine tectonics (Bertotti et al., 1993). Within the Piona and Musso (Val Colla) basement, a thermal anomaly developed at late Triassic as indicated by occurrence of sillimanite, andalusite and intrusion of pegmatites in the basement (Sanders et al., 1996).

During the Alpine orogenesis, the Late Permian - Early Triassic sequences accommodate alpine thrusting from Cretaceous (Schumacher 1997). Both, the basement and the sedimentary cover of the central Southern Alps have been thrusted and folded by the Alpine tectonics. Late E-W strike-slip, mainly driven by the Insubric Line, fragmented some of the Alpine thrusts and reactivated some others like the Musso Fault as transcurrent fault.

The Musso Fault Zone (MFZ)

In the area involved by the Musso Line (Musso Fault Zone, MFZ), the basement (Val Colla) comprehends three tectono-metamorphic units, from north: I) the Domaso-Cortafò Zone - DCZ, II) the Dervio-Olgiasca Zone - DOZ and III) the Monte Muggio Zone MMZ (see Fig. 2; El Tahlawi, 1965; Bertotti et al., 1993; Schumacher, 1996; Spalla et al., 2002), separated from each other by pre-Alpine mylonitic bands with tens of kilometers of extensions, reactivated in Alpine age. The MFZ is between the DCZ and DOZ (Schumacher and Laubscher, 1997) and the Lugano-Val Grande Line between the DOZ and the MMZ (Bertotti et al., 1993). The MFZ consists of 100-500 m wide fault rocks bands composed of mylonites, ultramylonites and phyllonites. Mylonites formed under greenschist metamorphic conditions. Along the northern border of the Musso Fault, DOZ metapelites are transformed into chlorite, white mica, albite and quartz ribbons ultramylonites and phyllonites with "s-c" structures, indicating a dextral shear sense of displacement (Bertotti et al., 1993; Spalla et al., 2002). Mylonites and ultramylonites are further reworked, fractured and often reduced to small slivers within a cataclastic breccia. pseudotachylytes, perhaps developed at different stages of fault activity, are common. The Musso Line has been interpreted in different ways: as the easternmost part of the Val Colla fault (El Tahlawi, 1965) within basement (Fumasoli, 1974), as a Permo-Mesozoic normal fault possibly active contemporarily to the Lugano-Val Grande Fault successively reactivated in brittle conditions (Bertotti, 1994; Gosso, 1996; Schumacher & Laubscher, 1996), as an Alpine right transcurrent fault (Schumacher, 1997), as a greenschist mylonitic band separating the metapsammitic basement of the Domaso-Cortafò Zone (DCZ) from the metapelites of the inner Val Colla Zone (Colombo, 1999) not affecting the Dolomia Principale of the Monte Pozzuolo and so predating the Norian. Bertotti et al., (1999) suggested that the Alpine contraction, roughly N-S, steepened Paleozoic to Mesozoic rocks and paleo-faults and caused upper and middle crust (ref. DOZ and DCZ) to detach from their substratum along the Musso fault and brought them into a steep south dipping position.

Geochronological constraints of basement of the Musso fault zone

The DOZ basement cropping out south of the MFZ was dated on pegmatite (K-feldspar-muscovite), schists (muscovite-biotite) and marble (calcite-white mica) by Rb/Sr, obtaining cooling ages between 195 and 215Ma (Bertotti et al., 1999); this age range was interpreted as due to a rapid cooling of the basement after the Mesozoic rifting. This cooling at the end of Trias is confirmed also for the MFZ, by the zircon fission track cooling age of 210±84Ma obtained in the basement just north of the Musso Line, to the E of the Monte Pozzuolo (Closure temperature for zircon fission tracks is approximately between 230-250°C). This results are comparable to

those obtained for the Monte Muggio zone. By contrast, south of the Musso Line, near the Piona Peninsula Bertotti (1999) obtained zircon fission tracks ages of 49±7Ma and interpreted this cooling as due to the Alpine deformation. This deformation is constrained by reliable Rb/Sr and K/Ar isotopic data (Del Moro et al., 1983) from the Adamello pluton (43–31 Ma) which crosscuts part of the fold and thrust structures of the central Southern Alps (Del Moro et al., 1983; Brack, 1984; Schönborn, 1992) and by U-Pb zircon data on magmatic bodies postdating the thrust faults (D'Adda et al., 2010) constraining a pre-Middle Eocene times thrust activity west of the Adamello. Several pseudotachylyte veins are associated to the Alpine thrusts as the Porcile and Orobic thrusts and they were extensively studied and dated (Siletto, 1990; Meier, 2003; Carminati & Siletto, 2005). In the Northern Lake Como basement pseudotachylites are associated to both the Musso Fault Zone and the Lugano-Val Grande Fault Zone (Bertotti, 1993; Schumacher, 1997; Spalla et al., 2002), but no one studied them in detail. Zwingmann & Mancktelow (2004) dated clay-rich fault gouge from a fault approximately parallel to and 50 m south of the Periadriatic Fault in Morobbia Valley, within the Scisti dei Laghi unit. They obtained K–Ar ages ranging from 19.6 to 28.2 Ma (Oligocene).

Fig. 4 Structural scheme of the Northern Lake Como area after: Fumasoli 1965, El Tahlawi 1974, Schumacher 2001, Mottana et al, Bertotti et al, Spalla et al 2002. Black points indicate the occurrence of pseudotachylites. Rb/Sr of basement rocks and pegmatites and zircon fission tracks (ZFT) ages after Bertotti et al., 1999.

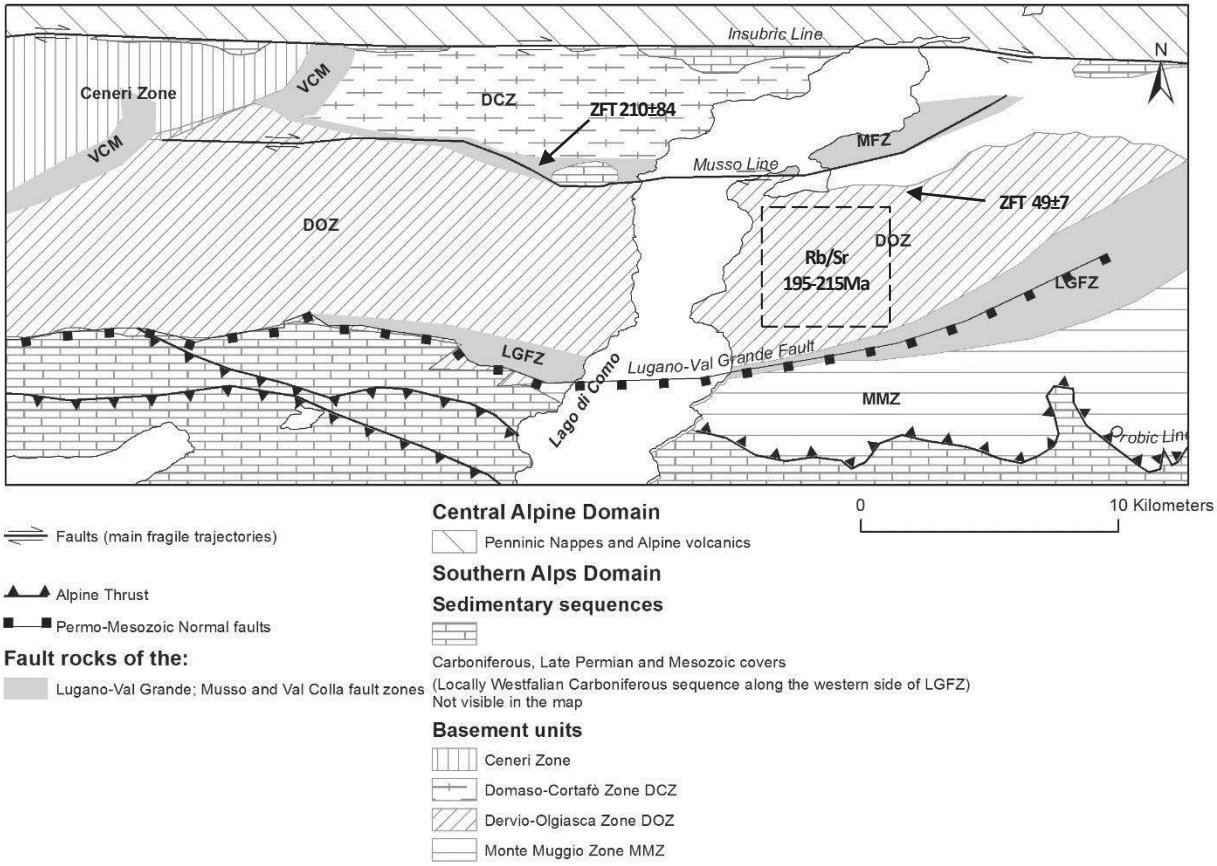

3.2 Methods

This study is based mostly on field survey of the Musso fault zone. The survey aimed at mapping the fault rocks, the tectonic structures such as faults with lineation's, cataclastic, mylonitic and ultramylonitic bands, and the Fe-carbonate and sulphide mineralizations. The field survey was then supported by analysis in thin section with ESEM microscopy technique (low vacuum SEM) and petrographic microscope. EWS semi-quantitative analysis were performed to determine the mineral phases. Those analysis are reported in APPENDIX 1.

3.2.1 Geo-structural database

After collecting 2.000 structural data (foliations, fold axial planes, axes and lineations) in the field, a dedicated database was created using the Excel software. The data have then been selectively represented in stereographic projection (Schmidt type, lower hemisphere, Tectonics FP software) and contemporarily visualized on the geological map.

3.3 Musso Fault Zone lithologies

Along the Musso Fault Zone following lithotypes crop out:

1. Fe-carbonate veins
2. Marble lenses
3. Pegmatites
4. Mylonitic micaschists and gneisses
5. Pseudotachylites

1. **Fe-CARBONATE VEINS**: They have been observed mostly near Dongo, Tegano, Peglio and Forte di Fuentes localities, but they are widespread along all the MFZ (Fig. 6). These veins are widespread in the basement and forms a network of hydrothermal origin Fe-carbonate veins, mainly constituted by siderite and minor ankerite. They range in thickness from <1 cm to >50cm. The veins origin, by correlation with other similar mineralizations in the Southern Alps, appears to be due to circulation of fluids in extensive tectonic regime during Early-Triassic, Olenekian (250-245Ma) (discussed extensively in Montorfano et al., 2014). In the Albano Valley the siderite veins mainly have E-W direction, but often they are boudined or folded or dislocated with both the mylonitic and cataclastic Musso Line rocks (Fig. 3E and F)

2. **MARBLE LENSES:** several lenses outcrop within the MFZ or to the south of it, with in the DOZ. The marble lenses generally range from a meter to hundreds of meters in length. The only exception is the Musso marble lens (MML) which reaches almost 3km in length and 300 meters in width. The marble lenses are boudinaged in the schists and are elongated in E-W direction following the Musso fault. The main foliation of the marble generally is concordant with the surrounding MFZ basement, beside for the MML. The marble can be found as: layered coarse grain marble with mica and sulphides, dolomitic coarse grain marble, fine grain marble mylonitic and fine grain banded marble only along the major fault planes. Within the MML hornblende and/or biotite rich metabasites are transposed. These show preserved structures interpreted as derived from the primary emplacement of metric size dykes, interfingering structures, and contact band rich in actinolite and sulphides. The MML and its metabasites are discussed extensively in chapter 2 of this work.

3. **MYLONITES**: These are widespread within the MFZ, and alternated to less deformed but still cataclastic rocks still belonging to the fault zone. Mylonitization interested several lithotypes along the Musso Line: marble, metabasites, biotite-garnet gneisses and chlorite-albite micaschists. Several degree of mylonitization are observable. In some cases original fabric is still recognizable while in others it can only be inferred. A general description for the mylonites belonging to the Musso Line (Fig. 3A,B,C,D). Mylonitic texture with well-developed foliation individuated by new crystallized very fine white mica and chlorite (Fig. 3A,B,C,D). In some areas embryonic of S-C, C-C' and S-C' structures can be observed. Two generations of white mica occur: the first is preserved as porphyroclast within the mylonitic foliation (mica fish), the second is sericite growing along foliation plane. Biotite is poorly preserved as it appears to be not stable during shear process that led to the formation of the mylonite. Chlorite substitutes for biotite growing together with sericite. Quartz is dynamically recrystallized, with a strong grain size reduction along the mylonitic foliation. Plagioclase porphyroclasts show no evidence for recrystallization and appear instead interested by brittle micro-fault and cataclasis. The stability of chlorite instead of biotite together with the brittle behavior of plagioclase and the dynamic recrystallization of quartz point to temperature conditions comprised between 250°C and 350°C during the formation of the mylonite.

4. **PSEUDOTACHYLITES** (Fig. 4): Pseudotachylytes (PST) outcrop along the Musso Line with E-W direction (Fig. 9). It is possible to distinguish fault veins and injection veins. PST sizes range from 0,5mm to 5mm for the fault veins and up to 10cm for the injection veins. Both

melt generation surfaces (MGS) as well as injection veins (sensu Sibson, 1975) of pseudotachylyte crosscut the cataclastic fabric. Within pseudotachylyte veins, the clast/matrix ratio is highly variable, with the lowest ratio displayed by some injection veins (ca. 10/90). Within the largest veins the clast/matrix ratio is close to 20/80. The matrix of both MGS and injections veins appears black-colored both at parallel and crossed nicols, with the exception of an injection veins where recrystallization of fine mica aggregates could be recognized at the microscope (crossed nicols). Compositional zoning is not always visible. When visible it appears reflecting differential cooling of the injected melts or fluidal structures. Most of the clasts are made of sub-rounded quartz, with minor lithic sub-rounded clasts and also biotite, plagioclase and ilmenite clasts with irregular shapes (Fig. 4A and B). Pseudotachylyte veins can be locally affected by brittle fractures almost perpendicular to the length direction of veins. The composition of the glass result having high content in Na_2O+K_2O (generally around 10% with minimum of approximately 6.3% and maximum of 11.1%). Glass composition results to range from foidite to dacite composition (Fig. 4C).

3.3.1 Ductile deformation

The mylonitic foliation ranges widely from north-dipping in the Motto della Tappa area to south and east dipping in the Pizzo di Gino area (Fig. 5). The trend remains constant in the Albano Valley. On the eastern shore of the Lake, in the Piona Peninsula, the mylonitic foliation generally maintain a E-W direction but it becomes NE-SE in the Forte di Fuentes hill.

3.3.2 Brittle deformation

Siderite veins (Fig. 6): In the Albano Valley the siderite veins probably represents the oldest brittle event because they are found boudined within the mylonitic rocks thus predating mylonitization. They are also present in un-deformed rocks. In the DCZ, siderite veins mainly have E-W direction. In the DOZ they have high dipping angle but two direction trends are visible: N-S and E-W.

Pseudotachylytes (Fig. 7): pseudotachylytes are widespread in the Musso Fault Zone. They are almost uniformly E-W trending, subvertical, and only in few cases, in the Albano Valley area show NE dipping direction (Plot Albano Valley Fig7).

Cataclastic bands (Fig. 8): they are widespread in the area and range from 20cm to more than 10m in width and extend in length from tens to hundreds of meters. They are developed in phyllonitic schists or mylonites or also within not previously deformed rocks. The clast size also vary largely, from <mm size (gouges) to large >3cm (breccia). South of the Musso Line, in the Albano Valley, they mainly dip southwards, while proceeding further south in the DOZ they

may also dip to the east. North of the Musso Line, cataclastic bands dip NE to east and display both extensional and compressive kinematics (plot DCZ Fig. 8). The Triassic dolostone cover of Monte Pozzuolo also displays several cataclastic bands (plot Triassic covers in Fig. 8) They also seem to be concordant with those of the basement.

Faults planes in the Dongo area, near the Musso Line (fig. 9):

In the DOZ (first plot on the right in fig. 9) three families appear: i) one is mostly E-W directed, transcurrent in both directions (it could not be define a main direction); ii) the second has NW to SE direction and is associated to a traspressive movement dominated by right and normal movements; iii) the third is a NNE to SSW family characterized by revers movements.

(in following description we used the same roman number to correlate fractures families)

In the MML (central plot in Fig. 9) zone fractures family i) is well represented and maintain the same transcurrent characteristics; ii) is not present; iii) is well represented but with a compressive-towards north movements.

In the DCZ (plot on the left in Fig. 9) fractures family i) is not represented; ii) is slightly present with different distensive sense of kinematic; iii) is not present; it appears a new fractures family iv) with NE-SW direction associated to both distensive and reverse movements.

DOZ and MML have fractures family i in common. DOZ and DCZ have family ii in common. DCZ do not have share fractures families with MML. DCZ have a fourth family not recognized in the other areas.

In conclusion DOZ and MML have very diffuse E-W directed faults, while these do not appear as much in the DCZ. DOZ and DCZ have NW-SE traspressive (right and normal) faults that do not crop out in the MML.

3.3.3 New structural map of the Musso Fault Zone

The interpolation of the structural data derived from this study and previous field survey campaigns (El Tahlawi, 1965; Fumasoli, 1974, Schumacher, 1996; Spalla et al., 2002) lead to a new maps of the Musso Fault Zone (Fig. 10A and B).

In the map the DCZ basement is composed of biotite and white mica schists with lenses rich in garnets and staurolite (Fumasoli, 1974) with associated bodies of amphibolites that ranges from very fine to coarse grained, hornblende rich types (Spalla et al., 2002). The DCZ basement rocks are covered by Permian, Lower Triassic Servino and Noric dolostones along the Insubric Line.

The DOZ basement is bordered by the Musso Fault Zone, but the limit is not clearly identifiable; it consists in E-W directed shear bands including brittle and ductile deformed rocks and bands of less deformed basement rocks. Mylonitic marble and other mylonitic rocks appear to occur within the northern portion of the DOZ. Mylonitization and fault rocks extend broader then what

previously documented therefore we preferred draw a Musso Fault Zone that includes also the northern portion of the DOZ (dotted line in Fig. 10B.

The MFZ extends to the W and E from the Motto della Tappa to the Forte di Fuentes areas. The Monte Pozzuolo Noric dolostone overlays part of the MFZ. The relationship with the Norian dolostone of Monte Pozzuolo is still not definitely clear since not Permian nor Lower Triassic rocks have been found between this dolostone and the basement. The dolostone bedding is not clear. Cataclastic bands are dominant in the dolostone and similar to those occurring within the MFZ (Fig. 8).

The lateral terminations of the MFZ are still not well determined: to the west there is a gradual decrease in volume of mylonitic rocks, while the brittle rocks and pseudotachylites still largely occur. To the east, the Forte di Fuentes hill definitely represent a portion of the MFZ, characterized by marble lenses, pseudotachylytes, large volumes of mylonitic rocks and siderite mineralization .

Main foliations trends are represented in Fig. 10B (continuous gray lines). In this figure we plotted together foliations from different localities. The Musso Fault Zone does not have a typical foliation but it shows alternating E-W trending bands of deformed and un-deformed rocks.

In the Piona Peninsula the DOZ basement shows a E-W trending foliation. To the west (Pizzo di Gino and Val Cavargna) the foliation changes and is N-S trending, therefore revealing a different tectonic asset not yet determined. The to the west the DCZ shows a N-S foliation, different from the E-W trending in the eastern portion.

Fig. 3 Fault rocks along the Musso Fault

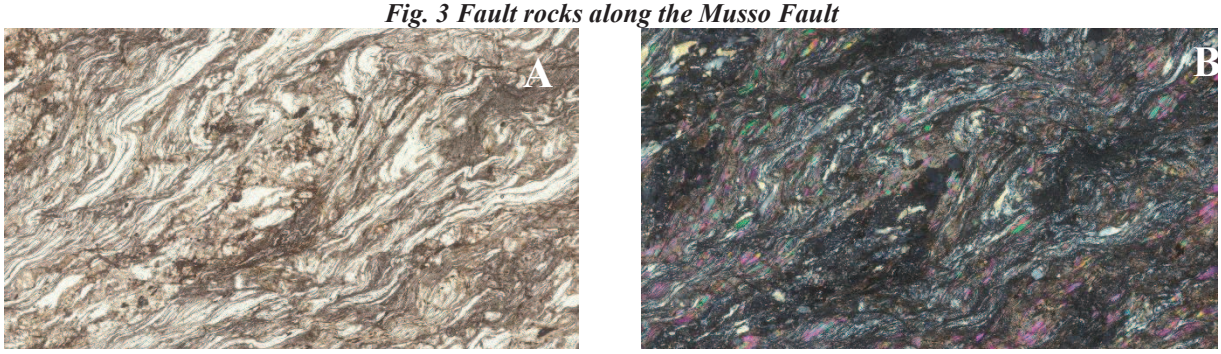

11 (sample ABB01) – Mylonitic micaschist

The sample has a mylonitic texture with a well developed mylonitic foliation individuated by newly crystallized white mica and chlorite. In some areas embryonic of s-c' structures could be observed. Two generation of white mica occur: the first is preserved as porhyroclast within the mylonitic foliation (mica fish), the second is sericite growing along foliation plane. Biotite is poorly preserved as it appears to be not stable during shear process that led to the formation of the mylonite. Chlorite substitutes for biotite and is also observed to grow together with sericite. Quartz is dynamically recrystallized, with a strong grain size reduction along the mylonitic foliation. Plagioclase porphyroclast show no evidence for recrystallization and appear instead interested by brittle micro-fault and cataclasi. The stability of chlorite instead of biotite together with the brittle behavior of plagioclase and the dynamic recrystallization of quartz point to temperature conditions comprised between 250°C and 350°C during the formation of the mylonite.

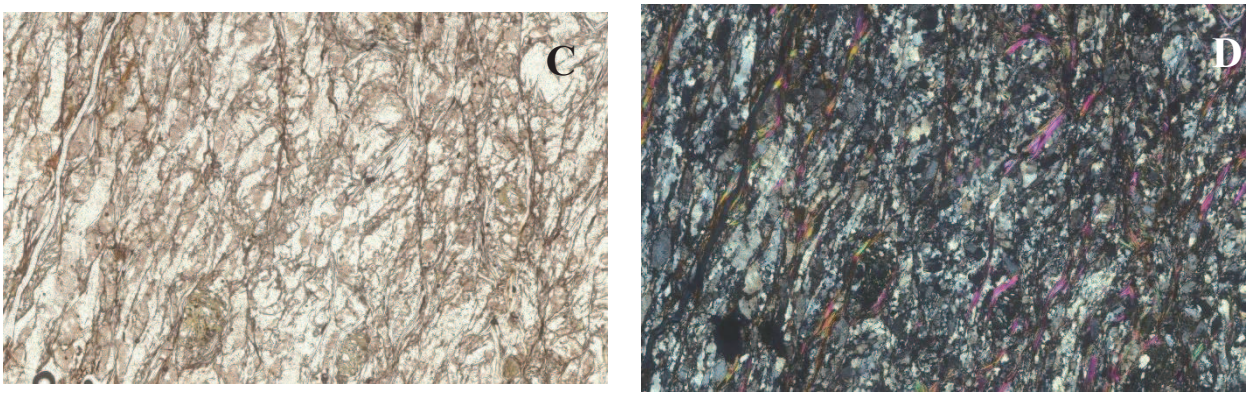

3 (sample GPS743E) – Two micas paragneiss

Garnet-bearing two-mica paragneiss with minor garnet relics. S-tectonitic fabric (i.e. foliated) with foliation marked by the (SPO) shape preferred orientation of white mica and biotite. Garnet occur as small (1-2 mm) porphyroblasts, pre-kinematic to the main foliation, which are almost completely substituted by aggregates of chlorite, quartz and minor oxides. Biotite shows evidence of retrogression as it is partly overgronw by chlorite. Within quartz-rich domains, a protomylonitic texture can be observed. Quartz crystals have high aspect ration (up to 1:5) and display evidence of dynamic recrystallization by subgrain rotations and grain boundary migration. Minor cataclastic phenomena affect the sample but the original texture is still well preserved.

Albano valley, road to Monti di Catasco: cataclastic band within phyllonites, with dismembered siderite veins (red).

Albano valley, near Punt de Reseg location: mylonitic gneisses with large quartz clast, and fragments of siderite veins.

Albano River bed: large grains mylonitic gneisses, showing shear bands and quartz clasts >10cm, and cm thick pseudotachylyte vein

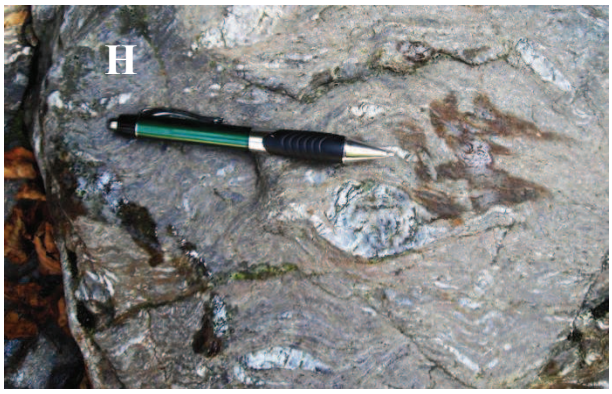

Albano River bed: mylonitc gneiss with large quartza clast showing right rotatio. Pencil oriented in E-W direction.

Piona Peninsula, entrance of the park of the Piona Abbey: fine grain mylonitic schists located to the S of the main Musso Fault.

Piona Peninsula, along the main Musso Fault: pseudotachylite withtin mylonitic gneisses

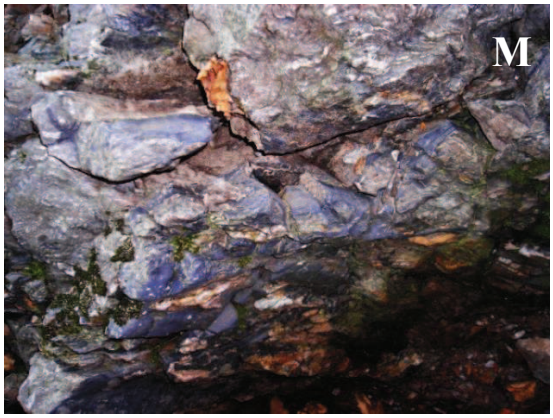

Albano Valley, near Punt de Reseg location: Pseudotachylites E-W directed within mylonitic gneisses

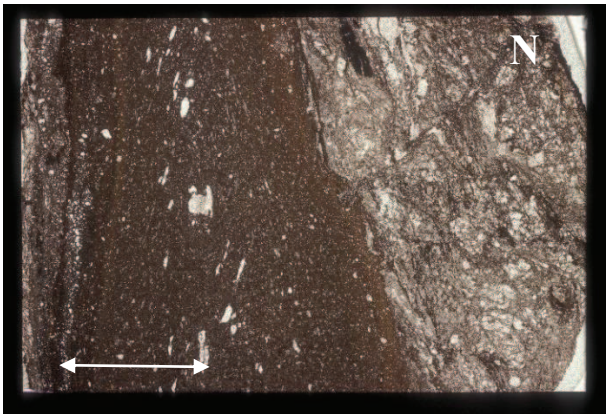

Albano Valley, near Punt de Reseg locality: pseudotachylyte (lateral injection vein) and its mylonitic and cataclastic host rock in thin section. White sign is one cm.

Fig. 4 Pseudotachylites of the Musso Fault ESEM analysis

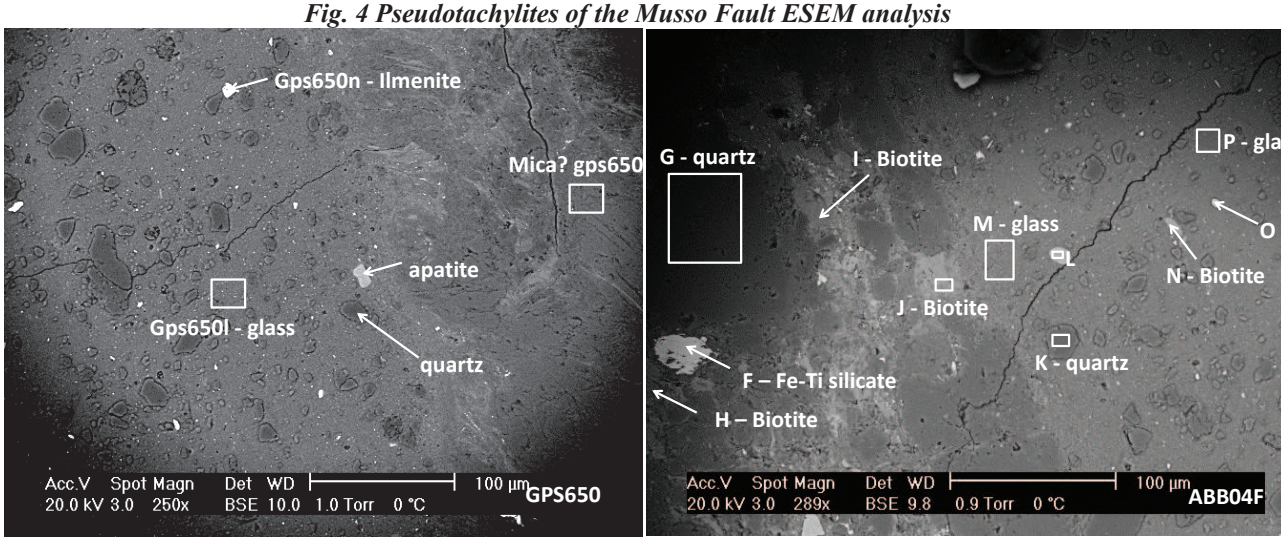

A: Albano Valley, Punt de Reseg locality: pseudotachylyte-hostrock contact (sample GPS650).

B: Piona Peninsula, near the Piona Abbey, along the Musso Fault: pseudotachylyte-host rock contact. In the glass quartz, biotite and apatite clasts.

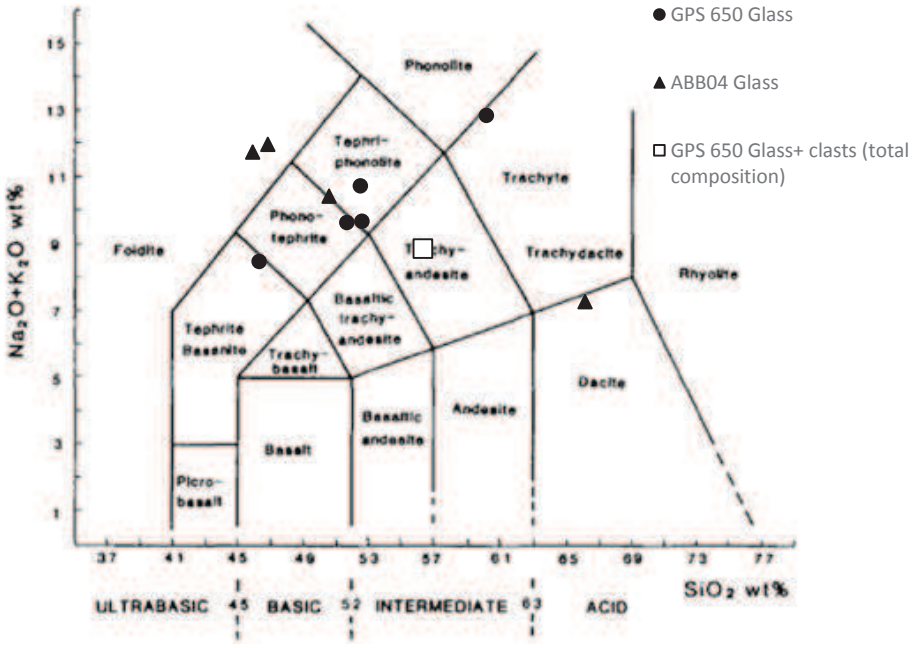

B

C: TAS diagram with semi-quantitative EWS analysis of pseudotachylytes glass. The composition of the glass result having high content in Na_2O+K_2O generally around 10% with minimum of approximately 6.3% and maximum of 11.1%. Glass composition results ranging from Foidite to Dacite composition.

Fig. 5 Structural data from the Musso Fault Zone and projection of the mylonitic foliation

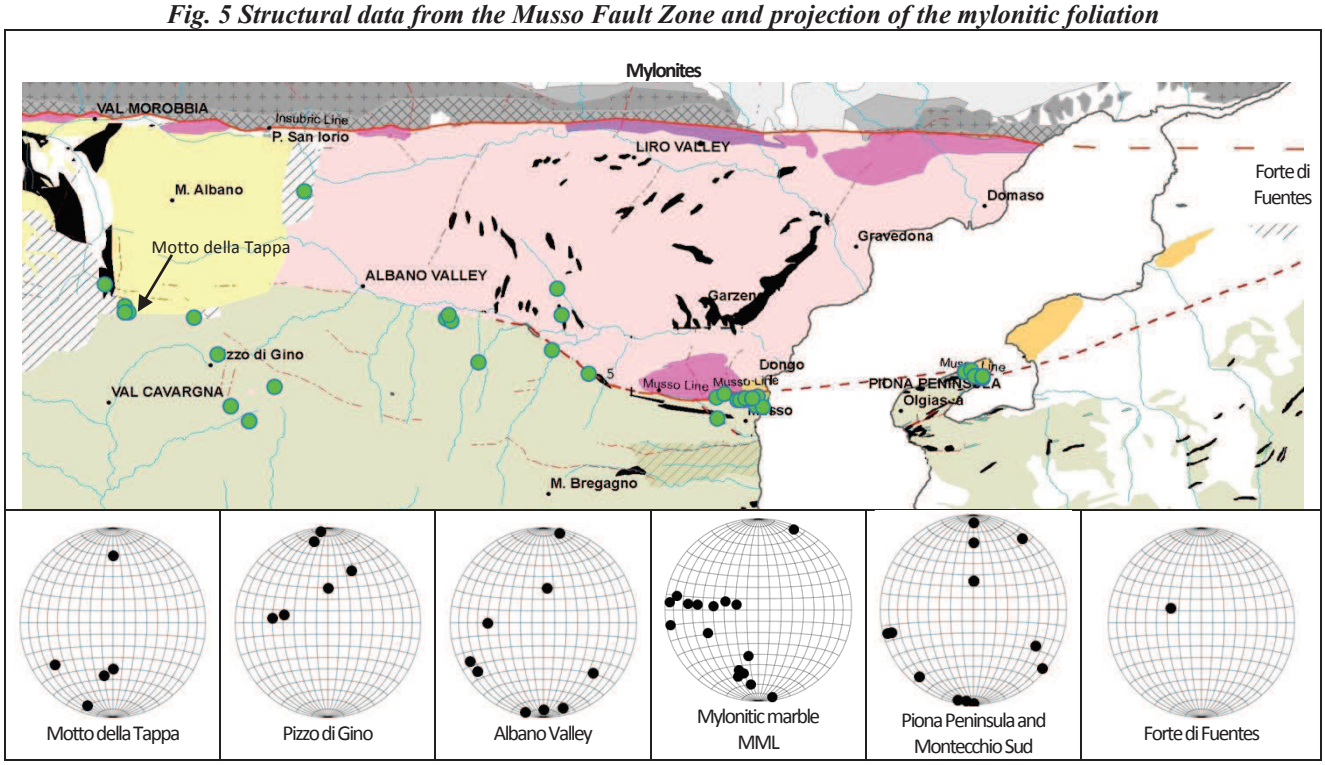

Fig. 5 Siderite veins

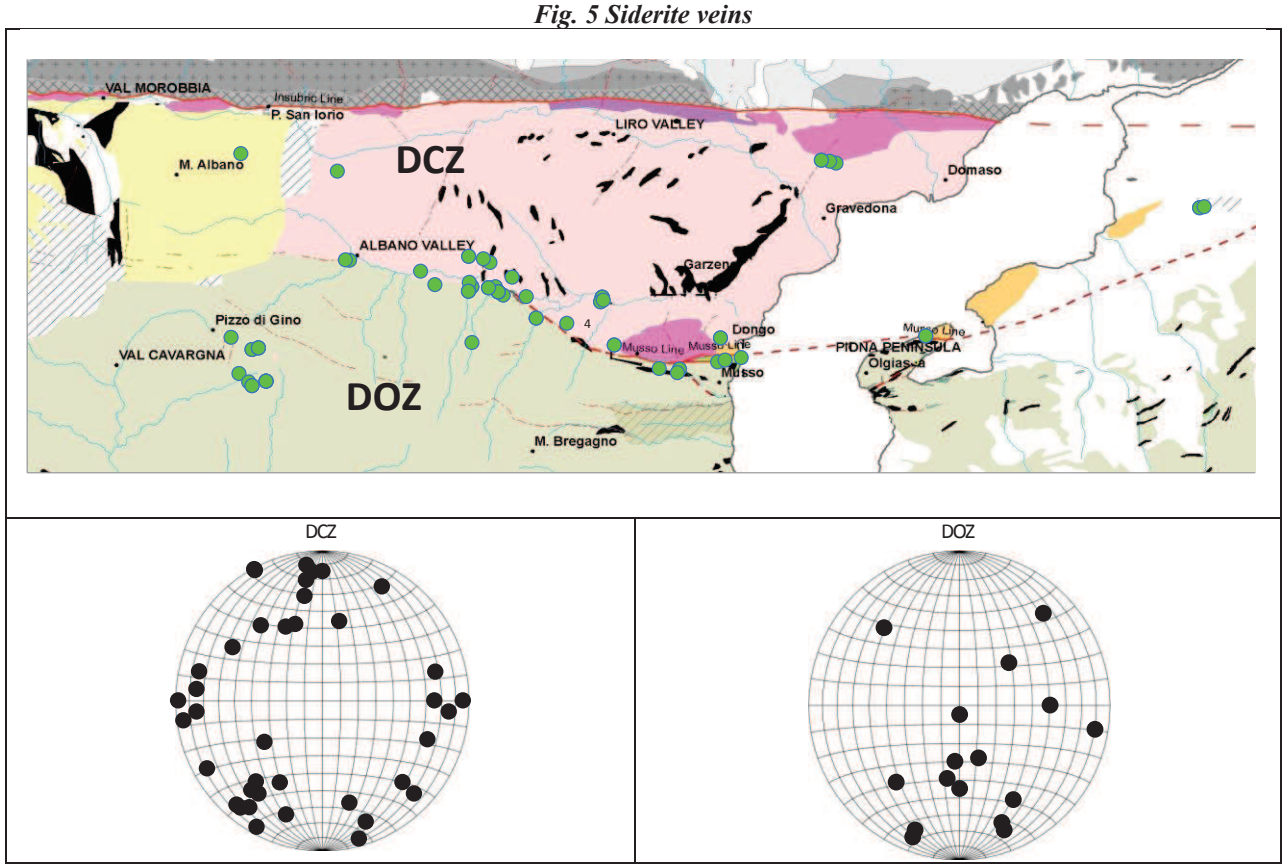

Fig. 6 Pseudotachylites of the Musso Fault Zone

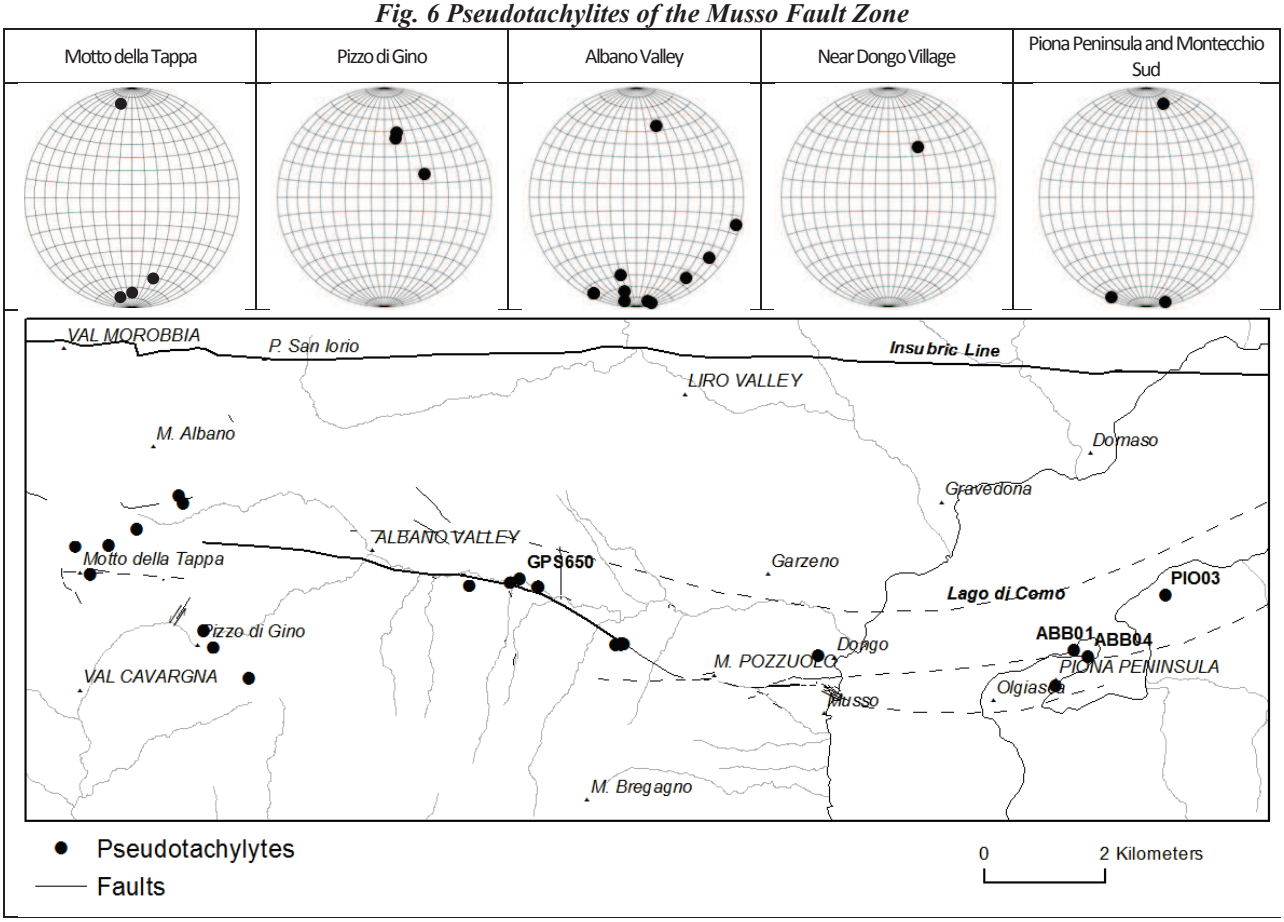

Fig. 7 Cataclastic bands

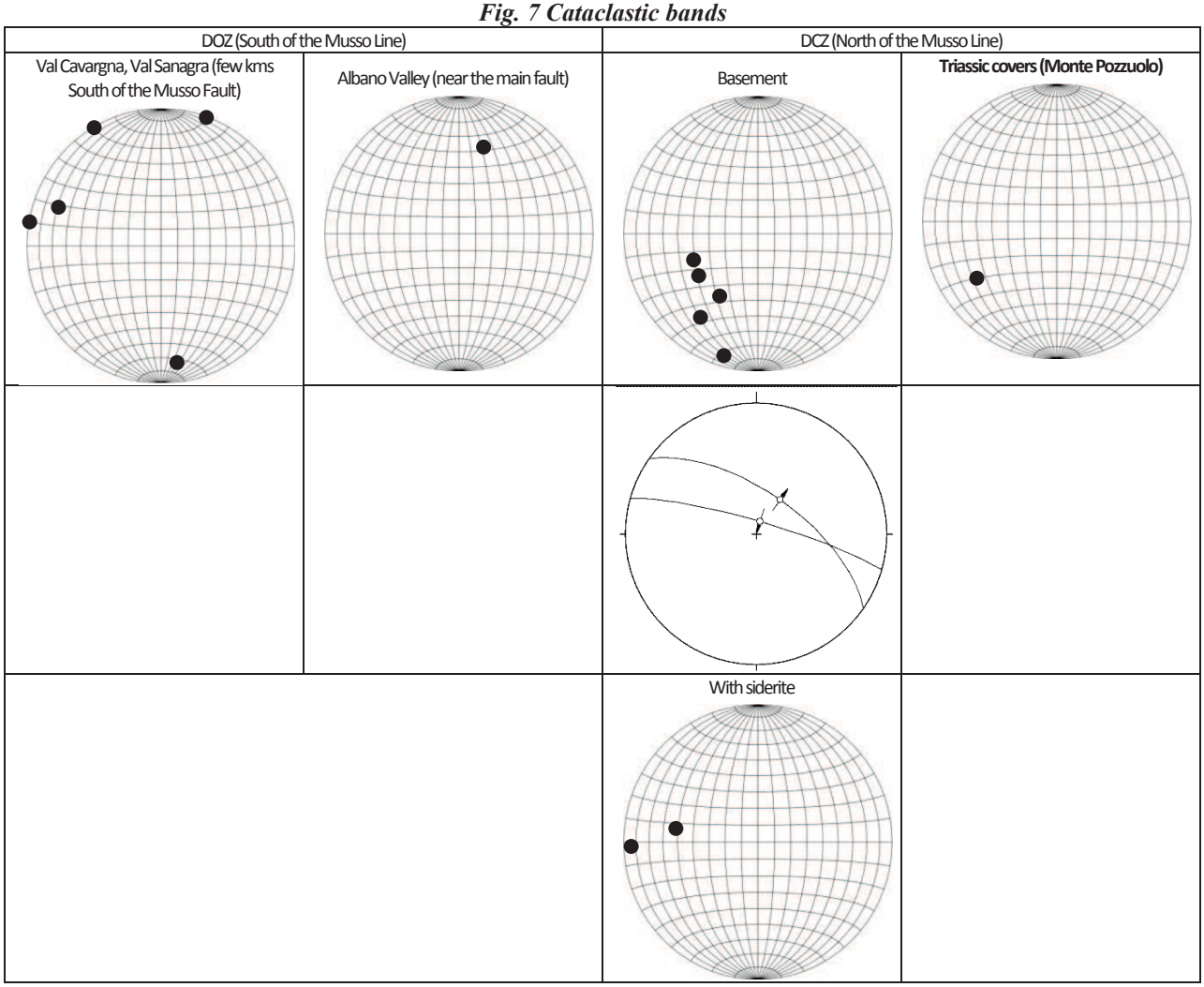

Fig. 8 Brittle deformation analysis between the Dongo and Musso villages, Western shore of Lake Como.

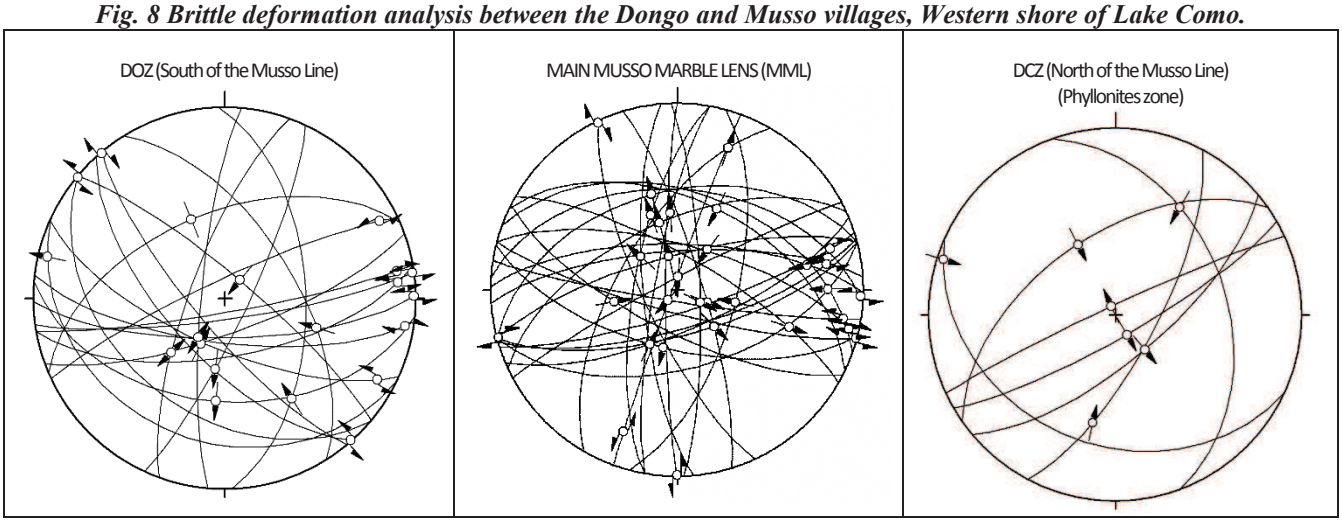

3.4 Discussion and conclusions

Marble lenses (Musso marble) are boudinaged along the Musso Fault Zone and represent the oldest rocks characterizing it. Their age is still not determined, but as widely discussed in chapter 2, the included metabasites have unique geochemical characteristics that do not allow to attribute them nor to DOZ nor the Strona Ceneri Border Zone amphibolite suites. There are no geochemical analysis of DCZ amphibolites. We speculate a Silurian-Devonian perhaps to Early Carboniferous age for the marble and the included metabasites due to partial geochemical similarity to the SCBZ amphibolites. Possibly the Musso Line developed in a Variscan context?
Geochronological and thermal data shows that the Northern Lake Como region experienced a late Variscan cooling and development of intrabasement shear zones thinning the Adriatic crust. These events were followed by sedimentation of Late Carboniferous and Permian sequences, intrusion of Permian plutons in the Orobic area. Development of a thermal anomaly at Middle Triassic in the area of the present Lake Como (Ferrara & lnnocenti, 1974; Mottana et al., 1985) was responsible of the emplacement of the Piona Peninsula pegmatites (Sanders et al., 1996).
In the Lake Como area continental extension started in the Norian (Bally et al., 1981; Bertotti, 1991) and continued to Liassic. The main structure, and the most studied, related to this event is the N -S trending, east dipping, Lugano-Val Grande normal fault zone. This fault is estimated to be listric at depth, bordering the Generoso sedimentary Basin. Onset of cooling roughly coincided with the first appearance of extensional faulting and continued during rifting. Therefore, absolute ages in the area are primarily controlled by the downward movement of isotherms and are not directly related to deformation (Bertotti et al., 1999). Could Musso Line belong to this group of regional faults thinning the Adria crust ?
In this context the oldest structures directly and incontrovertibly connected to the MFZ are the Fe-carbonate veins which are conserved also as boudinaged bodies within the mylonites. The Fe-mineralized veins belong, as discussed in Montorfano et al., 2014 (first chapter of this work), to the Early Trias, thus demonstrating that the Musso Line was already existing and allowing open fractures and circulation of the iron ore fluids. The same can be said also for the Grona Line, as demonstrated by extensive siderite mineralization presence and also mined in the Gaeta location and along the Lugano Val Grande Line in Val Cavargna (first chapter of this work).
Fe-mineralized veins are found in similar extensional context in all the Southern Alps. In other locations, siderite is emplaced also in the sedimentary covers up to the Servino Fm. It is possible that the MFZ was therefore bordering a small basin to the N, therefore justifying the presence of the sedimentary Monte Pozzuolo and Sasso Pelo

The mylonitic event of the MFZ possibly took place during Early Triassic thermal peak when temperature was low, around 250-350°C allowing crystallization of quartz-albite-chlorite-sericite associations, before the emplacement of the Piona pegmatites which do not show mylonitization even near the Musso Line. But was an other mylonitic event responsible of the strong deformation of the Musso marble near the Line?

From the Liassic to the onset of the Alpine compressive stage there is a long inactivity time span with no records for the Musso Fault. This would be concordant with the zircon fission tracks dated at 210±84Ma of Bertotti (1999) in the area that we consider as part of the MFZ and not of the DCZ, that shows a temperature lower than that estimated for the mylonites.

Alpine N-S contraction steepened Paleozoic to Mesozoic rocks and lineaments and caused upper and middle crust to detach from their substratum along the Musso Line and brought them into a steep south dipping position. This contraction was responsible of the ductile-britte deformation observed along the portion of the Musso Line with development of many pseudotachylytes. Pseudotachylyte veins were dated along the Orobic and Porcile thrusts and yielded ages of 79.9 ± 1.8 Ma for the Orobic and 73.2 ± 2.4 to 68.5 ± 1.9Ma for the Porcile indicating a Late Cretaceous (Campanian-Maastrichtian) activity (D'Adda, 2010). This was followed by uplift, erosion and deposition of deposits ("Lombardian flysch"?). A marked decrease in the terrigenous input (Bersezio et al. 1993; Di Giulio et al. 2001) up to the Middle Eocene, testifies for a period of relative tectonic quiescence. This indirect evidence suggests that no major deformation and thrusting occurred during Paleocene and the beginning of Eocene. Re-activation the Orobic and Porcile thrusts is constrained by a second generation of pseudotachylytes dated Eocene, between 56.4 ± 1.1 to 43.4 ± 2.1 Ma (D'Adda, 2010).

Between Middle and Late Eocene, E-W trending normal faults, affected the Orobic and Porcile previous compressive structures while widespread magmatic activity occurred in the Orobic Alps and in the Adamello area. The Adamello batholith was emplaced in a time interval of 43 to 31 Ma (Mayer et al. 2003), during which no evidence of compression was found (Brack 1984; John and Blundy 1993). Similar extensive deformation structures (distensive cataclastic bands Fig. 7) are found also in the Lake Como area, along the Musso and contiguous faults, possibly corresponding to the slightly younger but dated Oligocene in Val Morobbia by Zubringen (2009) and also mapped in this study along the MFZ. Finally, right strike-slip brittle deformation took place, visible along the largest fault planes, most probably driven by the Insubric Line.

Fig. 9: New structural map of the Musso Fault. Fig. A lithologies. B Main foliation trends. Black dots pseudotachylytes outcrops. Structural and lithological data: along and South of the Musso Fault from this study; North of the Musso Line after Fumasoli, 1974; East of Lake Como El Tahlawi, 1965; along the Lake shores Spalla et al., 2002

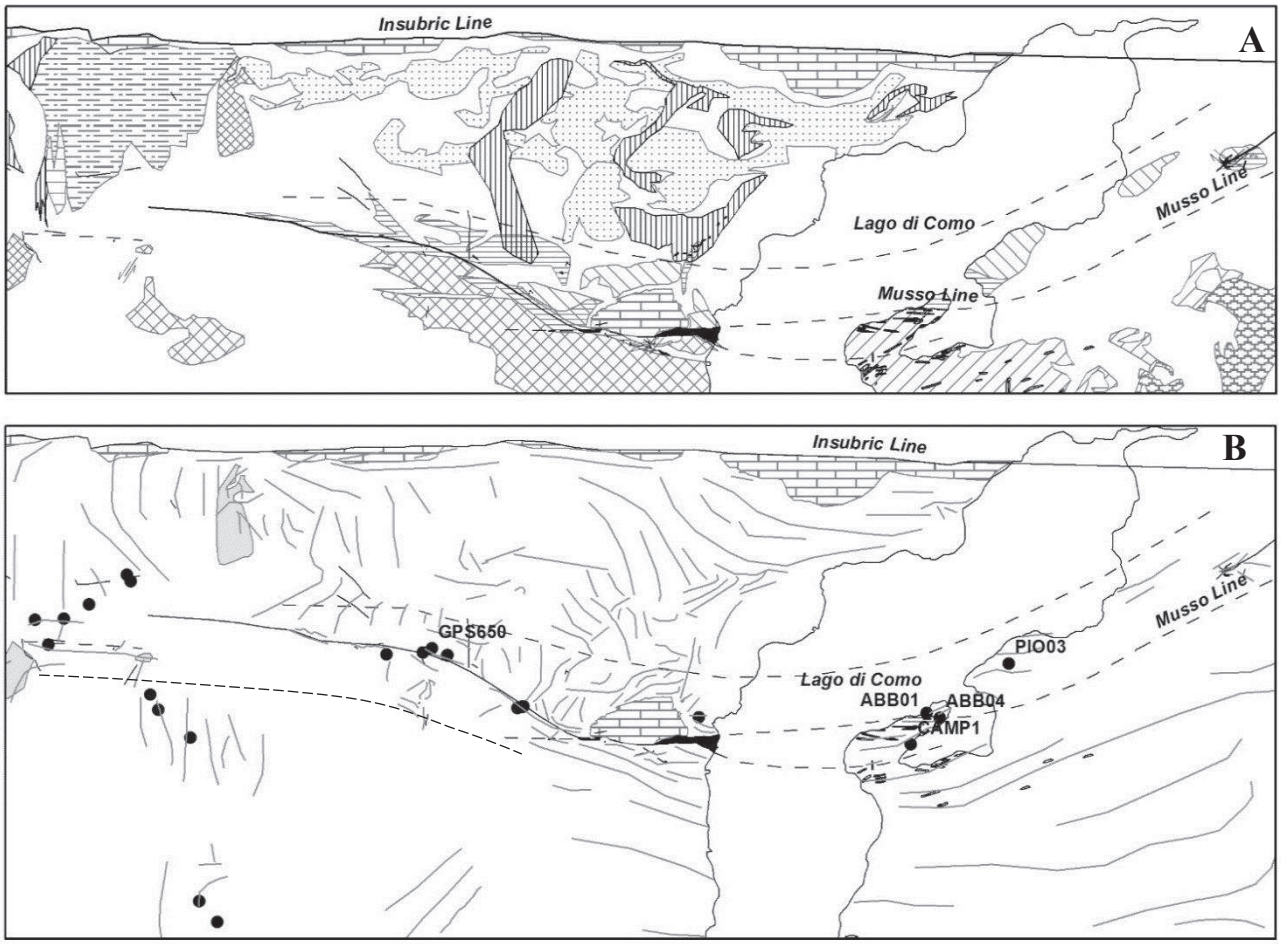

3.5 Appendix 1: Esem microscopy results

Sample GPS650 – Albano Valley

1. Generating vein
2. Injection vein

Note on semi-quantitative analysis: Semi-quantities shows matrix interaction causing not accurate Ox% determination.

1. Fault veins

	Elem	Na2O	MgO	Al2O3	SiO2	P2O5	K2O	CaO	TiO2	MnO	Fe2O3	Total	Mineral phase
gps650b	Wt%	0.89	6.10	26.74	46.15		6.46	1.30	1.30		11.06	100.00	Glass
gps650c	Wt%	0.89	10.71	25.20	33.89		1.59	0.51			27.21	100.00	Chlorite
gps650d	Wt%	1.17	2.10	6.53	86.10		1.51				2.59	100.00	Quartz
GPS650E	Wt%	1.87	2.77	10.12	19.37	29.44	2.67	31.38	0.35		2.04	100.00	Apatite
GPS650F	Wt%	1.06	1.71	8.44	83.70	0.00	2.05	0.56	0.66		1.82	100.00	Quartz
GPS650G	Wt%	0.96	2.28	13.20	75.53	0.00	3.57	0.37	0.83		3.26	100.00	Quartz
GPS650H	Wt%	0.74	4.01	27.29	52.49	0.00	7.64	0.70	1.47		5.67	100.00	Glass
GPS650I	Wt%	6.84	2.49	24.23	59.95		2.26	2.23			2.00	100.00	Albite
GPS650J	Wt%	1.89	4.75	25.95	52.40		7.39	0.83	1.74		5.04	100.00	Glass
GPS650K	Wt%	0.91	3.73	24.97	56.24	0.19	6.77	0.73	1.30		5.16	100.00	Glass+ clasts (total composition)
GPS650L	Wt%	1.58	4.41	25.94	51.55	1.06	6.76	1.19	1.62		5.89	100.00	Glass
GPS650M	Wt%	1.83	2.61	38.62	43.14	0.82	7.28	1.30	0.90		3.51	100.00	K-feldspar?
GPS650N	Wt%		2.31	12.98	21.49		2.59	0.55	31.78	2.58	25.72	100.00	Ilmenite

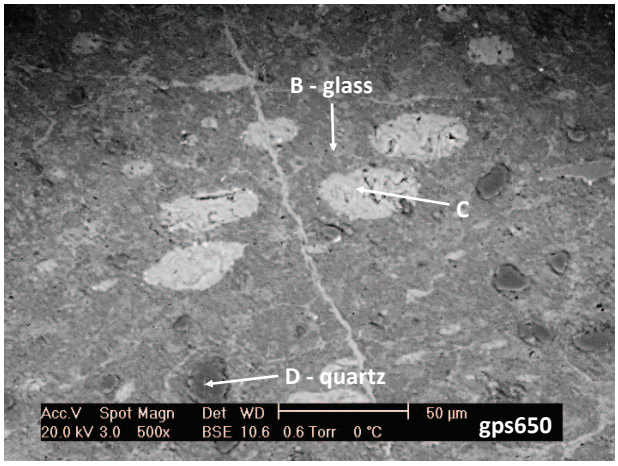

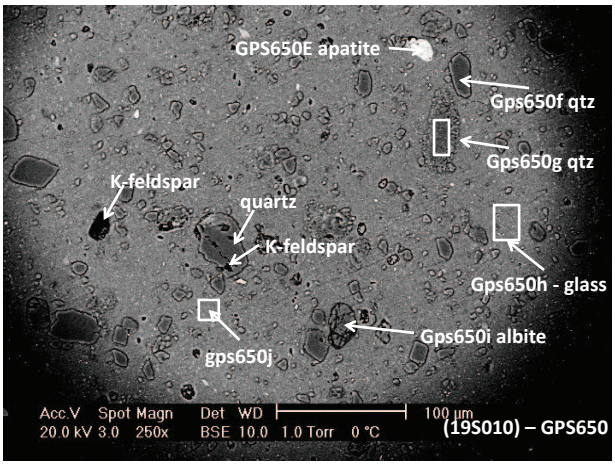

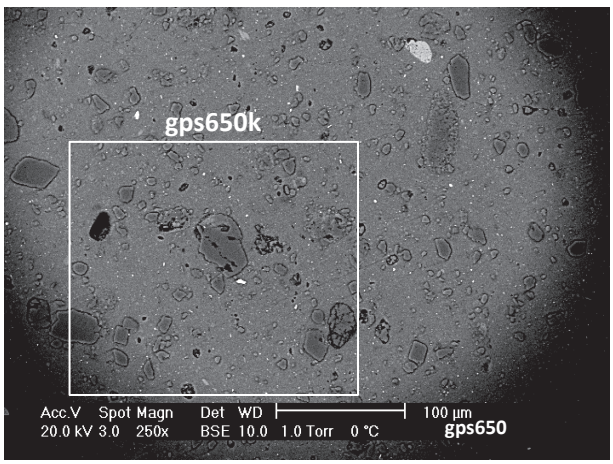

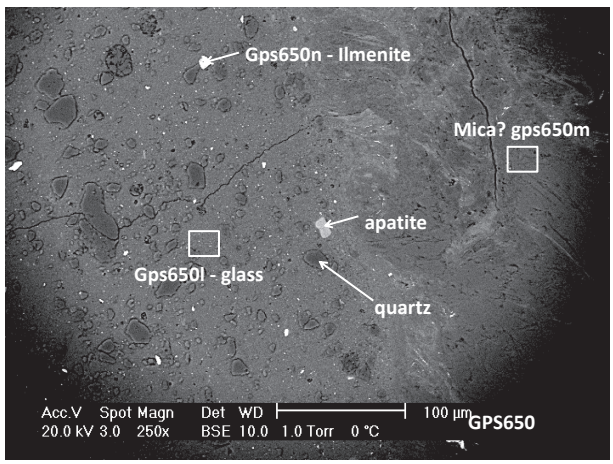

1. Injection vein

	Elem	Na2O	MgO	Al2O3	SiO2	P2O5	K2O	CaO	TiO2	MnO	Fe2O3	Total	Mineral phase
GP650B01	Wt%	2.07	3.09	19.06	60.16		9.01	1.56			5.05	100.00	Glass

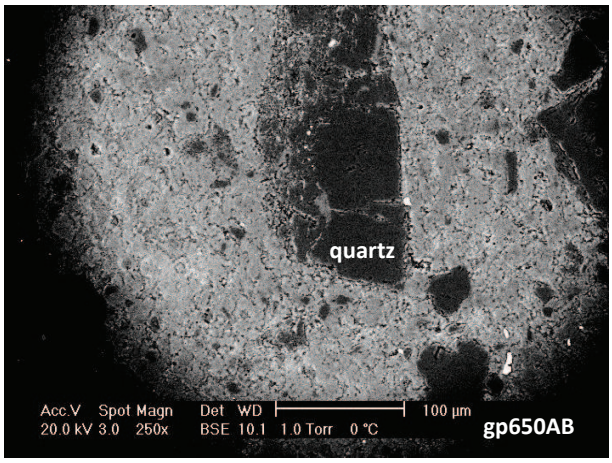

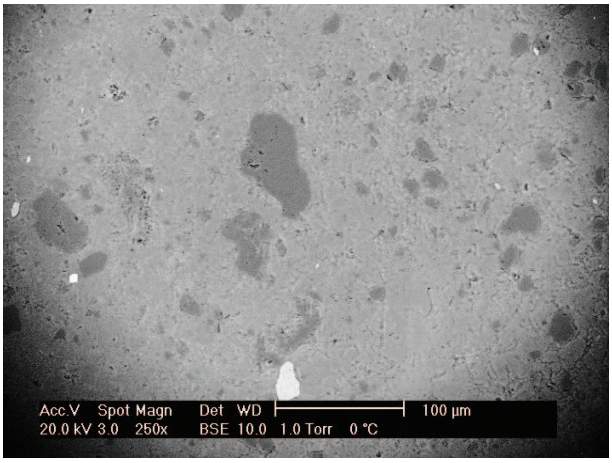

Sample ABB04 – Piona Peninsula

	Elem	Na2O	MgO	Al2O3	SiO2	P2O5	K2O	CaO	TiO2	Cr2O3	Fe2O3	Total	Mineral phase
ABB04A	Wt%	1.57	1.98	8.86	14.02	33.28	2.41	35.58			2.31	100.00	Apatite
ABB04B	Wt%	1.41	2.59	20.21	66.25	0.51	4.91	0.63			3.49	100.00	Glass
ABB04C	Wt%	7.45	2.06	25.90	56.66	0.90	1.97	3.41			1.65	100.00	Anorthoclase
ABB04D	Wt%	1.25	2.20	7.22	84.50	0.89	1.85	0.76			1.31	100.00	Quartz
ABB04E	Wt%	1.92	3.03	26.07	45.80	0.58	11.13	1.57			9.90	100.00	K-feldspar
ABB04F	Wt%	4.17	3.29	8.62	19.37		1.21	0.51	32.88	0.00	29.95	100.00	Ilmenite?
ABB04G	Wt%	1.52	1.75	5.61	86.41		1.19	0.52	0.77	0.39	1.86	100.00	Quartz
ABB04H	Wt%	1.64	6.52	22.12	42.53		7.44	1.11	2.61	0.35	15.69	100.00	Biotite
ABB04I	Wt%	1.46	6.95	21.64	43.87		7.87	1.24	1.95	0.00	15.03	100.00	Biotite
ABB04J	Wt%	2.80	8.02	23.76	40.70		7.62	0.77	1.72	0.30	14.32	100.00	Biotite
ABB04K	Wt%	2.60	2.67	9.22	79.42		1.91	0.53	0.56	0.23	2.86	100.00	Quartz
ABB04L	Wt%	2.58	2.46	10.20	15.91	30.89	2.46	32.85	0.45	0.00	2.18	100.00	Apatite
ABB04M	Wt%	2.91	4.76	27.69	46.69	1.16	7.43	1.24	1.52	0.11	6.47	100.00	Glass
ABB04N	Wt%	0.89	7.22	23.99	42.00	0.00	8.16	0.64	2.44	0.39	14.26	100.00	Biotite
ABB04O	Wt%	2.72	2.81	12.23	18.58	0.85	2.50	0.47	57.51	0.00	2.33	100.00	?
ABB04P	Wt%	2.37	4.68	28.67	45.76	1.69	7.77	1.20	1.93	0.23	5.71	100.00	Glass
ABB04Q	Wt%	1.34	3.71	28.03	50.46	0.00	7.68	1.08	1.68	0.43	5.59	100.00	Glass
ABB04R	Wt%	1.98	2.84	11.76	18.37	1.43	2.72	1.01	32.35	0.43	27.11	100.00	Ilmenite?
ABB04S	Wt%	5.78	2.72	26.57	54.02	0.72	3.34	2.65	0.84	0.30	3.07	100.00	Fractured clast

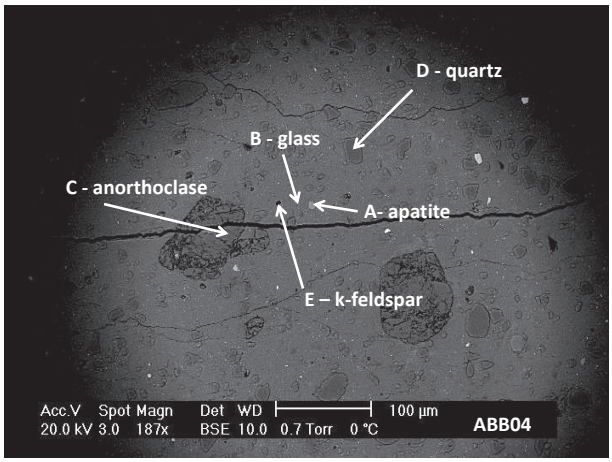

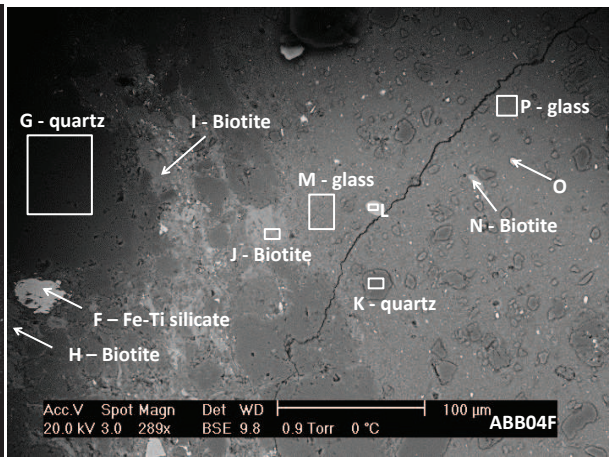

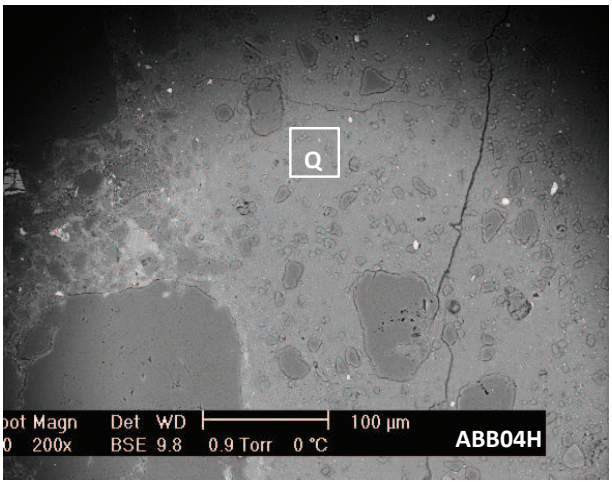

Geochemical data comparison

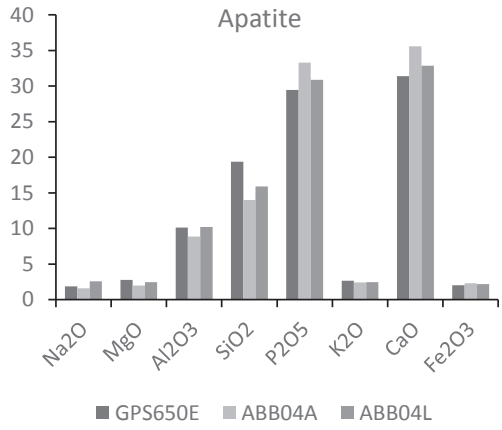

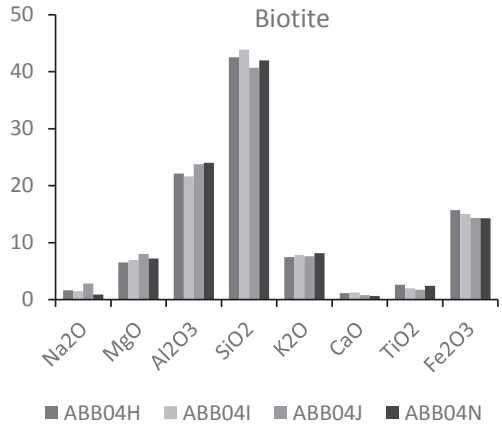

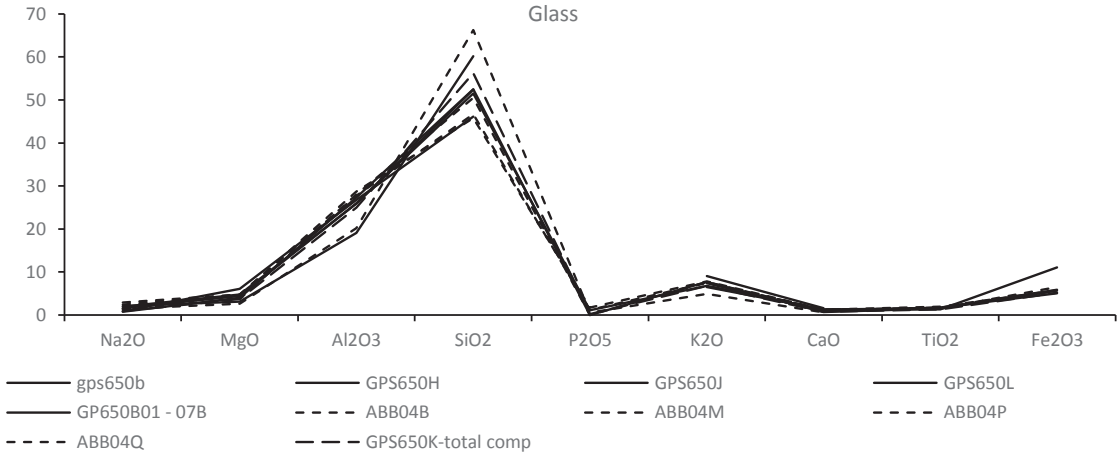

3.6 Appendix 2: samples descriptions and locations

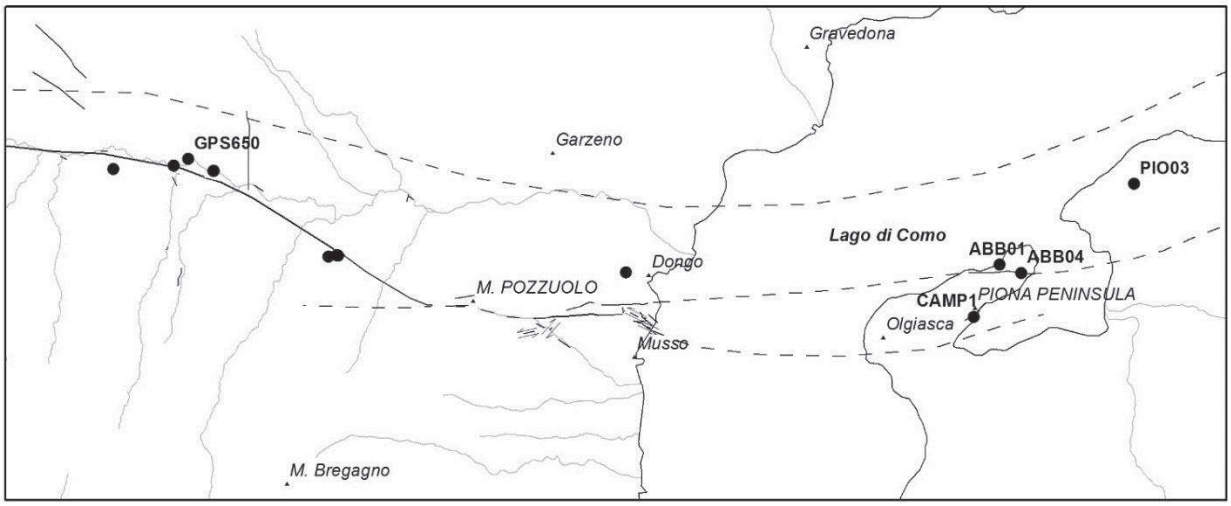

(CAMP01-PIO) 14 – Cataclastic gneiss with pseudotachylyte veins

The sample displays a cataclastic fabric characterized by the occurrence of pseudotachylyte (PST) veins of 0,1 – 2 mm thickness. PST appear to had developed from a cataclastic precursor. The mineralogy of host rock of the PST is made of quartz, plagioclase, biotite, chlorite, muscovite with abundant opaques minerals and apatite (trace amounts). Quartz aggregates are intensively fractured with the occurrence of transgranular fractures in most of crystals. Biotite is partly retrogressed to chlorite and show evidence of intracrystalline deformation as kink bands and microcracks.

Both melt generation surfaces (MGS) as well as injection veins (*sensu* Sibson, 1975) of pseudotachylyte crosscut the cataclastic fabric. Within PST veins the clast/matrix ratio is highly variable, with the lowest ratio displayed by some injection veins (ca. 10/90). The matrix of both MGS and injections veins appears black-colored both at parallel and crossed nicols, with the exception of an injection veins where recrystallization of fine mica aggregates could be observed at crossed nicols. No color or compositional zoning have been observed within the pseudotachylyte veins.

The inequigranular clast population consists mainly of quartz crystals and lithic grains of the host rock. Minor biotite clasts with evidence of partial resorption occur in a single injection vein. Quartz and lithic clasts are usually rounded to subrounded.

(GPS650) 7a – Garnet-biotite cataclastic gneiss with pseudotachylytes veins

The sample consists of a two micas gneiss with a cataclastic fabric characterized by the occurrence of peudotachylytes injection veins. The host rock of the pseudotachylyte veins is made of quartz, white mica, biotite, garnet, chlorite and accessory phases such as apatite and opaque minerals. White mica crystals aligned along the main foliation are partly substituted by fine-grained sericitic aggregates. The relic porphyroclasts of white mica show evidence of strong intracrystalline deformation resulting in undulose extinction and kink bands. Garnet occurs as 0,5-1,0 mm in size subidiomorphic porphyroclasts with skeletal texture. Both garnet and biotite show evidence of retrogression as they are substituted by chlorite.

Pseudotachylyte injection veins present in the sample are up to 2-2,5 mm wide. Observed at parallel nicols they show a poorly developed color zoning, in part visible also at crossed nicols. This zonation likely reflects differential cooling of the injected melts or fluidal structures.

Within the largest veins the clast/matrix ratio is close to 20/80. Most of the clasts are made of rounded quartz, with minor lithic subrounded clasts and also biotite clast with an irregular shape.

Pseudotachylyte veins are typically affected by brittle fractures almost perpendicular to the length direction of veins.

(GPS650) 7 – Biotite cataclastic gneiss with pseudotachylytes veins

The sample consists of a cataclastic to ultracataclastic biotite gneiss with small veinlets of pseudotachylyte.

In this sample, with respect to sample 7a, the cataclastic texture is more pronounced with 7-8 mm wide shear zone where strong comminution led to the development of partially matrix-supported ultracataclasite (clast/matrix ratio of ca. 40/60).

Both quartz and plagioclase show evidence of strong intracrystalline deformation (undulose extinction and deformation bands) accompanied by brittle transgranular fractures. Biotite is also deformed and partially substituted by chlorite, whereas fine grained sericitic aggregates substitute for white mica.

Pseudotachylyte occurs as a single vein formed by a melt generation surface with two reservoir veins. Other small veinlets of pseudotachylyte also occur (1-2 mm) but they are not further described as their relationships with the host rock are not completely visible.

The PST vein displays a variable thickness, ranging from 0,3 mm up to 3 mm where it enlarges to form a reservoir vein. Along the MGS segment the vein is homogeneous in color (grey-brown) but it has asymmetric margins: one more or less rectilinear, the other irregular. Along the irregular side a thin rim (ca 0,1 mm wide) of fine grained recrystallize quartz occurs. The clast/matrix ratio is about 20/80 with clasts mainly made by rounded to subrounded quartz crystals.

On the other side injection veins has a strong color zoning made by alternating dark-grey and brown levels, up to 1 mm wide. The color zoning highlights fluidal microstructures with lobes displaying a convex shape toward the host rock. The clast/matrix ratio is higher with respect to the MGS vein. It ranges from 30/70 up to 40/60 along vein margins. Clasts are chiefly subrounded but also minor angular clasts occur. Clasts consist of quartz, lithic fragments and minor plagioclase and biotite.

(ABB01) 11 – Mylonitic micaschist

The sample has a mylonitic texture with a well developed mylonitic foliation individuated by newly crystallized white mica and chlorite. In some areas embryonic of s-c' structures could be observed. Two generation of white mica occur: the first is preserved as porhyroclast within the mylonitic foliation (mica fish), the second is sericite growing along foliation plane. Biotite is poorly preserved as it appears to be not stable during shear process that led to the formation of the mylonite. Chlorite substitutes for biotite and is also obvserved to grow together with sericite.

Quartz is dynamically recrystallized, with a strong grain size reduction along the mylonitic foliation. Plagioclase porphyroclast show no evidence for recrystallization and appear instead interested by brittle micro-fault and cataclasi.

The stability of chlorite instead of biotite together with the brittle behavior of plagioclase and the dynamic recrystallization of quartz point to temperature conditions comprised between 250°C and 350°C during the formation of the mylonite.

4 References

Baccelle Scudeler L., Bartolomei G., Bosellini A., Dal Cin R., Lucchi Garavello A., Nardin M., Rossi D., Sacerdoti M., Semenza E., Sommavilla E., Zirpoli G., 1969, Note illustrative della Carta Geologica d'Italia alla scala 1:100.000, Foglio 11, M. Marmolada, Servizio Geologico Italiano, Roma, pp.89

Bally A., Bernoulli D., Davies G., Montadert L., 1981. Listric normal faults. In Blanchet R., Montadert L. Geology of continental margins. Oceanologica Acta, 4, suppl.: pp. 87-101

Balzarini A., Cani F., Zerboni A., 2001. Antiche cave nel territorio della Regio Insubrica. Como, Varese, Cantone Ticino, Soc. Archeologica Comense

Barth S., Oberli F., Meyer M., Blattner P., Bargossi M.G., Battistini G., 1993. The evolution of a calc-akaline basic to silicic magma system: geochemical and Rb-Sr, Sm-Nd and 18O/16O isotopc evidence from the Late Hercinian Atesina-Cima d'Asta volcano-plutonic complex, Northern Italy. Geochimica et Cosmochimica Acta, 57, 4285-4300

Bau, M. and Möller, P., 1992. Rare-earth element fractionation in metamorphogenic hydrothermal calcite, magnesite and siderite. Mineralogy Petrology, 45: 231-246.

Bernoulli, D., 1964. Zur Geologie des Monte Generoso (Lombardischen Alpen). Beitr. geol. Karte Schweiz, NF 118.

Bernoulli D., Govi M., Graeter P., Lehner P., Reinhard M., Spicher A., 1976. Geologischer Atlas der Schweiz 1:25000, Blatt 1353 Lugano Graph. Anstalt Wassermann, Basel.

Bernoulli, D., 2007. The pre-Alpine geodynamic evolution of the Southern Alps: a short summary. Bull. angew. Geol., Vol. 12/2, p. 3-10, Bern, Switzerland.

Bersezio R, Fornaciari M, Gelati R, Napolitano A, Valdisturlo A (1993) The significance of the Upper Cretaceous to Miocene clastic wedges in the deformation history of the Lombardian southern Alps. Geol Alp 69: 3-20

Bertotti G. 1988; The deep structure of the South-Alpine Mesozoic passive continental margin; Deep Structure of the Alps; Symposion 12-13; Dec. 1988 Paris, Abstract, 12.

Bertotti G. 1990 The deep structure of the Monte Generoso basin: an extensional basin in the south-Alpine Mesozoic passive continental margin, Deep Structure of the Alps, pp. 303-308.

Bertotti G., 1991. Early Mesozoic extension and Alpine shortening in the Western Southern Alps: the geology of the area between Lugano and Menaggio (Lombardy, Northern Italy). Meorie. Scienze Geologiche, vol. XLIII, 17-123.

Bertotti, G., Siletto, G.B., Spalla, M.I., 1993. Deformation and metamorphism associated with crustal rifting: Permian to Liassic evolution of the Lake Lugano-Lake Como area (Southern Alps). Tectonophysics 226, 271–284.

Bertotti G. Ter Voorde M. 1994. Thermal effects of normal faulting during rifted basin formation, 2. The Lugano-Val Grande normal fault and the role of pre-existing thermal anomalies. Tectonophysics, vol. 240, issue 1-4, pp. 145-157

Bertotti, G., Seward, D., Wijbrans, J., terVoorde, M. and Hurford, A.J., 1999. Crustal thermal regime prior to, during, and after rifting: a geochronological and modelling study of the Mesozoic South Alpine rifted margin. Tectonics, 18, 185–200.

Bigi G., Cosentino D., Parotto M., Sartori R., Scandone P., 1992. Structural Model of Italy; Scala 1:500.000. C.N.R. Progetto finalizzato geodinamica.

Bocchio, R., Crespi, R., Liborio, G., Mottana, A., 1980. Variazioni composizionali delle miche

chiare nel metamorfismo prograde degli scisti sudalpini dell'alto lago di Como. Memorie di Scienze

Geologiche (Padova) 34,153-176.

Bocchio R. And De Capitani L., 1998 - The amphibolites of the South-Alpine basement in the upper Lake Como region (Italy). Atti Soc. It. Sci. Nat., Milano, v. 139, pp. 101-125

Boriani A., Giobbi Origoni E., Borghi A., Caironi V; 1990; The evolution of the "Serie dei Laghi" (Strona –Ceneri and Scisti dei Laghi): the upper component of the Ivrea-Verbano crustal section, Southern Alps, Northern Italy and Ticino, Switzerland; Tectonophysics 182, pp. 103-118.

Boriani A. And Villa I. (1997) — Geochronology of regional metamorphism in the Ivrea-Verbano Zone and Serie dei Laghi, Italian Alps. Schweiz. Mineral. Petrogr. Mitt., 77, 381-401.

Boriani A., Bini A.. Berra F., 2012. Foglio 056 Sondrio, Note illustrative della Carta Geologica d'Italia alla scala 1:50.000, ISPRA, Servizio Geologico d'Italia

Brack P (1984) Geologie der Intrusiva und Rahmengesteine des Sudwest-Adamello (Nord-Italien). Mitt Geol Inst ETH Univ Zurich 7612: 253 pp

Braga Gp., Gatto G.O., Gatto P., Gregnanin A., Massari F., Medizza F., Nardin M., Perna G., Rossi D., Sacerdoti M., Semenza E., Sommavilla E., Zirpoli G. e Zulian T., 1971. Note illustrative della Carta Geologica d'Italia alla scala 1:100.000, Foglio 22 Feltre, Servizio Geologico d'Italia, Roma.

Brigo L. & Venerandi I., 2005. Le mineralizzazioni ferrifere nelle Alpi Meridionali centrali (Lombardia, Italia): revisione litostratigrafica e metallogenica. Bollettino della Società Geologica Italiana 3, volume 124, 493 – 510

Brondi A., Mittempergher M., Panizza M., Rossi D., Sommavilla E. & Vuillermin F., 1977. Note Illustrative della Carta Geologica díItalia alla scala 1:50.000, Foglio 028 La Marmolada. Servizio Geologico d'Italia, pp. 30, Roma

Brodie, K. H., and Rutter, E. H., 1987. The role of transiently fine-grained reaction products in the syntectonc metamorphism: natural and experimental examples. Canadian Journal of Earth Science, 24, 554-64

Brodie, K. H., Rex, D. & Rutter, E. H., 1989. On the age of deep crustal extensional faulting in the Ivrea Zone, northern Italy. In: Coward, M. P., Dietrich, D. & Park, R. G. Alpine Tectonics. Geological Society, London, Special Publication 45,203–210.

Cadel G., Cosi M., Pennacchioni G. & Spalla M.I., 1996. A new map of the Permo-Carboniferous cover and Variscan metamorphic basement in the central Orobic Alps, Southern Alps-Italy: structural and stratigraphic data. Memorie Scienze Geologiche, 48, 1-53, 1 geol. map 1:25.000, Padova.

Cassinis, G., Frizzo, P., Moroni, M., Rodeghiero, F., 1997. Le mineralizzazioni delle Alpi bresciane: aspetti geologicominerari e metallogenici. Atti della Giornata di Studio:"Le vene delle montagne", Brescia, 24 novembre 1995. Fondazione Bresciana per la Ricerca Scientifica: 97-119.

Cassinis G., Cortesogno L., Gaggero L., Massari F., Neri C., Nicosia U. & Pittau P., 1999. Stratigraphy and facies of the Permian deposits between Eastern Lombardy and the Western Dolomites. Field Trip Guidebook. In: «The continental Permian, International Congress, 15-25 Sept., 1999, Brescia»; 23-25 Sept. 1999, 157 pages, Earth Science Department, Pavia University

Cassinis G., 2007. Collio. In SGN, Periodici tecnici, I Quaderni, serie III, Volume 7 - Fascicolo VII – Unità tradizionali (2)/2007, pp 42-51

Cassinis G., Cortesogno L., Gaggero L., Perotti C. R., Buzzi L., 2008. Permian to Triassic geodynamic and magmatic evolution of the Brescian Prealps (eastern Lombardy, Italy). Bollettino Società Geologica Italiana (Ital.Journal of Geosciences.), Vol. 127, No. 3, pp. 501-518, 16 figs., 1 tab.

Carminati E, Siletto GB (2005) The Central Southern Alps (N. Italy) paleosismic zone: a comparison between field observations and predictions of fault mechanics. Tectonophysics 401:179-197

Cita Sironi M.B., Abbate E., Balini M., Conti M.A., Falorni P., Germani D., Groppelli, G. Manetti P., Petti F.M., 2007. Carta Geologica d'Italia 1:50.000. Catalogo delle formazioni. Fascicolo VII - Unità tradizionali (2). In: Quaderni del Servizio Geologico Nazionale, Serie III, vol. 7, fasc. VII, 382 pp.

Colombo A., Tunesi A. (1999): Alpine metamorphism of the Southern Alps west of the Giudicarie Line. Schweizerische Mineralogische und Petrographische Mitteilungen, 79,63-77.

Cortecci G. & Frizzo P., 1993. Origin of siderite deposits from the Lombardy valleys, northern Italy- A carbon, oxygen and strontium isotope study. Chemical geology, 105(4), pp. 293-303

Colombo A., Tunesi A., 1990. Alpine metamorphism of the Southern Alps west of the Giudicarie Line. Schweizerische Mineralogische und Petrographische Mitteilungen, 79, 63-77.

Crespi R., Liborio G. & Mottana A. 1981 Metamorfismo tardo-alpino di grado bassissimo nel basamento a Sud della linea Insubrica. Rend. Soc. Ital. Mineral. Petrol., 37: 813-824.

Crisci C. M. & Ferrara G., 1984. Geological and geochronological data on Triassic volcanism of the Southern Alps of Lombardy (Ialy), Geologische Rundscau, 73, 279-292.

D'adda P. 2010. Eo-Alpine Evolution Of The Central Southern Alps Insights From Structural Analysis And New Geochronological Constraints. University of Milan Bicocca, Unpublished PhD Thesis.

De Capitani L. Delitala M. C. Liborio G. Mottana A. Rodeghiero F. Thoni M., 1994. The granitoid rocks of Val Navazze, Val Torgola and Val di Rango (Val Trompia, Lombardy, Italy). Memorie di scienze geologiche, 46,, pp. 329-343

De Capitani L., Carnevale M., Fumagalli M., 2007. Gamma-ray spectroscopy determination of radioactive elements in late-Hercynian plutonic rocks of Val Biandino and Val Trompia (Lombardy, Italy). Per. Mineral., 76, 25-39.

De Sitter, L.U., De Sitter-Koomans, C.M, 1949. Geology of the Bergamasc Alps, Lombardia, Italy. Leidse Geol. Meded. 14 (1), 257.

De Zanche V. & Farabegoli E., 1981. Scythian tectonics in the Southern Alps: Recoardo phase. Geol. Palaont. Mitt. Insbruck, 10, 289-304

Del Moro A, Pardini G, Quercioli Q, Villa IM, Callegari E (1985) Rb/Sr and K/Ar chronology of Adamello granitoids, Southern Alps. In: Dal Piaz GV (ed) Il magmatismo tardo alpino nelle Alpi. Mem Soc Geol It 26: 285-299

Di Giulio A, Carrapa B, Fantoni R, Gorla L, Valdisturlo A (2001) Middle Eocene to Early Miocene sedimentary evolution of the western Lombardian segment of the South Alpine foredeep (Italy). Int J Earth Sci 90: 534-548

Di Paola S., Spalla M. I. 2000. Contrasting tectonic records in pre-Alpine metabasites of the Southern Alps (lake Como, Italy) Journal of Geodynamics, 30, 167-189

Di Paola S., Spalla M. I. 2006 Maps of foliation trajectories and metamorphic imprints: a tool for individuatine tectonometamorphic units in the Southalpine basement (Como Lake area). Mapping Geology in Italy G. Pasquarè, C. Venturini (eds.) e G. Groppelli (Ass.Ed.). Pp. 305-312, 1 carta geologica. Stampa SELCA Firenze

Diella V., Spalla M.I., Tunesi A. 1992. Contrasting thermochemical evolution in the Southalpine metamorphic basement of the Orobic Alps, (Central Alps, Italy). J.metam. Geol. 10, 203-219.

Doglioni, C. 1987. Tectonics of the Dolomites (Southern Alps, Northern Italy). Journal of structural Geology 9, 181-193.

Doglioni C. 1992. Relationships between Mesozoic extensional tectonics, stratigraphy and Alpine inversion in the Southern Alps. Eclogae Geologicae Helvetiae, 85, 1, 105-126.

El Tahlawi M.R.1965 Geologie und petrographie des nordöstlichen Comerseegebietes (Provinz Como, Italien). PhD Thesis, 199 pp, ETH Zurich

Elderfield, H. and Greaves, M.J. 1982. The Rare-Earth Elements in Sea-Water. Nature 296(5854), 214-219.

Ferrara, G. & Innocenti, F.. 1974. Radiometric age evidence of a Triassic thermal event in the Southern Alps.

Geologische Rundschau. 63, 572-581

Forcella F., Bigoni C., Bini A., Ferliga C., Ronchi A., Rossi S., 2012, Foglio 078 Breno. Note illustrative della Carta Geologica d'Italia alla scala 1:50.000, ISPRA, Servizio Geologico d'Italia

Forestier F.H., 1963. Métamorphisme hercynien dans les bassins du Haut Allier. Bull. Serv. Carte Géol. Fr., 271: 294 pp.

Frizzo P., 1970. Studio geominerario del territorio di Pisogne (Bassa Val Camonica – Brescia). Padova University, Unpublished Thesis

Frizzo P.. & Omenetto P.. 1974. Le manifestazioni metallifere nel basamento cristallino della Val Camonica (Lombardia). Memorie Museo Tridentino Scienze Naturali, 20, 1-75, Trento.

Frizzo P., Scudeler Baccelle L. 1983. Rapporti strutturali e tessiturali fra mineralizzazione a siderite e litotipi carbonatici nel Servino (Scitico) delle Valli Lombarde Padova. Scienze Geologiche, Vol. 36, 195-210

Frumento A., 1952. Imprese lombarde nella storia della siderurgia italiana: il contributo dei Falck. 1833-1913. Vol. I, Società "Acciaierie e ferriere lombarde Falck", 275

Fumasoli M. W., 1974. Geologie des gebietes nordlich und sudlich der Jiorio-Tonale-Linie im western von Gravedona (Como, Italia). PhD Thesis, unpublished, Zurich

Gaetani M., Gianotti R., Jadoul F., Ciarapica G., Cirilli S., Lualdi A., Passeri L., Pellegrini M., Tannoia G., 1986. Carbonifero superiore, Permiano e Triassico nell.area Lariana. Memorie Società Geologica Italiana, Vol. 32, 5-48

Gaetani, M., Jadoul, F., 1989. The structure of the Bergamasc Alps. Atti Accad. Naz. Lincei 66, 411–416.

Gianotti R., Perotti C.R. 1986. Introduzione alla tettonica e all'evoluzione strutturale delle Alpi Lariane. Memorie Società Geologica Italiana, Vol. 32, 67-99

Giobbi Mancini E., Boriani A. And Villa I. 2003 - Pre-Alpine ophiolites in the basement of Southern Alps: the presence of a bimodal association (LAG - Leptyno-Amphibolitic Group) in the Serie dei Laghi N-Italy, Ticino-CH). Atti dell'Accademia Nazionale dei Lincei, Classe di Scienze Fisiche, Matematiche e Naturali,14, 79-99.

Giobbi Mancini E, Bergomi Ma, Boriani A; 2004; Petrology and age of a bimodal association (LAG – leptyno-amphibolitic group) in the basement of Southern Alps (Serie dei Laghi, N-Italy, Ticino – CH). 32nd IGC (Florence, 2004), Abstract Volume, part 2, 1060 pp

Giobbi Origoni E., Zappone A., Boriani A., Bocchio R. And Morten L.; 1997; - Relics of pre-alpine ophiolites in the Serie dei Laghi (Western Southern Alps). Schweiz. miner. petrogr. Mitt., 77, 187-207.

Gosso G., Siletto G.B. & Spalla M.I. (1997) - International ophiolite symposium field excursion guide - continental rifting to ocean floor metamorphism (21st-23rd September 1995): first day: H-T/L-P metamorphism and structures in the Southalpine basement near Lake Como, Orobic Alps; intracontinental imprints of the Permo-Triassic rifting. Ofioliti, 22 (1), 133-145.

Gosso G., Spalla M.I., Bini A., Siletto G.B., Berra F. & Forcella F., 2012. Note Illustrative della Carta Geologica díItalia alla scala 1:50.000, Foglio 057 Malonno. APAT - Dipartimento Difesa del Suolo-Servizio Geologico díItalia, Roma.

Haskin, M.A. & Haskin, L.A., 1966. Rare earths in European shales; a redetermination. Science 154, 507-509

John BE, Blundy JD (1993) Emplacement-related deformation of granitoid magmas, southern Adamello Massif, Italy. Geol Soc Am Bull 105: 1517–1541

Jongmans W., 1960. Die Karbonflora der Schweiz. Beitr. Geol. Karte Schweiz, 108, XVI, 97

Kovach, W.L. 2007. MVSP – A Multivariate Statistical Package for Windows,Ver. 3.13. Kovach Computing Services, Pentraeth, Wales, UK

Lak Shatanov L.Z.& Stipp S.L.S., 2004, Experimental study of Eu(III) coprecipitation with calcite, Geochica et Cosmochimica Acta, 68-4, 819-827

Laubscher H.P., 1974. Evoluzione e struttura delle Alpi. Le Scienze, 72, 264 - 275.

Laubscher H.P., 1985. Large scale, thin–skinned thrusting in the Southern Alps: kinematic models. Geol. Soc. Am. Bull., 96, 710–718

Lardeaux J. M. & Spalla M.I., 1991. From granulites to eclogites in the Sesia zone (Italian Western Alps): a record of the opening and closure of the Piedmont ocean. Journal of Metamorphic Geology, 9, 35-59

Magloughlin, J.F., Spray, J.G., 1992. Frictional melting processes and products in geological materials: introduction and discussion. In: Magloughlin, J.F., Spray, J.G. (Eds.), Frictional Melting Processes and Products in Geological Materials. Tectonophysics 204, 197–204.

Meier A. 2003. The Periadriatic Fault System in Valtellina (N-Italy) and the Evolution of the Southwestern Segment of the Eastern Alps. [Ph.D thesis] : 190 pp. Zurich, Switzerland, ETH

Meschede M. 1986 A method of discriminating between different types of mid-ocean ridge basalts and continental tholeiites with the Nb–Zr–Y diagram. Chemical Geology 56, 207 218

Montorfano C., Martin S., Viganò A., 2008. Database cartografici: un'applicazione nelle Alpi centro-orientali. Rendiconti Online Società Geologica Italiana, Volume 3, Fascicolo 2, 573-574,

Montorfano C. Martin S., Carugati G. Secco L. Toffolo L. Vezzoli L. Frizzo P.. 2014. Siderite mineralization in the Southern Alps: a signal of the Permo—Triassic rifting? Lithos, currently in revision

Mottana A., Nicoletti M., Petrucciani C., Liborio, G., De Capitani L., Bocchio R., 1985. Pre-alpine and alpine evolution of the South-alpine basement of the Orobic Alps. Geologische Rundschau, Vol. 74, Issue 2, 353-366

Mullen E. D. 1983 MnO/TiO2/P2O5: a minor element discriminant for basaltic rocks of oceanic enviroments and its implications for petrogenesis Earth and Planetary Science Letters 62, 53 62

Nakamura N., 1974. Determination of REE, Ba, Fe, Mg, Na, and K in carbonaceous and ordinary chondrites. Geochimica et Cosmochimica Acta 38, 757-775

Philippe S., Vilemaire C., Lancelot J.R., Girod M.,Girod M., Mercadier H., 1987. Données minéralogiques et isotopiques sur duex gites hydrothermeaux uraniferes du basin volcano-sedimentaire permien de Collio Orobico (Alpes Bergamasques): mise en evidence d'une phase de remobilisation cretacée. Bull. Minéral., 110, 283-303

Poli M.E. & Zanferrari A. 1992. Agordo basement (NE Italy): a 500 MA-LONG geological record in the Southalpine crust. In: Contributions to the geology of Italy with special regard to the Paleozoic basements. (Ed. By Carmignani L., Sassi F.P.). IGCP 276, vol. 5, 283-296

Pourmand A., Dauphas N., Ireland T. J, 2012. A novel extraction chromatography and MC-ICP-MS technique for rapid analysis of REE, Sc and Y: Revising CI-chondrite and Post-Archean Australian Shale (PAAS) abundances. Chemical Geology 291, 38–54

Rodeghiero, F. & Zuffardi, P., 1985. Stratiform and strata-bound siderite and barite deposits of the Central Italian Alps. Monografie Ser. Mineralium Deposita, 25, 121-135

Sanders C.A.E., Bertotti G., Tomasini S., Davis G.R., Wijbrans J.R., 1996. Triassic pegmatites in the Mesozoic middle crust of the Southern Alps (Italy): Fluid inclusions, radiometric dating and tectonic implications. Eclogae Geologicae Helvetiae, Vol. 89, 505– 525.

Schönborn G., 1992. Kinematics of a transverse zone in the Southern Alps, Italy. Thrust Tectonics, 299-310

Schumacher M., 1997A. Verformungsgeschichte der sudalpen zwischen Lago Maggiore und Lago di Como. Unpublished thesis, ETH Zurich

Schumacher M.E., Schönborn G., Bernoulli D. & Laubscher H.P. 1997B - Rifting and collision in the Southern Alps. In: (Pfiffner O.A., Lehner P., Heitzmann P., Mueller S. and Steck A. - Ed.), Deep Structure of the Swiss Alps, Birkhäuser, Basel, 186-204.

Sciunnach D., Garzanti E., Posenato R., Rodeghiero F., 1999. Stratigraphy of the Servino Formation (Lombardy, Southern Alps): towards a refined correlation with the Werfen Formation of the Dolomites. Memorie di Scienze Geologiche, Padova, 51, 103-118

Schaltegger U., Brack P. 2007. Crustal-scale magmatic systems during intracontinental strike-slip tectonics. U, Pb and Hf isotopic constraints from Permian magmatic rocks of the Southern Alps. Int J Earth Sci (Geol Rundsch), 96, 1131-1151.

Sibson, R., 1975. Generation of pseudotachylite by ancient seismic faulting. Geophys. J. Royal Astronom. Soc. 43, 775–794.

Siletto G.B., Spalla M.I., Tunesi A., De Nardo M.T., Soldo-L. 1990; Structural analysis in the Lario Basement (Central Southern Alps, Italy), Mem. Soc. Geo. It.; Vol 45; pp. 93-100; 3ff.

Siletto, G. B., Spalla, M. I., Tunesi, A., Lardeaux, J. M., Colombo, A., 1993. Pre-Alpine structural and metamorphic histories in the Orobic Southern Alps, Italy. In: Pre-Alpine basement in the Alps. Springer-Verlag, Heidelberg, 585–598.

Sloman L.E,. 1989. Triassic shoshonites from the Dolomites, northern Italy: alkaline arc rocks in a strike-slip setting. Journal Geophys. Res., 94, 4655-4666.

Spalla, M.I., Gosso, G., Siletto, G.B., Di Paola, S., Magistroni, C., 1998. Strumenti per individuare unità tettonico-metamorfiche nel rilevamento geologico del basamento crsitallino. Memorie di Scienze Geologiche (Padova) 50, 155-164.

Spalla, M.I., Gosso, G., Siletto, G.B., Di Paola, S. 2000; The role of structural and metamorphic memory in the distinction of tectono-metamorphic units: the basement of the Como lake in the Southern Alps; Journal of Geodynamics 30 191-204.

Spalla M.I., Di Paola S., Siletto G.B., Bistacchi A. 2002. Mapping tectono-metamorphic histories in the Lake Como Basement (Southern Alps, Italy). Memorie di Scienze Geologiche Padova, Vol. 54, 1-25

Swanson, M.T., 1992. Fault structure, wear mechanism and rupture processes in pseudotachylyte generation. Tectonophysics 204, 223–242.

Zimák J., Losos Z., Novotný P., Dobeš P., Hladíková J. 2002. Study of vein carbonates and notes to the genesis of the hydrothermal mineralization in ithe Moravo-Silesian Culm. Journal of the Czech Geological Society, Vol. 47, issue 3-4, 111 - 122

Zwingmann, H., Mancktelow, N. 2004: Timing of Alpine fault gouges. EPSL, 223, 415-425.